7-29-2022 10:00 AM

Flexural Behaviour of Concrete Beams with High Strength Reinforcement

Sohaib Akbar, *The University of Western Ontario*

Supervisor: Bartlett, F. Michael, *The University of Western Ontario*
Co-Supervisor: Youssef, Maged A., *The University of Western Ontario*
A thesis submitted in partial fulfillment of the requirements for the Master of Engineering Science degree in Civil and Environmental Engineering

ABSTRACT

Using High Strength Reinforcement (HSR) in concrete construction allows steel volumes to be reduced, and economies to be realized. CSA Standard A23.3:19 “Design of Concrete Structures” limits the maximum yield strength for design to 500 MPa. This thesis investigates the flexural behavior of concrete beams reinforced with HSR to assess whether current code provisions are appropriate. Curvature ductility ratios are calculated for cross sections with varying concrete compressive strengths, and reinforcement types and quantities. The effects of utilizing HSR on extreme fibre concrete compressive strains at Ultimate Limit State (ULS), moment redistribution at ULS, and deflections at Serviceability Limit States, are investigated. It was found that curvature ductility factors for sections reinforced with HSR are relatively less; A23.3:19 Clause 9.2.4, which specifies the maximum permissible moment redistribution at ULS, is appropriate for all beams investigated; and designs that meet the minimum height requirements of A23.3:19 Table 9.2 satisfy the deflection limits in A23.3:19 Table 9.3 for all beams investigated.

SUMMARY FOR LAY AUDIENCE

This thesis investigates the behavior of concrete beams reinforced with High Strength Reinforcement (HSR) that are not covered by the current Canadian Standards. Using HSR reduces the volume of steel, easing construction and potentially saving costs. Numerical simulations are conducted to quantify the behavior of beams reinforced with High Strength Reinforcement. Ductility is a desirable characteristic as it provides warning of imminent failure. Beams reinforced with HSR were found to be less ductile than those with conventional reinforcement, which should be considered in the design stage. Other flexural characteristics for members with HSR subjected to both in-service and failure loads are investigated, and the current design standards are adequate for these cases.

ACKNOWLEDGEMENTS

I would like to express my sincere gratitude to Dr. F. Michael Bartlett, and Dr. Maged A. Youssef for their continuous support, for always motivating me to try my best, and for consistently hosting weekly meetings for my guidance. Working with them has inspired in me a strong work ethic, and has made me a better technical writer, engineer, and person. I truly believe this thesis would not have been possible without their supervision.

I appreciate the financial support from Natural Sciences and Engineering Research Council of Canada.

TABLE OF CONTENTS

LIST OF TABLES

LIST OF FIGURES

LIST OF APPENDICES

NOMENCLATURE

EVW	External Virtual Work
HSC	High Strength Concrete
HSR	High Strength Reinforcement
IVW	Internal Virtual Work
SLS	Serviceability Limit State
UDL	Uniformly Distributed Load
ULS	Ultimate Limit State

a	Depth of the stress block approximation in A23.3
$A_s^{+/-}$	Reinforcement area at the critical positive or negative section of the beam
A_t	Transformed cross section area of a beam
B	Carreira & Chu concrete idealization parameter
b	Cross section width
C_c	Concrete compressive force
C_{ci}	Concrete compressive force in a compressive region layer, i
C_s	Shrinkage coefficient
C_u	Ultimate creep coefficient
c	Distance from the extreme compressive fibre to the plastic neutral axis

c_{cl}	Clear concrete cover to flexural reinforcement
d	Effective depth of the beam cross section
E_c	Concrete modulus of elasticity
$E_{c,7}$	Concrete modulus of elasticity at 7 days
$E_{c,28}$	Concrete modulus of elasticity at 28 days
E_{it}	Initial tangent modulus
E_s	Steel modulus of elasticity
E_{sh}	Steel reinforcement tangent modulus at the onset of strain hardening
f_c'	Specified minimum concrete compressive strength in A23.3:19, and also peak concrete compressive stress, reached after 28 days of curing
$f_{c,7}$	Peak concrete compressive stress, reached after 7 days of curing
f_r	Concrete rupture stress
f_s	Steel stress at Serviceability Limit State
f_u	Steel stress at ultimate
f_{su}	Steel stress at ultimate moment capacity
f_y	Steel yield stress
$\bar{f}_y$	Steel mean yield stress
h	Height of beam cross section
$I_{cr}^{+/-}$	Cracked moment of inertia at the critical positive (span) and negative (support) sections

I_e	Effective moment of inertia about the x-axis using Bischoff's equation
I_i	Indicator variable for the steel grade, where 'i' ranges from 1 to 4
I_t	Transformed moment of inertia about the x-axis
K	Ratio of specified live to dead loads
k	Depth factor to calculate the distance from extreme compressive fibre to the neutral axis, when the steel reinforcement yields
k_N	Axial stiffness of a reinforced beam
L	Span length
L_n	Effective span length
M	Moment in the moment-curvature analysis
M_1	Moment at the location of the second plastic hinge, corresponding to the formation of the first plastic hinge
M_2	Additional moment the second plastic hinge is able to resist after the formation of the first plastic hinge
M_{cr}	Cracking moment
$M_{cr}(t)$	Long term cracking moment
M_d	Applied moment due to specified dead load
$M_{el}^{+/-}$	Linear-elastic moment at the critical positive or negative sections of the beam
M_f^e	Factored applied moment on the beam, assuming computed assuming linear-elastic behaviour

M_i	Moment about the extreme compressive fibre due to the compressive force in layer ‘i’
M_l	Applied moment due to specified live load
M_{OW}	Moment due to a beam’s own weight
M_{SDL}	Moment due to superimposed dead load on a beam
M_s	Applied service load moment
$M_u^{+/-}$	Ultimate moment capacity at the critical positive or negative section of the beam
$M_y^{+/-}$	Yielding moment at the critical positive or negative section of the beam
n	Modular ratio
n_{28}	Modular ratio after 28 days
n_7	Modular ratio after 7 days
p	Mander & Matamoros steel idealization parameter
Q_{cr}	Correction factor for creep coefficient
r	Moment redistribution percentage
s	reinforcement bar spacing
T_s	Steel reinforcement tensile force
t	Elapsed time
t_{dse}	Time after deflection sensitive elements are installed
V_1	Shear force at the external support due to w_1

V_{if}	Shear force at the internal support due to the failure load
w	Applied uniformly distributed load
w_1	Uniformly distributed load required to create the first plastic hinge
w_2	Additional uniformly distributed load required to create the second plastic hinge
w_c	Failure load corresponding to the case where a full collapse mechanism forms.
w_d	Applied dead load
w_f	Failure uniformly distributed load
w_l	Applied service live load
x	Half length of the first plastic hinge which forms in the beam
y_i	Distance from the top compressive fibre to the top of a layer, i, in the compression region
$\bar{y}_c$	Centroid of a cross section in the y-axis (along the beam height)
$\bar{y}_t$	Transformed centroid of a cross section in the y-axis (along the beam height)
$\bar{y}_{ti}$	Distance from the top of a layer, i, in the compression region to its centroid along the y-axis (along the beam height)
$\bar{y}_i$	Distance from the top compressive fibre to the centroid of a layer, i, in the compression region

$\propto$	Distance from the external support to the span plastic hinge, expressed as a fraction of the span length
α_1	Concrete stress block parameter in A23.3
β	Reliability index
β_1	Concrete stress block parameter in A23.3
β_i	Parameter estimate calculated from regression analysis, where 'i' is a numeric value and its range varies based on the fitted model
γ_c	Unit weight of concrete
γ_M	Ratio of magnitudes of interior support and span moment capacities, $\left\lvert\frac{M_u^-}{M_u^+}\right\rvert$
Δ	Total midspan deflection
Δ_1	Span deflection due to w_1
Δ_2	Span deflection due to w_2
Δ_c	Creep deflection
Δ_i	Instantaneous deflection
$\Delta_{LL,i}$	Instantaneous deflection due to transient live loads
$\Delta_{OW,c}$	Creep deflection due to beam's own weight
$\Delta_{OW,i}$	Instantaneous deflection due to beam's own weight
Δ_{sh}	Shrinkage deflection
$\Delta_{SLD,c}$	Creep deflection due to superimposed dead load

$\Delta_{SLD,i}$	Instantaneous deflection due to superimposed dead load
$\Delta_{SLL,c}$	Creep deflection due to sustained live load
$\Delta_{SLL,i}$	Instantaneous deflection due to sustained live load
ε	Error term in regression analysis
ε_c	Concrete compressive strain
ε_{ci}	Concrete compressive strain at the top of layer ‘i’ in the compression region
$\varepsilon_{c,max}$	Concrete compressive strain at the extreme fibre
ε_{cu}	Concrete compressive strain at the extreme fibre, corresponding to maximum moment or the A23.3 limit of 0.0035
ε_f	Steel strain at fracture of the reinforcing bar
ε_0	Strain corresponding to peak compressive stress
ε_s	Steel tensile strain
ε_{sh}	Steel strain on the onset of strain hardening
ε_{shu}	The ultimate shrinkage strain
ε_u	Steel strain at ultimate
ε_y	Steel strain corresponding to the yielding stress
ζ	Curvature weights

$\theta^{+/-}$	Inelastic rotations of first plastic hinge to form. The +/- superscripts indicate the hinge location: + for a span hinge subjected to positive moment and – for a support hinge subjected to negative moment
θ_{id}	Inelastic rotational demand
$\rho^{+/-}$	Geometric reinforcement ratio at the critical positive or negative section of the beam
σ_c	Concrete compressive stress
σ_{ci}	Concrete compressive stress at the top of a layer, i, in the compression region
$\overline{\sigma}_{ci}$	Mean concrete compressive stress of a layer, i, in the compression region
σ_s	Steel tensile stress
τ_c	Fraction of the total creep deflection that occurs in the time interval 't_{dse}'
τ_s	Fraction of the total shrinkage deflection that occurs in the time interval 't'
ϕ_c	Concrete resistance factor taken as 0.65
ϕ_s	Steel resistance factor taken as 0.85
φ	Curvature in the moment-curvature analysis
$\varphi_{avl,c}$	Average creep curvature at left support of a beam span
$\varphi_{avl,sh}$	Average shrinkage curvature at left support of a beam span
$\varphi_{avm,c}$	Average creep curvature at midspan of a beam
$\varphi_{avm,sh}$	Average shrinkage curvature at midspan of a beam

$\varphi_{avr,c}$	Average creep curvature at right support of a beam span
$\varphi_{avr,sh}$	Average shrinkage curvature at right support of a beam span
$\varphi_{c,cr}$	Cracked creep curvature
$\varphi_{c,un}$	Uncracked creep curvature
$\varphi_{cr}^{+/-}$	Cracking curvature at critical positive or negative cross section of the beam
φ_{l}	Beam left support instantaneous curvature
φ_{m}	Beam midspan instantaneous curvature
φ_{r}	Beam right support instantaneous curvature
$\varphi_{sh,cr}$	Cracked shrinkage curvature
$\varphi_{sh,un}$	Uncracked shrinkage curvature
$\varphi_{u}^{+/-}$	Ultimate curvature at critical positive or negative cross section of the beam
$\varphi_{y}^{+/-}$	Yielding curvature at critical positive or negative cross section of the beam
ω	Mechanical reinforcement ratio

Chapter 1

1 Background And Literature Review

1.1 INTRODUCTION

Concrete is a core construction material because it is relatively inexpensive. It can effectively resist compression stresses but has a low tensile resistance. Hence the tensile zones of structural concrete components are conventionally reinforced with steel. The tensile resistance is the product of the reinforcement (steel) cross sectional area and the steel yield stress, which corresponds to the linear-elastic limit of the stress-strain relationship. An increase in the yield stress of steel facilitates a decrease in the steel area necessary to meet load requirements. This reduction lowers the material costs and construction time in addition to reducing congestion in concrete components (Mast et al, 2008). At the present time, the maximum yield stress of steel used in calculations is limited to 500 MPa in Clause of 8.5.1 of CSA Standard A23.3:19 “Design of Concrete Structures” (CSA 2019). ACI 318:19 (ACI 2019) allows concrete beams to be reinforced with HSR in non-seismic applications but the yield stress is limited to 80 ksi (550 MPa). For a tension-controlled failure, the steel strain has to be greater than ε_y+0.003, where ε_y is the strain at yield. For a compression-controlled failure, the steel strain is less than ε_y when the concrete strain reaches 0.003.

Steel reinforcements with higher yield stresses have been proposed for reinforced concrete construction. The Canadian Standards Association CSA G30.18 “Carbon Steel Bars for Concrete Reinforcement” (CSA 2021) specifies Grade 400, 500 and 600 reinforcing bars with minimum yield strengths of 400, 500, and 600 MPa, respectively. In the United States of America, conventional steels conform to ASTM A615/615M Grade 60 (ASTM 2020), and A706/706M Grade 60 (ASTM 2016). The statistical bias and variability for G30.18 Grade 400R (regular) and Grade 400W (weldable) bars are likely similar to those for A615/615M Grade 60 and A706/706M Grade 60, respectively. The ASTM A615/615M Grade 60 Standard (ASTM 2020a), first published in 1968, specifies a minimum yield strength of 60,000 psi (420 MPa). The A706/706M Grade 60 and Grade 80 Standard

(ASTM 2016), first published in 1974, specifies a minimum yield strength of 60,000 psi (420 MPa) and 80,000 psi (550 MPa), respectively and also specifies a maximum yield strength and minimum ductility requirements. Other common High Strength Reinforcement (HSR) steels conform to ASTM A615/615M Grade 100 (ASTM 2020b) and A1035/1035M Grade 100 (ASTM 2020c) Standards. ASTM A615/615M Grade 100, which was first published in 2015, specifies a minimum yield strength of 100,000 psi (690 MPa). A1035/1035M Grade 100 Standard, first published in 2004, also specifies a minimum yield strength of 100,000 psi (690 MPa).

Table 1.1, from Mander and Matamoros (2019), shows the mechanical properties for ASTM A615/615M Grade 60 & 100, ASTM A706/706M Grade 60 & 80, and A1035/1035M Grade 100, which will be investigated in this thesis because few data concerning CSA G30.18: 2021 Grade 600 material in particular are available. The column headings are as follows: $\bar{f}_y$ is the mean yield strength; ε_{sh} and E_{sh} are the strain and tangent moduli, respectively, at the onset of strain hardening; f_u and ε_u are the stress and strain, respectively, at ultimate; and ε_f is the strain at fracture of the reinforcing bar.

Table 1.1: Mechanical properties for various steel grades (Mander and Matamoros, 2019)

ASTM standard	Grade in ksi (MPa)	$\bar{f}_y$ (MPa)	ε_{sh}	E_{sh} (MPa)	ε_u	f_u (MPa)	$f_u / \bar{f}_y$	ε_f
A 615	60 (413)	496	0.009	8300	0.10	725	1.462	0.13
A 615	100 (690)	827	0.008	6900	0.06	980	1.185	0.08
A 706	60 (413)	480	0.013	6900	0.13	655	1.365	0.16
A 706	80 (551)	593	0.008	7200	0.12	785	1.324	0.14
A 1035	100 (690)	724	$= \varepsilon_y$	53 600	0.06	1120	1.547	0.08

Figure 1.1 shows the stress-strain relationships for the various grades shown in Table 1.1. All grades except ASTM A1035/A1035M exhibit a distinct yielding point while A1035/A1035M shows a roundhouse behavior. With an increase in steel grade, the yield strength is increased and the ductility, as represented by the strain at fracture, is reduced. ASTM A706/706M Grade 60 has a greater ductility than A615/615M Grade 60.

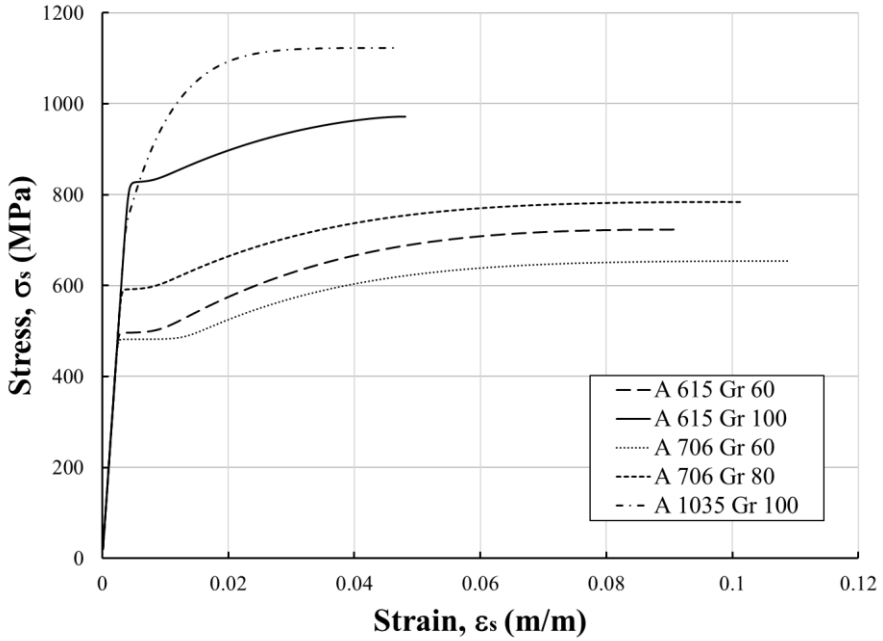

Figure 1.1: Stress-strain relationships for various high-strength steel grades

1.2 LITERATURE REVIEW

Mast et al (2008) considered beams reinforced with A615/615M Grade 60 and A1035/1035M Grade 100 steels. They computed the ultimate steel stresses using three stress-strain relationships: the actual relationship for the steel, a linear-elastic perfectly plastic idealization, and a linear-elastic perfectly plastic idealization with the yield stress capped at the ACI limit of 550 MPa. The results showed that using ASTM A1035/1035M Grade 100 reinforcement increases the nominal moment capacity by 95% and 31% when using the actual steel relationship and the capped ACI limit model, respectively, compared to a beam reinforced with A615/615M Grade 60 steel. The curvature ductility in the beam reinforced with A615/615M Grade 60 steel at a steel strain of 0.005 was the same as the

curvature ductility in the beam reinforced with A1035/1035M Grade 100 steel at a strain of 0.0067, when the actual stress model was used, or 0.009 when a bilinear idealized stress model (not capped at 550 MPa) was used. The ductility sections reinforced with HSR is therefore smaller than that for sections reinforced with conventional steel at the same steel strain. These findings are applicable for HSR that do not show a distinct yielding point which excludes A615/615M Grade 100 steel.

Shahrooz et al (2010) conducted a study involving A1035/1035M reinforcement to evaluate the steel strains corresponding to tension- and compression-controlled failure limits. Approximate linear-elastic-perfectly plastic steel stress-strain idealizations were assumed with yielding stresses defined using various approaches, including the 0.2% offset strain method. They proposed defining a flexural failure to be tension-controlled if the tensile steel strain at Ultimate Limit States exceeds 0.008. This finding is again only applicable for HSR which does not show a distinct yielding point.

Yosefani (2018) investigated experimentally the curvature ductility in beams reinforced with A615/615M Grade 60, A615/615M Grade 100, and A1035/1035M Grade 100 steels. The results showed that the curvature ductility of the beam with A615/615M Grade 60 steel at a tensile strain of 0.005, which is the steel strain needed to achieve the tensile controlled failure in ACI 318-19 (ACI 2019), was comparable to that of the beam reinforced with A615/615M Grade 100 steel at a tensile strain of 0.008, and to that of the beam reinforced with A10355/1035M Grade 100 steel at a tensile strain of 0.01. It was also concluded that A1035/1035M Grade 100 HSR is less ductile than A615/615M Grade 100 HSR. The comparison of curvature ductilities with reinforcement ratios for beams reinforced with HSR and conventional steel grades was not reported.

Both long term and immediate deflections were also investigated by Yosefani (2018), as it was predicted that using HSR would lead to a reduced steel area which will increase deflections. One simply supported beam, reinforced with A1035/1035M Grade 120 steel, was subjected to an applied load for a span of 1 year to check the validity of the provisions of ACI 318. It was concluded that ACI provisions overestimated the observed long-term deflections, because the ACI long-term deflection multiplier, λ, is independent of concrete

compressive strength. It was also concluded that it would be desirable to further investigate the effects of specific beam configurations, including the concrete compressive strengths and reinforcement ratios, on short- and long-term deflections.

Yosefani (2018) also checked the cracking of HSR-reinforced beams at Serviceability Limit States as it was envisaged that the higher steel strains would lead to higher crack widths. The crack widths were acceptable according to ACI 318 code provisions for beams reinforced with HSR (Grade 100), although they were relatively greater than those for beams reinforced with conventional steel.

Yosefani's (2018) investigation considered only simply supported beams so moment redistribution, which is a property of indeterminate structures including continuous beams, was not considered. Designing a continuous beam and accounting for moment redistribution can potentially reduce steel area at critical moment sections and increase the ratio of SLS steel stresses to ULS steel stresses. Hence, crack widths should be checked in continuous beams as well, particularly those where the steel area has been reduced by accounting for moment redistribution at Ultimate Limit States.

1.3 RESEARCH OBJECTIVES

The objective of the research reported in this thesis is to investigate the flexural behavior of concrete beams reinforced with HSR to determine whether current provisions for conventional steel grades in CSA A23.3:19 "Design of Concrete Structures" (CSA 2019) are applicable to HSR. In particular,

1. Determine whether the flexural ductility of a beam is adversely affected if it is reinforced with HSR.
2. Assess whether the current provisions that limit the amount of permissible moment redistribution in the CSA 23.3:19 standard apply to beams reinforced with HSR.
3. Determine whether the current provisions for deflections in the CSA A23.3 Standard apply to beams reinforced with HSR.

1.3.1 Research Significance

Ductility is essential to provide warning of an impending failure, and higher target reliability indices are usually required for elements with reduced ductility (CSA 2011). The ductility of a beam also defines the inelastic rotational capacity at a plastic hinge, which is necessary for moment redistribution in continuous beams. As noted previously, the use of HSR reduces the steel cross sectional area in beams, potentially reducing the cracked and effective moments of inertia and so increasing flexural deflections.

1.4 THESIS OUTLINE

Chapter 2 presents a parametric study that investigates the influence of steel quantity, type and grade, concrete strength, and other factors on the curvature ductility of reinforced concrete beams. A methodology for deriving moment-curvature relationships from first principles and creating idealized bilinear responses for cross sections that do not exhibit a marked yield moment are presented. The variation of flexural curvature ductilities and steel stresses at the nominal ultimate moment with reinforcement ratios are quantified using regression analyses. The application of the equation in A23.3:19 ensures that the tension-initiated flexural failure is investigated for beams with high strength reinforcements.

Chapter 3 presents a parametric study that investigates how moment redistribution is influenced by different reinforcing steel quantities, types and grades in two-span beams that are continuous over the interior support. The methodology to quantify moment redistribution is presented and used to compare the moment redistribution exhibited by beams reinforced with HSR and conventional reinforcing steel. It is shown that designs based on moment redistribution at Ultimate Limit States can have excessive crack widths at Serviceability Limit States.

Chapter 4 investigates the short- and long- term deflections in simply supported beams, two-span beams with one end continuous, and three-span beams with both ends continuous. Gilbert's method (Gilbert 2011) is applied to determine the short- and long-term deflections. The yield strength correction factor specified in a note to Table 9.2 of A23.3:19

to increase the minimum beam height, necessary if deflection calculations are to be avoided, is reviewed.

Chapter 5 summarizes the thesis, lists the conclusions, and proposes some recommendations for future investigations.

Three appendices supplement material presented in the main body of the thesis. Appendix 2A shows the concrete stress-strain idealizations by Thorenfeldt et al (1987), and Wee et al (1996). Appendix 2B shows the steel reinforcement idealizations by Mast et al (2008) for MMFX A1035/1035M Grade 100 steel, and Yosefani (2018). Appendix 4A shows the variation in incremental deflections, and ratio of effective span length to incremental deflections with reinforcement ratios in simply supported beams, two-span beams with one continuous end, and three-span beams with both ends continuous, when concrete compressive strength is 50 MPa.

Chapter 2

2 Flexural Ductility of Cross Sections with High Strength Reinforcement

2.1 INTRODUCTION

High strength reinforcement (HSR) allows the use of smaller diameter bars in concrete construction, lessening reinforcing congestion and reducing costs. Reinforcement bars with 400 MPa yield strength are most commonly used in Canada: in this chapter, bars with greater yield strengths are considered to be "high strength". The new edition of CSA G30.18 "Carbon Steel Bars for Concrete Reinforcement" (CSA 2021) specifies mechanical properties for reinforcing bars with minimum yield strength of 400, 500, and 600 MPa. In the United States, the American Society for Testing and Materials (ASTM) A1035/A1035M (ASTM, 2020a), A615/A615M (ASTM, 2020), and A706/A706M (ASTM, 2016) specifications allow bars with minimum yield strengths of 60, 80, and 100 ksi (420, 560, and 690 MPa).

Clause 4.1.3 of CSA A23.3: 19 "Design of Concrete Structures" (CSA 2019) only permits the use of deformed reinforcing bars complying with CSA G30.18. The 2005 edition of ACI 318 (ACI 2005) included provisions for ASTM A615/A615M and A706/A706M reinforcing bars, and the provisions for ASTM A1035/1035M Grade 100 bars were added in the 2008 edition (ACI 2008). As previously illustrated in Figure 1.1, ductility is reduced when yield stresses are increased for steel bars.

Clause 8.5.1 of CSA A23.3:19 limits the yield strength of steel reinforcement, f_y, used in design calculations to 500 MPa. The Technical Committee responsible for A23.3 has created a Task Group to develop design provisions for bars with higher yield strengths to allow this limitation to be relaxed where it is appropriate to do so.

2.1.1 Research Objectives

The objectives of the research reported in this chapter are as follows:

1. Quantify the flexural ductility of members reinforced with HSR and compare this with that of members reinforced with conventional reinforcement. This is a necessary first step towards determining whether the resistance factor currently specified for steel reinforcement, ϕ_s, of 0.85 is applicable to HSR. CSA S408-11 "Guidelines for the Development of Limit States Design Standards" (CSA 2011) typically requires more stringent target reliability indices for members that exhibit less ductile failures.

2. As is clear from Figure 1.1, bars with the various steel grades specified in ASTM Standards exhibit significant strain hardening, and ASTM A1035/A1035M bars exhibit a "roundhouse" behavior with an undefined yield point. Therefore, a second objective of the research reported in this chapter is to develop means to allow designers to quantify the tensile steel stress in the reinforcement bars at the ultimate moment.

3. Clause 10.1.3 of CSA A23.3:19 allows the concrete strain at the extreme compression fibre at ultimate to be 0.0035. A third objective of the research is to assess whether this extreme fibre strain value is appropriate for beams reinforced with HSR.

4. Clause 10.5.2 of CSA A23.3:19 limits the area of tension reinforcement in beams, requiring that

   [2.1] $$\frac{c}{d} < 0.8\frac{700}{(700 + f_y)}$$

   where c is the distance from the extreme compression fibre to the neutral axis at ultimate, and d is the effective depth of the reinforcing steel. If this criterion is satisfied, it can be assumed that the tensile reinforcement has yielded (CSA 2019).

A fourth objective of the research is to determine if this limit is appropriate for beams reinforced with HSR.

2.1.2 Chapter Outline

The four research objectives in this chapter can be achieved if accurate moment-curvature relationships are derived for beams reinforced with conventional steel reinforcement or HSR. Section 2.3 therefore presents the methodology used to derive the moment-curvature relationship, including the assumptions, specific procedural steps, and the material idealizations adopted for steel and concrete. The moment-curvature relationships for sections with reinforcement that exhibit a roundhouse stress-strain behavior do not have a well-defined yield moment, so a method to idealize the response using an equivalent bilinear idealization is presented. The analysis method is validated by comparison with test data obtained by others.

Section 2.4 quantifies the variation of the curvature ductility factor, as obtained from the moment-curvature analysis, with the mechanical reinforcement ratio, ω. The ductility factor is defined as the ratio of the ultimate to yielding curvature values, φ_y and φ_u, respectively. The relationship between φ_u/φ_y and ω is quantified for the reinforcing steel grades shown in Table 1.1, and concrete with specified compressive strengths, f_c', of 30, 50, and 70 MPa.

Section 2.5 presents a review of the impact of the use of HSR on other flexural quantities of interest to designers. In particular, relationships between the ultimate steel stress, f_u, and ω are developed to facilitate the design of flexural members with reinforcement that exhibits a roundhouse behaviour and an undefined yield point. Concrete strains at the extreme compression fibre corresponding to the maximum moment, as obtained from the moment-curvature analysis for the various reinforcement grades and concrete strengths investigated, are compared to the strain of 0.0035, as specified in A23.3:19 (CSA 2019). The applicability of current code provisions that define “balanced” flexural conditions, where the steel yielding simultaneously with the concrete crushing in compression, are assessed for beams reinforced with high-strength reinforcement.

Finally, in Section 2.6 the research presented in the chapter is briefly summarized and the conclusions are presented.

2.2 LITERATURE REVIEW

2.2.1 Moment-Curvature Relationship

Figure 2.1 shows a trilinear approximation of the relationship between the curvature, φ, of a reinforced concrete flexural cross section, and the applied moment, M. Such an idealization was utilized by Park and Pauley (1975) and is defined by the states of cracking, yielding, and ultimate. The cracking moment, M_{cr}, is defined as the moment required to initiate concrete flexural cracks at the extreme tensile fibre and occurs when the tensile stress at extreme fibre reaches the modulus of rupture, f_r. The yielding moment, M_y, is the moment required to initiate yielding of the steel reinforcement and corresponds to the tensile stress in the steel reinforcement reaching the yield stress. The ultimate moment, M_u, corresponds to the maximum moment that the cross section can resist. The corresponding curvatures are φ_{cr}, φ_y and φ_u, at cracking, yielding and ultimate, respectively.

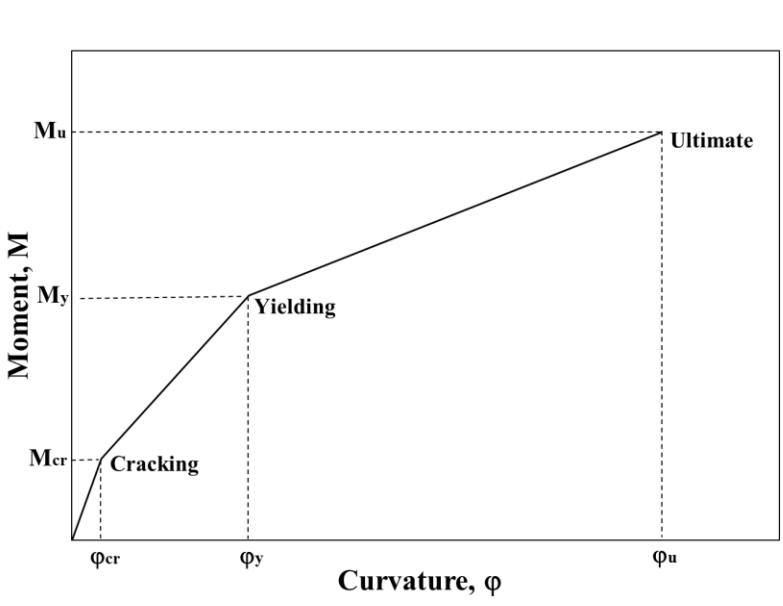

Figure 2.1:Trilinear moment-curvature relationship

Assuming linear-elastic-cracked behaviour, the yield moment can be computed as (e.g., MacGregor & Bartlett, 2000)

$$\textbf{[2.2]}\quad M_y = \frac{I_{cr} f_y}{nd\,(1 - k)}$$

where n is the ratio of Young's modulus of steel, E_s, to that of concrete, E_c. The depth of the compressive stress region, assumed triangular as shown in Figure 2.2 (b), is kd, where k is computed as

$$\textbf{[2.3]}\quad k = \sqrt{n\rho^2 + 2n\rho} - n\rho$$

where ρ is the geometric reinforcement ratio, A_s/bd, A_s is the cross-sectional area of the steel reinforcement in tension, and b is the width of the beam cross section. The cracked moment of inertia, I_{cr}, in Equation [2.2] is computed as

$$\textbf{[2.4]}\quad I_{cr} = \frac{b(kd)^3}{3} + nA_s\,(d - kd)^2$$

From the strain diagram in Figure 2.2(b), the yield curvature is computed as

$$\textbf{[2.5]}\quad \varphi_y = \frac{\varepsilon_y}{d(1-k)}$$

where ε_y is the yield strain of the steel reinforcement.

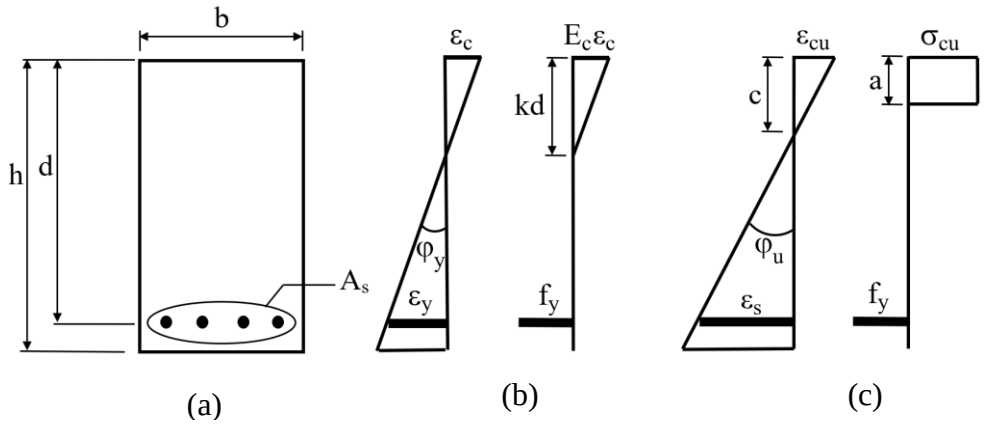

Figure 2.2: (a)Typical rectangular beam cross section (b) Stress and strain diagrams at yield (c) Stress and strain diagrams at ultimate

The ultimate moment can be calculated, assuming the concrete in compression is represented by an equivalent rectangular stress block, as

[2.6] $M_u = A_s f_y \left(d - \frac{a}{2}\right)$

where a is the depth of the concrete stress block as defined by A23.3:19, shown in Figure 2.2(c). If no applied axial force is present, horizontal force equilibrium requires that

[2.7] $a = \frac{A_s f_y}{\alpha_1 f_c' b}$

Stress block parameters β_1 and α_1 have evolved from the idealization originally proposed by Whitney (1937). Parameter β_1 is the ratio of the stress block depth to the neutral axis depth, a/c. In CSA A23.3:19 (CSA 2019), α_1 and β_1 are functions of f_c'

[2.8a] $\alpha_1 = 0.85\text{-}0.0015 f_c'$

[2.8b] $\beta_1 = 0.97\text{-}0.0025 f_c'$

From the strain diagram at ultimate, Figure 2.2 (c), the ultimate curvature is

[2.9] $\varphi_u = \frac{\varepsilon_{cu}}{c}$

From Eq. 2.7, increasing f'_c reduces the depths of the stress block, a, and the neutral axis, c, and so increases the ultimate curvature if ε_{cu} is assumed constant. Similarly increasing $A_s f_y$ increases 'a' and 'c' and so reduces the ultimate curvature. It is readily shown that the ultimate curvature is inversely proportional to the mechanical reinforcement ratio, ω, defined as

[2.10] $$\omega = \frac{A_s f_y}{b d f'_c}$$

Substitution of Equations [2.10] and [2.7] into Equation [2.9] and resolving yields

[2.11] $$\varphi_u = \frac{\varepsilon_{cu}\, \alpha_1 \beta_1}{d} \quad \frac{1}{\omega}$$

Thus, the ultimate curvature is inversely proportional to ω.

From Equations [2.5] and [2.11], the curvature ductility ratio, φ_u/φ_y, can be expressed in terms of ω as

[2.12] $$\frac{\varphi_u}{\varphi_y} = \frac{\varepsilon_{cu}\, \alpha_1 \beta_1\, (1 - k)}{\varepsilon_y d} \quad \frac{1}{\omega}$$

As the variation of k with ω is slight, the curvature ductility ratio is essentially inversely proportional to ω.

2.2.2 Steel Yield Point

As shown in Figure 1.1, A1035/A1035M steel does not exhibit a distinct yield point. In such cases, ASTM A370 (ASTM, 2021) permits use of the 0.2% strain offset method to determine the yield stress. As shown in Figure 2.3, a line is drawn parallel to the linear-elastic part of the stress-strain curve with horizontal intercept of 0.2%. The yield point is defined as the intersection of this line and the strain-strain curve. The linear-elastic limit can also be used as an alternative to the yield point. It is defined as the upper limit of the linear-elastic stress-strain behaviour, Point A on Figure 2.3.

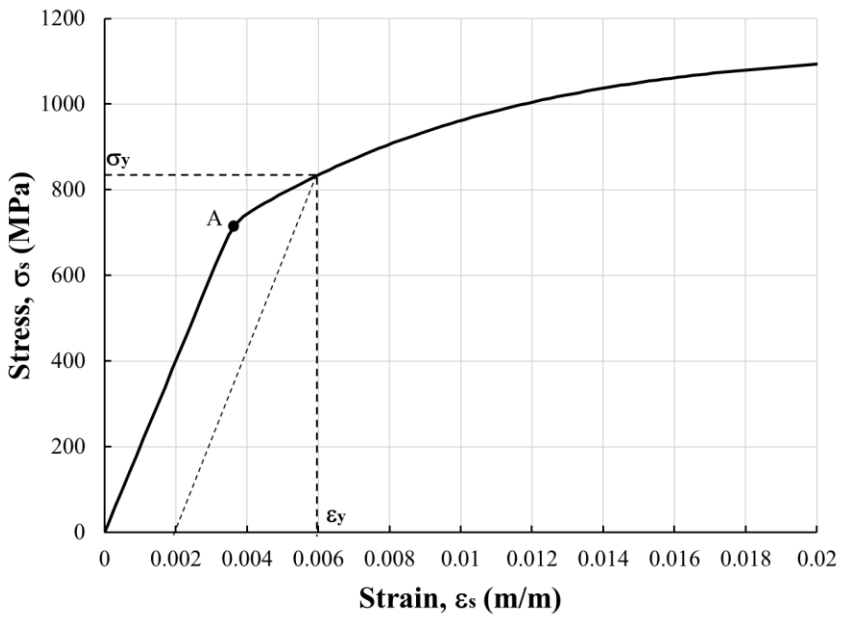

Figure 2.3: Determination of 0.2% offset yield stress

2.3 MOMENT-CURVATURE RELATIONSHIP

As noted in Section 2.1, the moment-curvature relationship essentially captures the load-deformation response for a cross section in flexure, and so is uniquely defined by the geometric properties of the section and reinforcement, and by the strengths and stress-strain relationships of the concrete and steel materials. These material idealizations and the computation procedure adopted are presented in this section. Some simplifications and assumptions used in derivation of the moment-curvature analysis are as follows:

1. Concrete tensile strength is ignored.
2. Steel and concrete have a perfect bond.
3. Plane sections remain plane.

2.3.1 Concrete Material Idealization

Several empirical stress-strain relationships for concrete in compression have been considered, as shown in Appendix 2A. The Carreira and Chu (1985) relationship was

selected for its simplicity and because it gives similar results to other concrete idealizations, as shown in Figure 2.4. The ascending branches of the curves are similar but the graphs diverge after peak stress is achieved. The equations for the different concrete stress-strain idealizations are presented in Appendix 2A.

$$\textbf{[2.13]}\ \sigma_c = f_c' \left(\frac{B\left(\frac{\varepsilon_c}{\varepsilon_o}\right)}{B-1+\left(\frac{\varepsilon_c}{\varepsilon_o}\right)^B} \right)$$

where σ_c and ε_c are the concrete stress and strain, respectively and ε_o is the strain corresponding to the maximum compressive stress, f_c' calculated as

$$\textbf{[2.14]}\ \varepsilon_o = 0.00078\, f_c'^{\frac{1}{4}}$$

The parameter B is defined as

$$\textbf{[2.15]}\ B = \frac{1}{1-\frac{f_c'}{E_{it}\varepsilon_o}}$$

where E_{it} is the initial tangent modulus, calculated as $10200 f_c'^{\frac{1}{3}}$, and f_c' ranges between 20 and 120 Mega pascals (MPa). The concrete equivalent stress block presented in A23.3:19 cannot be used to derive the full moment-curvature response because it is valid for ultimate moments only. A note to Clause 10.1.6 of CSA A23.3:19 specifies that the peak stress adopted for analysis using stress-strain curves derived from cylinder test results should not exceed 0.9 f'$_c$. This reduction is somewhat arbitrary and was ignored in the present study.

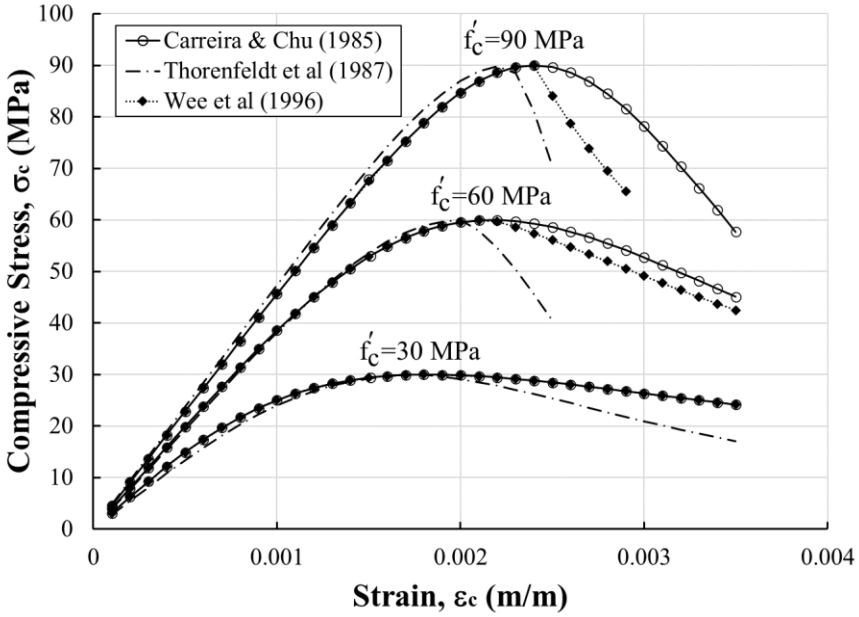

Figure 2.4: Comparison between different concrete stress-strain idealizations

2.3.2 Steel Material Idealization

The different steel idealizations shown in Appendix 2B were investigated. The stress-strain relationship proposed by Mander and Matamoros (2019) was selected because it requires a single equation to model the linear-elastic and strain-hardening regions. The idealizations proposed by others require two equations to model these two distinct regions. The single idealization equation is

$$\textbf{[2.16]}\quad \sigma_s = \frac{E_s\varepsilon_s}{\left\{1+\left|\frac{\varepsilon_s}{\varepsilon_y}\right|^{20}\right\}^{0.05}+\left|\frac{\varepsilon_s}{\varepsilon_f}\right|^{20}} + \frac{f_u-f_y}{1+\left|\frac{\varepsilon_s}{\varepsilon_f}\right|^{20}} \times \left|1-\frac{|\varepsilon_u-\varepsilon_s|^p}{\left\{|\varepsilon_u-\varepsilon_{sh}|^{20p}+|\varepsilon_u-\varepsilon_s|^{20p}\right\}^{0.05}}\right|$$

where the various symbols are defined in the discussion of Table 1.1. The parameter p is defined as

$$\textbf{[2.17]}\quad p = \frac{E_{sh}(\varepsilon_u - \varepsilon_{sh})}{(f_u-f_y)} < 10$$

Figure 2.5 shows the application of Equations [2.16] and [2.17] to idealize the stress-strain response of A615/615M Grade 100 and A1035/1035M Grade 100 steels which exhibit defined and undefined yield points, respectively. The stress-strain relationships proposed by Mast (2008) for A1035/1035M Grade 100 steel and by Yosefani (2018) for A615/615M Grade 100 steels are presented in Appendix 2B.

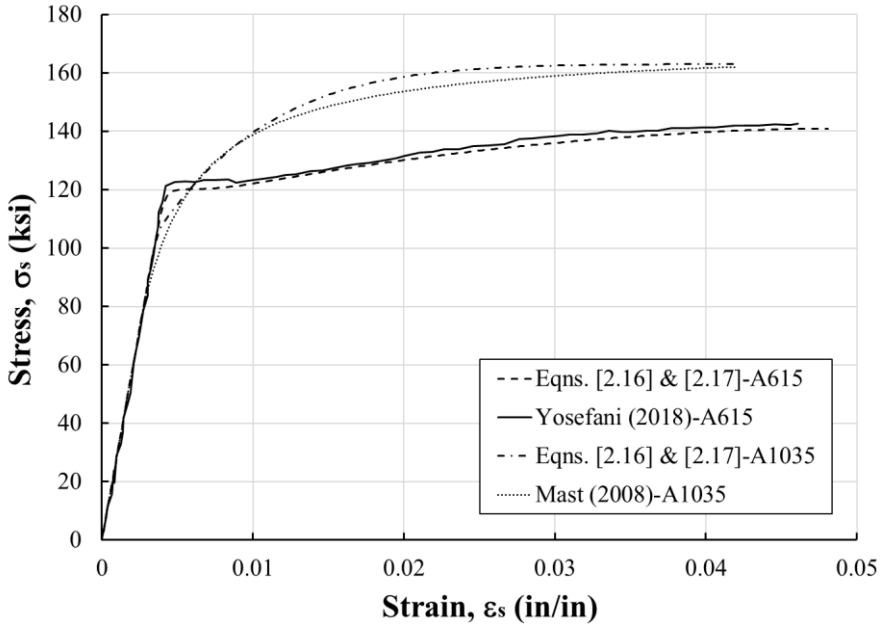

Figure 2.5: Comparing stress-strain idealizations for steel grades exhibiting a defined and undefined yield point

2.3.3 Procedure To Obtain Moment-Curvature Relationship

Figure 2.2(a) shows the cross section geometry adopted for the moment-curvature analysis. Compressive steel reinforcement was ignored because adding compressive reinforcement increases the ultimate curvature (Park & Pauley, 1975). Compressive strains, stresses and forces are assumed positive in the analysis.

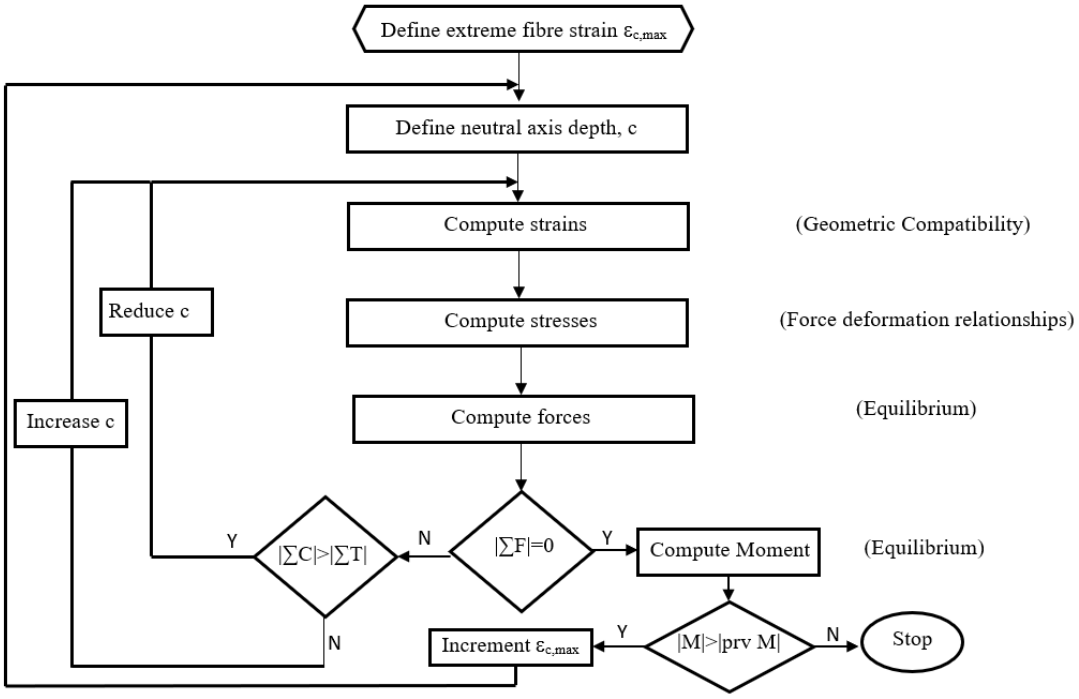

Figure 2.6: Flowchart for determining moment-curvature response

Figure 2.6 is a flowchart that outlines the essential steps for calculating the moment-curvature relationship. The steps are as follows:

1. Define the concrete strain at the extreme compression fibre $\varepsilon_{c,max}$.

2. Assume an initial neutral axis depth, c. Typically, the neutral axis depth reduces as the applied moment increases.

3. Calculate the steel tensile strain, ε_s. Assuming that plane sections remain plane, Figure 2.7b, and perfect bond between the steel and concrete

   [2.18] $$\varepsilon_s = \varepsilon_{c,max} \frac{c - d}{c}$$

4. Calculate the steel stress using Equation [2.16] and the steel force, T_s, as

   [2.19] $$T_s = \sigma_s A_s$$

5. Calculate the concrete stress and force by dividing the compression region into 30 layers of thickness c/30, as shown in Figure 2.7. Sensitivity analysis determined that the error in the compressive force calculation using 30 layers is less than 2%. The layers are labelled i = 1, 2,…30, where the first layer is at the bottom, immediately above the neutral axis, as shown.

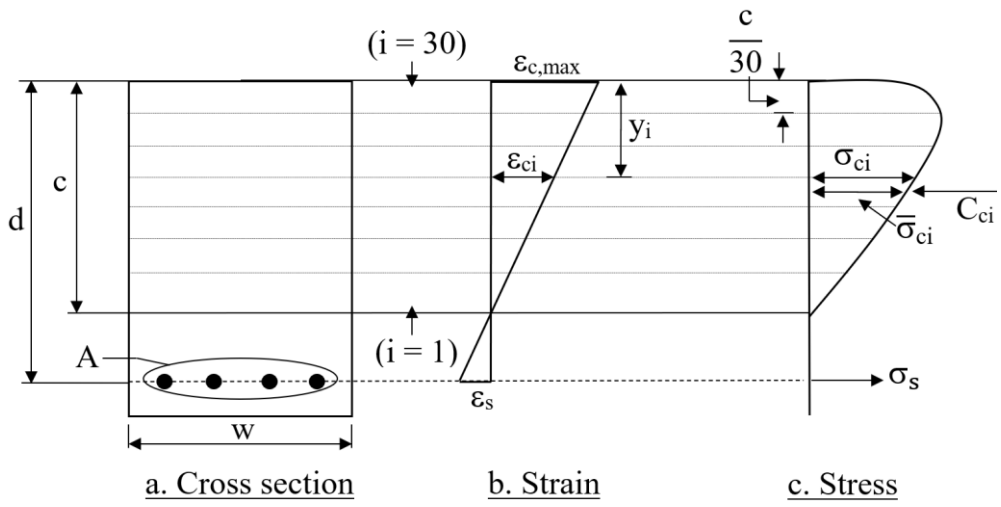

Figure 2.7: Layered division of concrete compressive zone with layer thickness 'c/30'

For each layer,

a. Determine the compressive strain, ε_{ci}, at the top of each layer, assuming plane sections remain plane

[2.20] $$\varepsilon_{ci}=\left(\frac{i}{30}\right)\varepsilon_{c,max}$$

b. Calculate concrete stress σ_{ci} at the top of each layer using Equation [2.13] and substituting ε_{ci} for ε_c.

c. Calculate the average concrete stress for each layer, $\overline{\sigma}_{ci}$.

[2.21] $$\overline{\sigma}_{ci}=\{\sigma_{ci}+\sigma_{c(i-1)}\}/2$$

d. Calculate the concrete force, C_{ci}, in each layer.

[2.22] $C_{ci} = \bar{\sigma}_{ci}(i)\left(\frac{c}{30}\right)b$

e. Add the contribution of the force in layer i to the total concrete force, $\sum C_i$.

[2.23] $\sum C_i = \sum C_{(i-1)} + C_{ci}$

6. Check whether horizontal force equilibrium is satisfied. Here equilibrium is considered satisfied if the sum of horizontal forces is less than 1 kN. If the absolute magnitude of total concrete force, $|\sum C_i|$ is smaller than that of the tensile steel force, $|T_s|$ by more than 1 kN then increase the neutral axis depth and repeat Steps 2 through 6. Similarly, if $|T_s|$ is smaller than that of $|\sum C_i|$, reduce the neutral axis depth and repeat Steps 2 though 6.

7. When the neutral axis depth determined from Steps 2 through 5 satisfies horizontal force equilibrium, compute the corresponding moment. For each layer,

   a. Find the distance from the extreme compressive fibre to the top of each layer, y_i.

   b. Determine the distance, $\bar{y}_{ti}$ from the top of each layer to the centroid of the trapezoidal stress region

   [2.24] $\bar{y}_{ti} = \frac{c}{30}\frac{2\sigma_{c(i-1)}+\sigma_{ci}}{3\sigma_{c(i-1)}+\sigma_{ci}}$

   c. Add y_i and $\bar{y}_{ti}$ to get the total distance, $\bar{y}_i$, from the extreme compression fibre to the location of the compressive force resultant, C_{ci} of each layer.

   d. Take the moment about the extreme compressive fibre due to the concrete force in layer i

   [2.25] $M_i = C_{ci}\,\bar{y}_i$

   e. Add this contribution to the total moment $\sum M_i$

$$\textbf{[2.26]} \quad \sum M_i = \sum M_{(i-1)} + M_i$$

8. Determine the total moment

$$\textbf{[2.27]} \quad M = \sum_{i=1}^{30} M_i + T_s d$$

where T_s is negative while C_{ci} are positive so M is negative.

9. Calculate the curvature as $\varepsilon_{c,max}/c$.

10. Increment the extreme fibre strain and repeat Steps 2 through 9, stopping when either the maximum moment or a concrete extreme fibre strain of 0.0035 is reached.

2.3.4 Yield Moment for Steel with Undefined Yield Point

If the reinforcing steel stress-strain relationship features a distinct yield point, the yield moment is that corresponding to attainment of the yield strain ε_y in the reinforcement. As shown in Figure 1.1, however, the stress-strain relationship for A1035/A1035M Gr 100 steel does not have a distinct yield point. In this case an approximate bilinear moment-curvature relationship can be derived following the procedure shown schematically in Figure 2.8. The dashed line represents the actual moment-curvature relationship, and the solid line represents the approximate bilinear idealization. The curvature and moment co-ordinates of the approximate yield point, $\varphi_{y,eq}$ and $M_{y,eq}$ respectively, are obtained by satisfying the following criteria

1. The area under the actual moment-curvature relationship equals the area under the approximate bilinear idealization. This is equivalent to requiring that Areas 1 and 2 as shown are equal.

2. The slope of the actual and approximate bilinear moment-curvature relationships at the origin are equal.

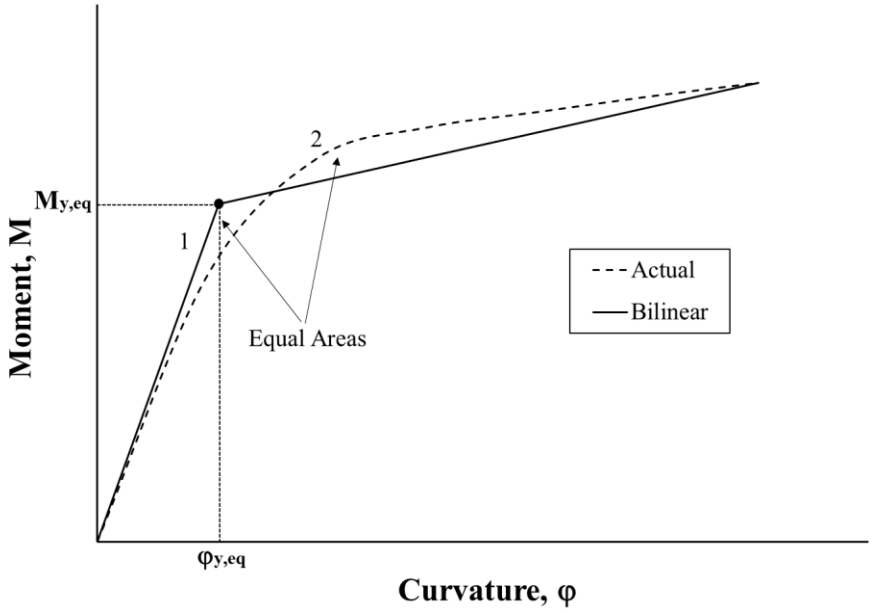

Figure 2.8: Approximate bilinear idealization

2.3.5 Validation

The moment-curvature analysis was validated by comparing predicted load-deflection responses to those observed in tests by Yosefani (2018). Figure 2.9 shows the four-point loading applied to Yosefani's Beams B1 (designated 5: A615/615M Grade 60), and B2 and B4 (designated 8: A615/615M Grade 100 and 13: A615/A615 M Grade 100, respectively). The beams were simply supported on a 2.44 m span with a 0.81 m long constant moment region at midspan. The cross section, 152 mm x 254 mm, was cast using concrete with the compressive strengths shown in Table 2.1. The grade and yield strength of the reinforcement of the beams are also shown in Table 2.1.

Table 2.1: Yosefani (2018) test beams: material properties

Property	**B1**	**B2**	**B4**
f_c' (MPa)	38.6	55.8	90
Reinforcement	A615M Gr.60	A615M Gr.100	A615M Gr.100
A_s (mm^2)	387	213	213
f_y (MPa)	479	838	838

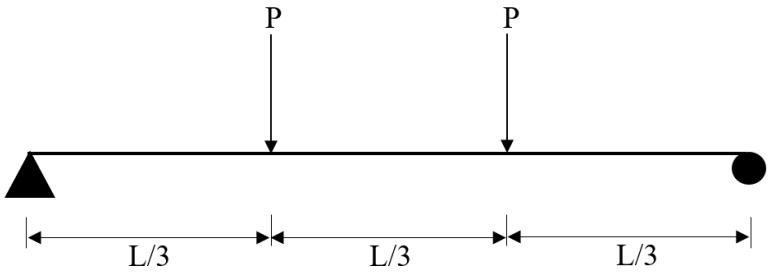

Figure 2.9: Idealization of beams tested by Yosefani (2018): four-point bending

Figures 2.10, 2.11, and 2.12 show the experimentally observed and predicted load-deflection responses of Beams B1, B2, and B4, respectively. The predicted responses shown are computed using the procedure presented in Section 2.3.3. The maximum experimental deflection at the midspan was 42, 43, and 46 mm for Beams B1, B2, and B3, respectively. The load-deflection responses were determined using moment-area theorem, ignoring tension stiffening. The deflections at the yield were computed assuming a linear increase of curvature from zero at the supports to the yield curvature at and between the applied point loads. The deflections at ultimate were computed assuming a similar curvature distribution except that the curvature between the applied point loads is the ultimate curvature. It was assumed that the extreme fibre concrete compressive strain could exceed a magnitude of 0.0035. In all cases, the agreement with the experimental result is good.

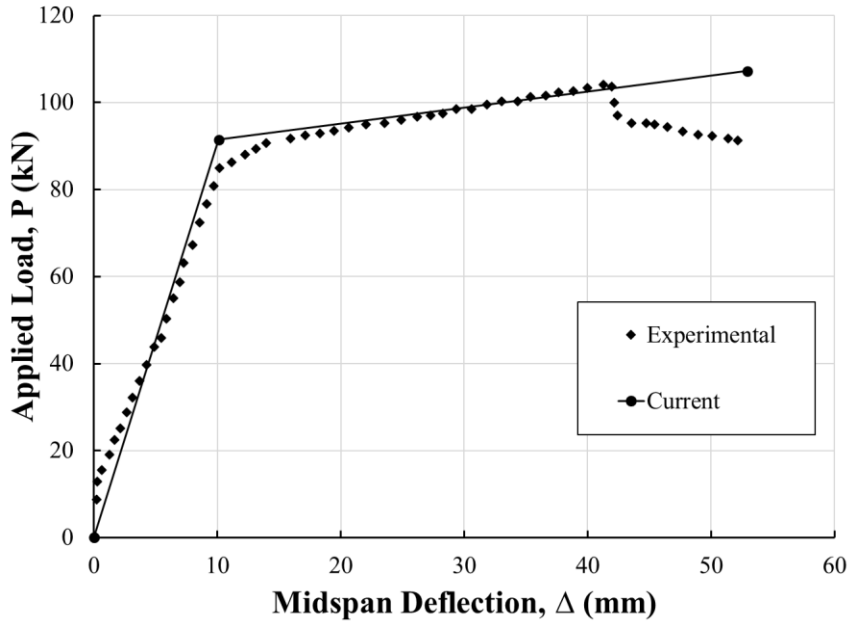

Figure 2.10: Load deflection response Beam B1

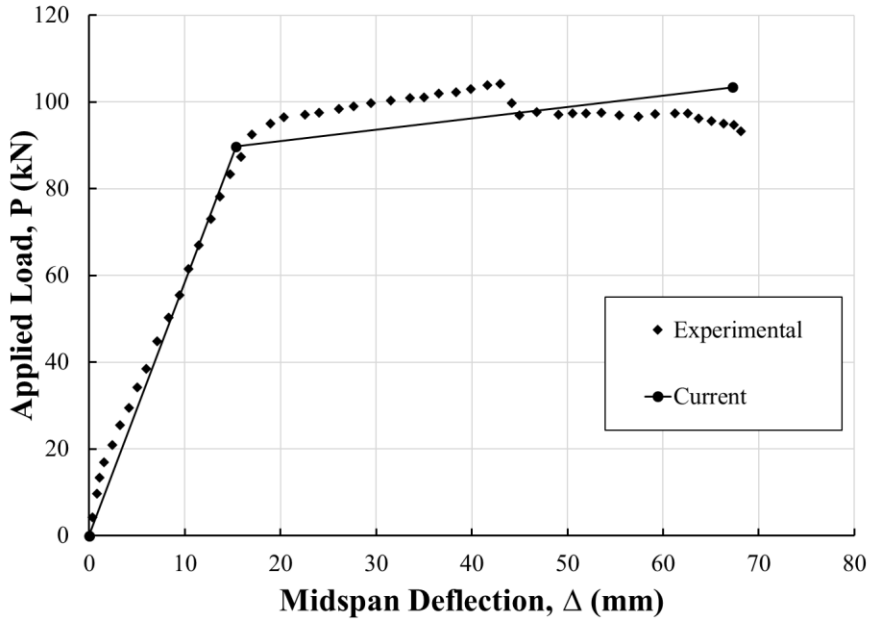

Figure 2.11: Load deflection response Beam B2

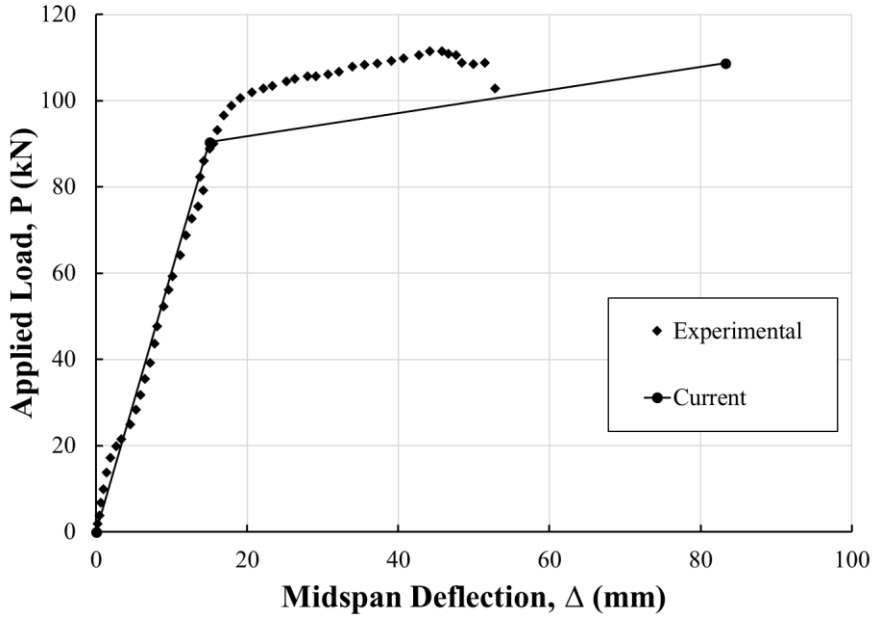

Figure 2.12: Load deflection response Beam B4

Table 2.2 compares the load-deflection results from Yosefani's experiments, and the current analysis. In the experiments, the top cover spalled, which reduced the concrete compressive neutral axis depth, reducing the total moment capacity, causing the beam to fail at a much smaller extreme fibre strain. The concrete strain was not limited to 0.0035 in the 'current' results so the ultimate deflections are greater.

Table 2.2: Load-deflection results for Yosefani's experimental analysis, and current analysis

Quantity	**P_y (kN)**			**Δ_y (mm)**			**P_u (kN)**			**Δ_u (mm)**		
Beam	**B1**	**B2**	**B4**	**B1**	**B2**	**B4**	**B1**	**B2**	**B4**	**B1**	**B2**	**B4**
Experimental	85.0	92.5	96.6	10.2	17.0	16.9	104	104.2	111	41.3	43.0	45.8
Current	91.5	89.7	90.4	10.1	15.4	15.0	107	103.4	109	52.9	67.2	83.3

2.4 IMPACT OF HIGH STRENGTH REINFORCEMENT ON CURVATURE DUCTILITY

Curvature ductilities were computed for beam cross sections reinforced with steel types ASTM A615/A615M Grade 60 & 100, A706/706M Grade 60 & 80, and A1035/1035M Grade 100 with ω ranging between 0.05 and 0.36. Concrete compressive strengths of 30, 50, and 70 MPa were investigated. Two sets of analyses were conducted: one with the extreme fibre concrete strain constrained to 0.0035 and a second with this limit removed.

Figure 2.13 shows the effect of increasing the reinforcement ratio on the curvature ductility. A615/615M Grade 60 steel was used at reinforcement ratios of 0.3, 0.6, 0.9, 1.2, and 1.5% with f_c' of 30 MPa. With increasing reinforcement ratio, the neutral axis depth increases to satisfy horizontal force equilibrium and the ultimate curvature is decreased. A higher steel tensile force at higher ρ increases the moment capacity of the cross section. An increase in reinforcement ratio increases ω according to Equation [2.10] and curvature ductility and ω are approximately inversely proportional, Equation [2.12].

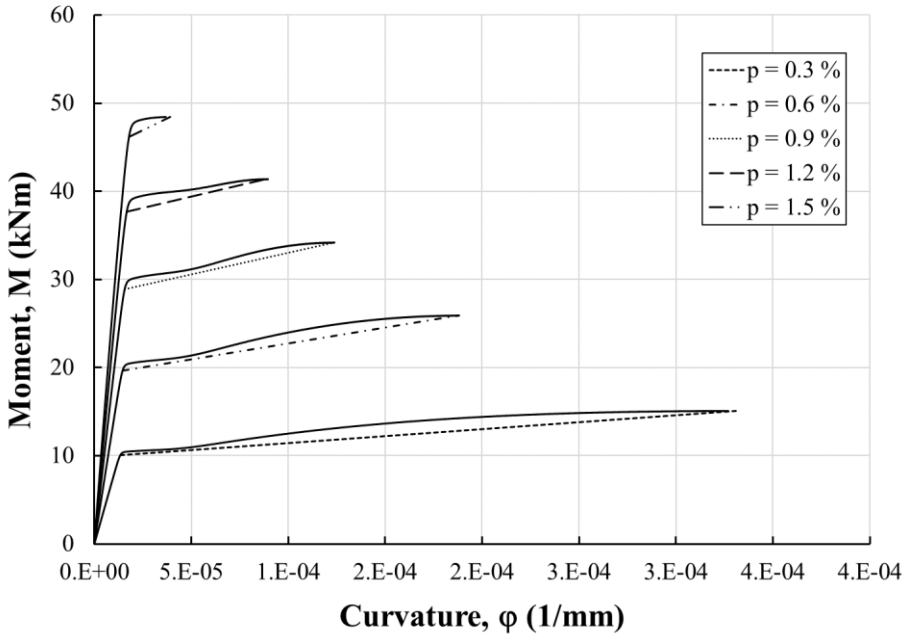

Figure 2.13: Moment-curvature relationship for A615/615M Grade 60 steel with increasing reinforcement ratios and f_c'=30 MPa

Figure 2.14 shows the variation of yielding and ultimate curvatures with the mechanical reinforcement ratio ω when the reinforcement is A615/615M Grade 60. As ω increases, the yielding curvatures increase very slightly while the ultimate curvatures, φ_u, reduce markedly. This is because a higher ω value increases c and reduces φ_u. Yielding curvatures, Equation [2.5], increase with k, Equation [2.3], which is only slightly affected with increased ρ, so φ_y is almost unaffected. The variation of the curvature ductility ratio, φ_u/φ_y, with ω should therefore look similar to that shown for φ_u in Figure 2.14.

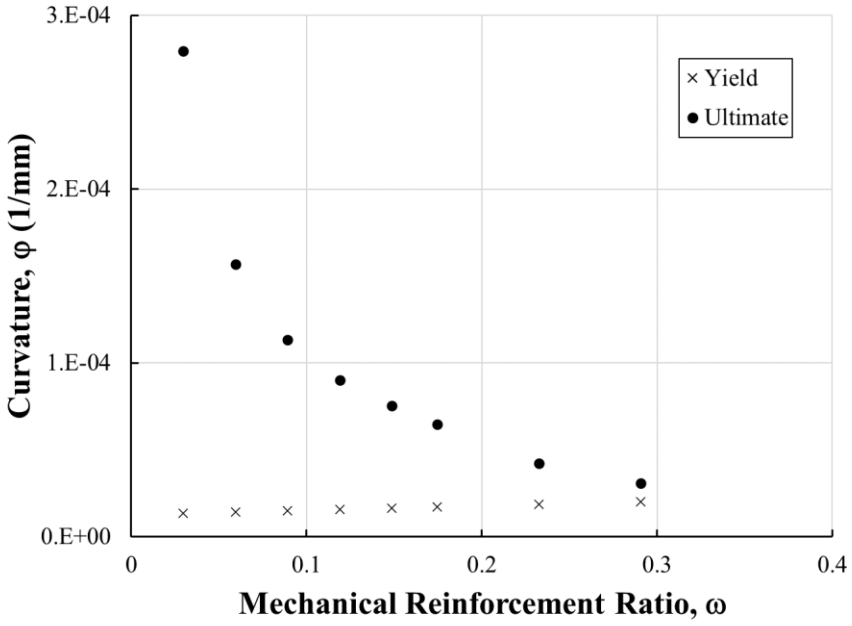

Figure 2.14: Yielding and ultimate curvature versus mechanical reinforcement ratio for cross section reinforced with A615/A615M Gr.60 steel

Figure 2.15 shows the variation of curvature ductility ratio with ω for the case where the extreme fibre concrete compressive strain is limited to a maximum of 0.0035. It confirms that these quantities are approximately inversely proportional, and therefore that neutral axis depth c is proportional to ω. This relationship for cross sections reinforced with A1035/1035M Grade 100 and A615/615M Grade 100 steels suggest a more linear correlation.

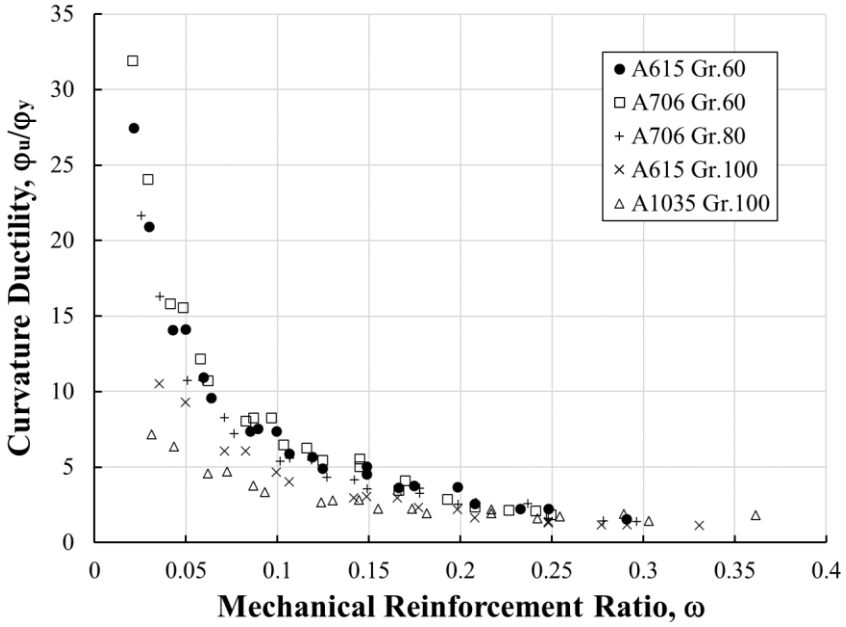

Figure 2.15: Curvature ductility versus mechanical reinforcement ratio (strain limit of 0.0035)

Regression analyses were performed to fit relationships to the data using indicator variables to distinguish between the various reinforcement grades. The form of the model was

[2.28] $\varphi_u/\varphi_y = \left(\beta_0 + \beta_1 I_1 + \beta_2 I_2 + \beta_3 I_3 + \beta_4 I_4\right)\left(1/\omega\right) + \varepsilon$

where: $\beta_0 \ldots \beta_4$ are parameters estimated by regression analysis, and ε is the error term. Indicator variable I_1 equals 1 if the steel is ASTM A706/706M Grade 60 or 0 otherwise, I_2 equals 1 if the steel is ASTM A706/706M Grade 80 or 0 otherwise, I_3 equals 1 if the steel is ASTM A615/615M Grade 100 or 0 otherwise, and I_4 equals 1 if the steel is ASTM A1035/1035M Grade 100 or 0 otherwise. The parameter estimates for all indicator variables were significantly different from zero ($p \leq 0.05$), suggesting that the relationship between the curvature ductility factor and the mechanical reinforcement ratio is different for each steel grade. The fitted equation is

[2.29] $\varphi_u/\varphi_y = (0.6 + 0.06\, I_1 - 0.05\, I_2 - 0.21\, I_3 - 0.34\, I_4)\left(1/\omega\right)$

The coefficient of determination, R^2, is 0.99 and the standard error is 0.62. Table 2.3 presents the standard error and the ratio of estimate and error for each coefficient. Because this ratio is greater than 4.2 for all coefficients, all the parameter estimates are statistically significant. For a given ω, Equation [2.29] indicates that the curvature ductility factor for ASTM A706/706M Grade 60 reinforcement is greater than that for the other grades of reinforcement. This is probably because the strain at the onset of strain hardening for this material, 0.0013 (Table 1.1), is markedly greater than that of the others. Similarly, the curvature ductility factor for ASTM A615/A615M & A1035/1035M Grade 100 reinforcement at a given ω is markedly smaller than that for all the other reinforcement grades. Similarly, A1035/1035M Grade 100 has a smaller curvature ductility factor at any given ω than all the steel grades except A615/615M Grade 100. This suggests that a more stringent target reliability index should be used to calibrate the resistance factor for ASTM A615/615M Grade 100 and ASTM A1035/1035M Grade 100 reinforcement.

Table 2.3: Regression analysis results

	β_0	β_1	β_2	β_3	β_4
Estimate	0.6	0.06	-0.05	-0.21	-0.34
Standard Error	0.009	0.012	0.013	0.016	0.015
Estimate/Error	63.6	5.4	4.2	12.7	23.1

Figure 2.16 shows the variation of φ_u/φ_y with ω for the case where the maximum extreme fibre concrete strain is not constrained. The maximum compressive strains exceed 0.7% for certain combinations of steel type, ρ and f_c' which may not be realistic because the concrete cover would likely spall when subjected to such high strains. The model represented by Equation [2.28] was applied again, and the parameter estimates, standard errors and ratio of parameter estimate to error are shown in Table 2.4. The parameter estimate for indicator variable I_2 was not significantly different from zero, which means that the variation of φ_u/φ_y with ω for ASTM A706/706M Grade 80, and ASTM A615/615M Grade 60 steels are similar. The fitted equation is

[2.30] $\varphi_u/\varphi_y = (0.7 + 0.12\ I_1 - 0.22\ I_3 - 0.46\ I_4)(1/\omega)$

The coefficient of determination, R^2, is 0.89 and the standard error is 2.5. The reinforcing steel A706/706M Grade 60 has the highest curvature ductility while A1035/1035M Grade 100 and A615/615M Grade 100 have relatively lower curvature ductilities.

Table 2.4: Regression analysis results for a data with no concrete strain constraint

	β_0	β_1	β_3	β_4
Estimate	0.7	0.12	-0.22	-0.46
Standard Error	0.03	0.04	0.06	0.05
Estimate/Error	22.7	3.1	3.8	8.6

Figure 2.16 shows the variation in flexural curvature ductility for the range of ω values investigated when the extreme fibre concrete strain is not limited. The relationships for A615/615M and A1035/1035M Grade 100 steels are essentially as shown in Figure 2.15: the extreme fibre concrete strain at ultimate for these steels is less than 0.0035. The ductility ratios for the other steel grades, particularly A706/706M Grade 60, are markedly higher than those shown on Figure 2.15, particularly for low ω. In these cases, the extreme fibre compression strain is markedly greater than 0.0035 and the ultimate curvature and ductility ratio are increased.

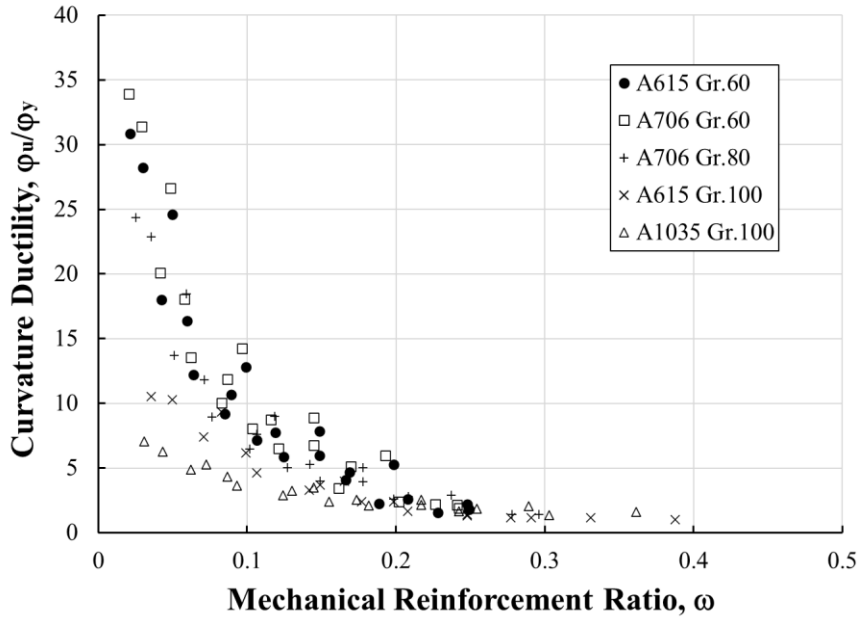

Figure 2.16: Curvature ductility versus mechanical reinforcement ratio (no strain limit)

2.5 IMPACT OF HIGH STRENGTH REINFORCEMENT ON OTHER DESIGN PARAMETERS

2.5.1 Ultimate Steel Stress

Figure 2.17 shows the relationship between the steel stress at ultimate, f_{su}, and the mechanical reinforcement ratio, ω. The open markers correspond to instances where the ultimate moment is the maximum computed, while the filled markers correspond to instances where the ultimate moment corresponds to a 0.0035 extreme fibre strain. As ω increases, the f_{su} decreases because the neutral axis depth increases to maintain horizontal force equilibrium and the steel strain is decreased according to Equation [2.18]. The nominal moment capacity, M_n, is defined in A23.3:19 using Equation [2.6]. It can be expressed in dimensionless form as

[2.31] $$\frac{M_n}{bd^2 f_c'} = \frac{A_s f_y d}{bd^2 f_c'} - \frac{(A_s f_y)^2}{2\alpha_1 f_c'^2 b^2 d^2} = \omega - \frac{\omega^2}{2\alpha_1}$$

For small values of ω, the higher-order term has only a slight effect, so the dimensionless moment is approximately proportional to ω and so inversely proportional to the curvature ductility ratio.

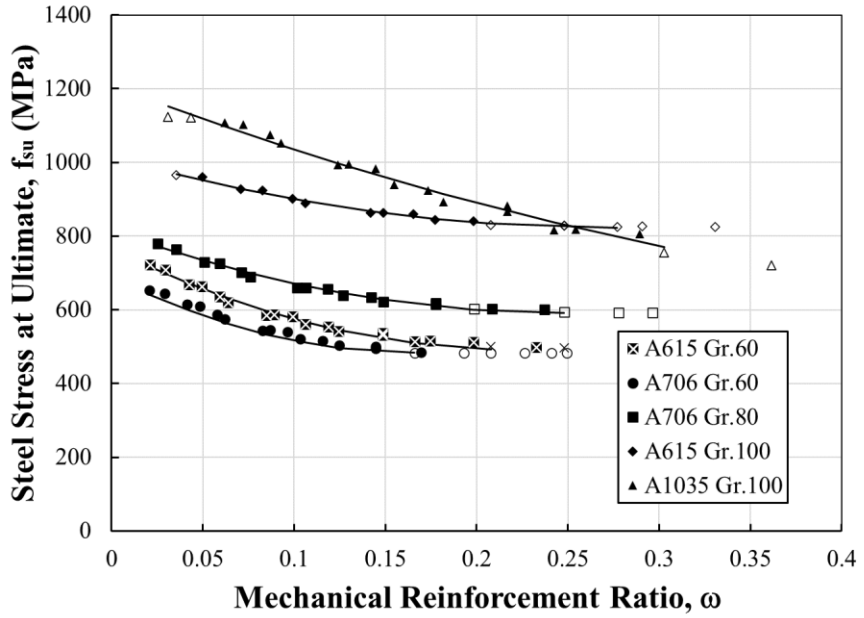

Figure 2.17: Ultimate steel stress versus mechanical reinforcement ratio

Linear regression was conducted to fit quadratic relationships to the data using a model with the following form

[2.32] $$f_{su} = (\beta_{10}+\beta_1 I_{11}+\beta_{12} I_2+\beta_{13} I_3+\beta_{14} I_4)\omega^2+(\beta_5+\beta_6 I_1+\beta_7 I_2+\beta_8 I_3+\beta_9 I_4)\omega+ \left(\beta_0+\beta_1 I_1+\beta_2 I_2+\beta_3 I_3+\beta_4 I_4\right)+\varepsilon$$

where: $\beta_0 \ldots \beta_{14}$ are parameters estimated by regression analysis and ε is the model error. Indicator variable I_1 equals 1 if the steel is ASTM A615/615M Grade 60 or 0 otherwise, I_2 equals 1 if the steel is ASTM A706/706M Grade 80 or 0 otherwise, I_3 equals 1 if the steel

is ASTM A615/615M Grade 100 or 0 otherwise, and I_4 equals 1 if the steel is ASTM A1035/1035M Grade 100 or 0 otherwise. The parameter 'β_6' was removed because it was not statistically significant. Tables 2.5 and 2.6 show the significant estimates 'Est.' and Standards Errors 'Err.' for the investigated steel grades. The R^2 value is 0.99 and the standard error is 14.8 MPa. Table 2.7 shows the fitted equations.

Table 2.5: Parameter estimates from regression analysis, β_0 to β_7

	β_7	β_5	β_4	β_3	β_2	β_1	β_0
Est.	632	-2452	519	325	128	78	688
Err.	213	121	15	17	15	6	8
Est./Err.	2.9	20.3	35.3	19.6	8.8	12.1	82.8

Table 2.6: Parameter estimates from regression analysis, β_8 to β_{14}

	β_{14}	β_{13}	β_{12}	β_{11}	β_{10}	β_9	β_8
Est.	-5946	-4836	-3632	-1844	7322	589	1070
Err.	568	660	685	205	413	191	220
Est./Err.	10.5	7.3	5.3	8.9	17.7	3.1	4.9

Table 2.7: Fitted equations for the investigated steel grades

Steel grade	Fitted equation
A706/706M Grade 60	$f_{su} = 7322\ \omega^2 - 2452\ \omega + 688$
A615/615M Grade 60	$f_{su} = 5478\ \omega^2 - 2452\ \omega + 766$
A706/706M Grade 80	$f_{su} = 3690\ \omega^2 - 1821\ \omega + 817$
A615/615M Grade 100	$f_{su} = 2486\ \omega^2 - 1382\ \omega + 1014$
A1035/1035M Grade 100	$f_{su} = 1376\ \omega^2 - 1863\ \omega + 1208$

For a given design moment, Equation [2.31] can be used to determine ω. This value can be refined, using the equations in Table 2.6 to obtain a more accurate value of the steel stress, f_{su}. The regression analysis results, Equations [2.29] and [2.30], can then be used to find the corresponding curvature ductility. This is particularly useful for A1035/A1035M steel which exhibits a roundhouse curve (as shown in Figure 1.1) and a yield point is not defined.

2.5.2 Ultimate Extreme Fibre Concrete Compressive Strain

Figure 2.18 shows the relationship between the extreme fibre concrete compressive strain at ultimate moment, ε_{cu}, and ω for the various steel grades and f_c' values. The horizontal line shows the value of 0.0035 as specified in A23.3:19. The computed values exceed this limit for virtually all steel grades investigated with ω less than approximately 0.2. The ultimate concrete strain is affected primarily by f_c': lower f'c values correspond to stress-strain relationships with more gradual descending branches, Figure 2.18a, and so exhibit higher ultimate extreme fibre strains. The steel grade has a relatively smaller effect.

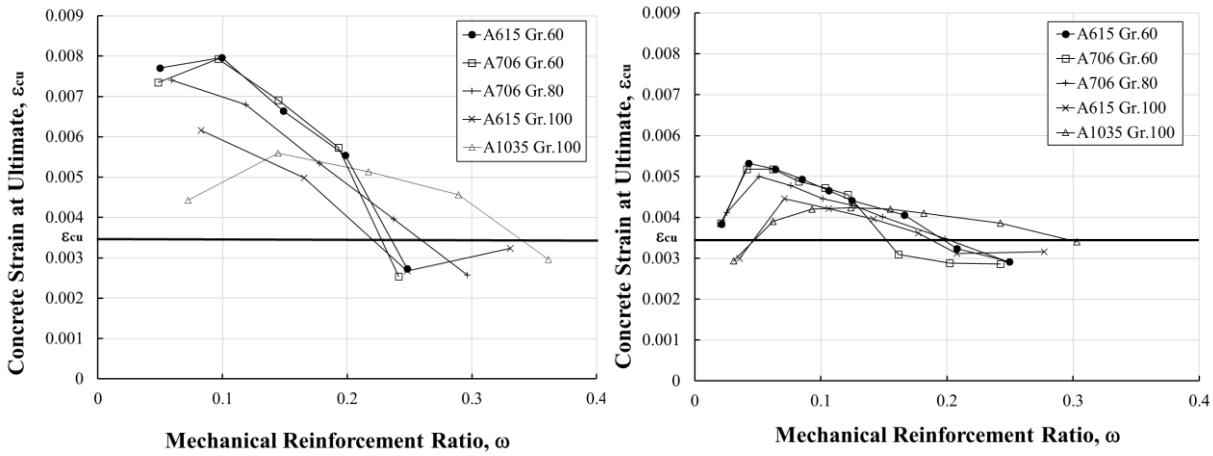

(a) (b)

Figure 2.18: Extreme fibre concrete compressive strain at ultimate versus mechanical reinforcement ratio: (a) f_c'=30 MPa (b) f_c'=70 MPa

2.5.3 Balanced Flexural Failure

A ‘balanced’ flexural failure occurs when the steel yields in tension and the concrete crushes in compression, at a specified strain of 0.0035, simultaneously. Table 2.8 compares the critical c/d ratio obtained from the moment-curvature analysis with the limits specified in the 2014 and 2019 editions of A23.3 computed using the nominal stress yield strength. The limit defined using the moment-curvature relationship, was obtained by increasing the steel reinforcement ratio, ρ, until the reinforcement yielded when the concrete strain was 0.0035. The corresponding c/d value was recorded.

The A23.3:14 (CSA 2014) limit is

[2.33] $$\frac{c}{d} = \frac{700}{700+f_y}$$

The A23.3:19 (CSA 2019) was previously given in Equation [2.1]. The two right columns in the table are the ratios of the c/d ratios from the moment-curvature analysis to the limits computed according to A23.3. Ratios greater than 1.0 indicate that the code-computed limit is conservative as it underestimates the actual critical c/d ratio. In other words, the code limits defined by Equations [2.1] and [2.33] are the specified maximum c/d values, and are conservative because the limiting values from the moment-curvature analysis are greater than these code-specified limits. On this basis, the provisions of A23.3:14 are unconservative for all steel grades investigated whereas those in A23.3:19 are conservative.

Table 2.8: Balanced condition based on nominal yield strength for steel reinforcement

Steel type	c/d	Nominal f_y ksi (MPa)	A23.3:14 limit	A23.3:19 limit	(c/d)/ A23.3:14	(c/d)/ A23.3:19
A615 Gr.60	0.58	60 (413)	0.629	0.503	0.93	1.16
A615 Gr.100	0.46	100 (690)	0.504	0.403	0.91	1.14
A706 Gr.60	0.59	60 (413)	0.629	0.503	0.94	1.18
A706 Gr.80	0.54	80 (550)	0.559	0.448	0.97	1.21
A1035 Gr.100	0.49	100 (690)	0.504	0.403	0.98	1.22

Table 2.9 presents similar information except that the code-specified c/d limits are computed using the mean yield stress values from Table 1.1, instead of the specified minimum yield stress. The provisions of in A23.3:14 and A23.3:19 are conservative for all steel grades investigated.

Table 2.9: Balanced condition based on mean yield strength for steel reinforcement

Steel Type	c/d	Mean f_y ksi (MPa)	A23.3:14 Limit	A23.3:19 Limit	(c/d)/ A23.3:14	(c/d)/ A23.3:19
A615 Gr.60	0.58	72 (496)	0.585	0.468	1.0	1.250
A615 Gr.100	0.46	120 (827)	0.458	0.367	1.0	1.260
A706 Gr.60	0.59	70 (496)	0.592	0.474	1.0	1.250
A706 Gr.80	0.54	86 (593)	0.542	0.433	1.0	1.250
A1035 Gr.100	0.49	105 (723)	0.492	0.393	1.0	1.250

2.6 SUMMARY AND CONCLUSIONS

CSA Standard A23.3:19 limits the maximum reinforcing steel yield strength that can be assumed in calculations to 500 MPa. An initiative is underway to relax this requirement to allow the full potential of steels with higher yield strengths to be realized. The primary objective of the research reported in this chapter is to compare the curvature ductility ratios, φ_u/φ_y, of cross sections reinforced with High Strength Reinforcement (HSR) with those of sections with conventional reinforcement. If the ductility is reduced, the target reliability index must be increased and the resistance factor for steel reinforcement, ϕ_s, must be reduced. Moment-curvature relationships were therefore derived for cross sections reinforced with ASTM A706/706M Grade 60 (410 MPa) and Grade 80 (560 MPa) steels, ASTM A615/615M Grade 60 (410 MPa) and Grade 100 (690 MPa) steels, and ASTM A1035/1035M Grade 100 (690 MPa) steel. Steel and concrete stress-strain relationships by Mander & Matamoros (2019) and Carreira & Chu (1985) were used, respectively.

An idealized bilinear moment-curvature relationship was defined using the yielding and ultimate points of the response. Yielding corresponds to the steel tensile strain exceeding the steel yielding strain. For sections reinforced with A1035/A2035M Grade 100 steel, which exhibits a roundhouse behaviour, an approximate bilinear moment-curvature relationship was derived. Ultimate moment corresponds to either the maximum moment or the concrete extreme fibre compressive strain reaching a value of 0.0035. A MATLAB code was programmed to determine the moment-curvature response, construct the bilinear idealizations and record the yielding and ultimate curvatures, moments, concrete strains, and steel stresses. These data were used to investigate curvature ductility ratios, steel stresses and extreme fibre concrete compressive strains at ultimate, and the applicability of A23.3:19 criteria to ensure balanced flexural failure for the difference steel grades.

The following conclusions are drawn from the research reported in this chapter:

1. The curvature ductility ratio, φ_u/φ_y, is approximately inversely proportional to the mechanical reinforcement ratio, ω, defined as A_sf_y/bdf_c'. Thus ω increases, and

φ_u/φ_y reduces, as the steel area, A_s, or yield strength, f_y, increases or the concrete compressive strength, f_c', reduces.

2. For a given value of ω, beams reinforced with A 706 Grade 60 steel have the highest curvature ductility ratios, with respect to other steel grades investigated.

3. For a given value of ω, beams reinforced with ASTM A615 Grade 100 and A1035/1035M Grade 100 reinforcements have the lowest curvature ductility ratios. It may be necessary to calibrate a new, more stringent, resistance factors ϕ_s for these steel grades.

4. If extreme fibre concrete compressive strain, $\varepsilon_{c,max}$, at ultimate is limited to 0.0035, then the difference in variation of φ_u/φ_y with ω is statistically significant for cross sections reinforced with all steel grades investigated. If $\varepsilon_{c,max}$ is not limited, then then the difference in variation of φ_u/φ_y with ω is not statistically significant only for cross sections reinforced with ASTM A615/615M Grade 60 and ASTM A706/706M Grade 80 reinforcement.

5. Equations are derived for compiling the ultimate steel stress as a function of ω for the steel grades investigated that are suitable for design-office use.

6. The extreme fibre concrete compressive strain at ultimate is reduced significantly as f'_c increases while the steel type has a relatively smaller impact. The A23.3:19 limit of 0.0035 can be unconservative when ω is greater than 0.20.

7. The c/d limitation, where c is the depth of the compression region and d is the effective reinforcement depth, specified in A23.3:19 to ensure a balanced failure condition occurs are appropriate for cross sections reinforced with high strength reinforcement. The '0.8' factor introduced in the 2019 edition of A23.3 ensures that the limitation is appropriate even if the limiting c/d limit is computed using the nominal reinforcement yield strength, f_y, while the actual response is computed using the mean reinforcement yield strength, $\bar{f}_y$.

Chapter 3

3 Moment Redistribution Limits for Beams with High Strength Reinforcement

3.1 INTRODUCTION

High Strength Reinforcement (HSR) reduces steel volumes in reinforced concrete construction, decreasing congestion and making the design more cost-efficient. CSA Standard A23.3:19 (CSA 2019) currently requires the maximum yield strength used in design calculations to be no greater than 500 MPa. A reduction in steel volume may result in serviceability issues, including larger crack widths. This problem may be exacerbated in continuous beams considering the effects of moment redistribution.

Moment redistribution can occur only in indeterminate structures. As the failure load is reached, plastic hinges form and the distribution of moment due to changes in subsequent load increments. In continuous beams, maximum positive and negative moments develop at the span and support regions, respectively, for a particular load case. Plastic hinges form when the steel reinforcement yields at these critical moment sections. If the hinge region is sufficiently ductile, it will undergo inelastic rotation, without attracting additional moment. To satisfy equilibrium, the additional moment predicted using linear-elastic analysis is redistributed to other critical sections that have not formed plastic hinges. The collapse load is reached when a sufficient number of plastic hinges form to make the beam statistically unstable, and a plastic collapse mechanism forms. If the first plastic hinges to form are at sections with low curvature ductility ratios, φ_u/φ_y, they may have insufficient inelastic rotation capacity to allow subsequent plastic hinges to form. In this case, a complete plastic collapse mechanism does not form, and the failure load corresponds to the cross section with the initial plastic hinge reaching its ultimate moment capacity. Clause 9.2.4 in A23.3:19 (CSA 2019) limits the maximum moment redistribution in continuous beams to a maximum of the lesser of 20% or (30-50c/d) % where c is the depth of the neutral axis at failure and d is the effective depth of reinforcement. Cross sections with

high c/d ratios have relatively small ultimate curvatures, φ_u, and so smaller inelastic rotation capacities.

As presented in Chapter 2, beams reinforced with HSR can have smaller curvature ductility than beams reinforced with conventional reinforcement. It is therefore necessary to investigate whether the provisions of A23.3:19 Clause 9.2.4 are applicable for beams with HSR.

3.1.1 Moment Redistribution at Ultimate Limit State

Figure 3.1a illustrates moment redistribution for a two-span beam that is continuous over its interior support and subjected to a uniformly distributed load w on both spans. The linear-elastic moment at the interior support and critical span cross sections are $\frac{wL^2}{8}$ and $\frac{wL^2}{14}$ respectively, where L is the span length. If the magnitudes of the bending moment capacities at the span and support sections are as shown in Figure 3.1c, the support section will reach its yield moment capacity, M_y^-, first. Figure 3.1b shows the linear-elastic moment diagram. The moment-curvature relationships, Figure 3.1c, are assumed bilinear. The curvature ductility ratio, φ_u/φ_y, at the support is smaller than that at the span. A plastic hinge first forms at the support section, Figure 3.1d, and additional load Δw is applied until the yield capacity of the span section, M_y^+, is reached, Figure 3.1e. These new plastic hinges at the span sections cause the beam to become unstable. It collapses as the complete mechanism shown in Figure 3.1f. The collapse mechanism is not developed when the yield capacity at the spans is not reached before the plastic hinge at the support fails. In this case, the inelastic rotational capacity at the support is insufficient to allow the span hinge to form.

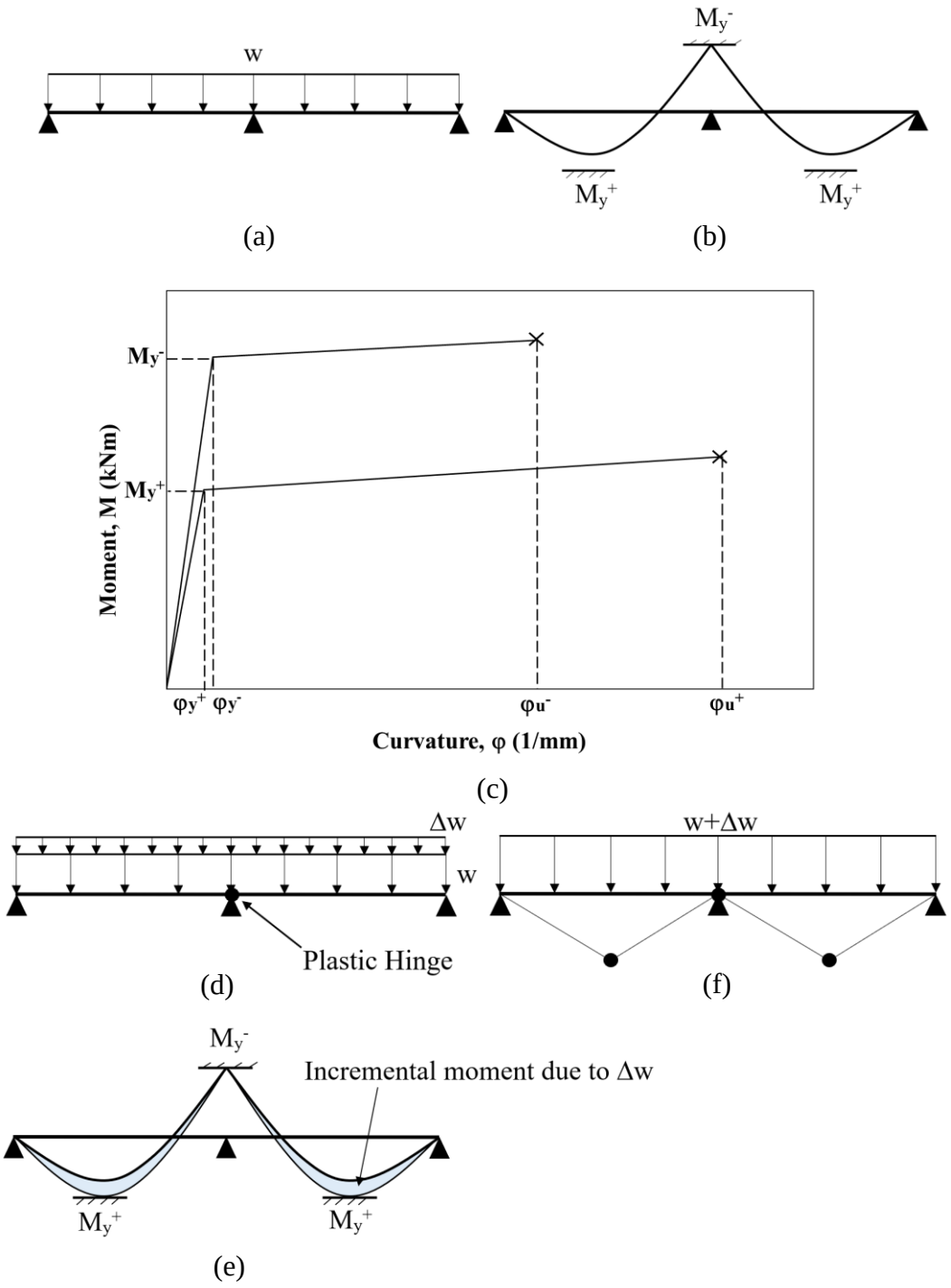

Figure 3.1: Development of plastic collapse mechanism: (a) Beam and loading (b) Linear-elastic bending moment diagram (c) Moment-curvature relationship (d) Formation of first plastic hinge (e) Incremental moment due to Δw (f) Full collapse mechanism

3.1.2 Impact of Moment Redistribution at Serviceability Limit States

Moment redistribution may cause excessive crack widths at Serviceability Limit State (SLS). Crack widths are proportional to the stress in the reinforcing steel stress, f_s. Clause 10.6.1 in A23.3:19 allows the designer to assume that f_s equals 0.6 f_y instead of computing it using equations based on elastic-cracked cross section behaviour. If the reinforcing steel area necessary to satisfy Ultimate Limit States at a particular cross section has been significantly reduced using moment redistribution, f_s can markedly exceed $0.6f_y$. In this case, crack widths may be unacceptably large. This situation is made worse if live loads are relatively small with respect to the dead loads. It is therefore important that beams with HSR designed at ULS accounting for moment redistribution are checked at SLS because a lower steel area, A_s is required to provide a given ultimate moment capacity so the in-service steel stresses, f_s will increase further. This is not addressed in A23.3:19.

3.1.3 Research Objectives

1. The primary objective of the research presented in this chapter is to determine whether the current provisions in Clause 9.2.4 of A23.3 are appropriate for beams reinforced with high strength reinforcement.

2. A secondary objective is to assess how the combinations of moment redistribution and HSR may lead to unacceptable crack widths.

3.1.4 Chapter Outline

The moment redistribution that occurs in beams reinforced with conventional and high strength steel reinforcement is compared in this chapter. A brief literature review is presented in Section 3.2. Section 3.3 outlines a procedure for designing the critical cross sections of a beam, determining the moment-curvature relationships for these critical sections, and using these relationships to determine the failure load of the beam using nonlinear analysis by SAP2000.

Section 3.4 illustrates the moment redistribution phenomenon by considering two beams: one that forms a complete mechanism at collapse and the other that does not form a

complete collapse mechanism. The corresponding load-deflection responses in each case are illustrated.

Section 3.5 presents a parametric study that investigates the effects of concrete compressive strength, f_c', of 30 and 70 MPa and steel grades ASTM A615/615M Grade 100 and ASTM A706/706M Grade 60 on the moment redistribution of beams with different reinforcement ratios. These two steel grades have been selected for study because, as shown in Chapter 2, A706/706M Grade 60 has the highest curvature ductility while A615/615M Grade 100 has a relatively low ductility for a given mechanical reinforcement ratio, ω.

Section 3.6 compares the results of the parametric analysis to the provisions concerning moment redistribution in A23.3:19 (CSA 2019).

Section 3.7 discusses Serviceability Limit States (SLS) in a beam designed at ULS using moment redistribution. A procedure to determine the maximum permissible moment redistribution that satisfies the critical width/reinforcement spacing criteria in ACI 318:19 (ACI 2019) is derived and typical results are presented.

Section 3.8 presents the summary and conclusions of the research reported in this chapter.

3.2 LITERATURE REVIEW

For a concrete beam with a rectangular cross section at the Ultimate Limit State, horizontal force equilibrium of the concrete compressive force and the steel tensile force requires

[3.1] $\phi_c \, \alpha_1 \, \beta_1 \, c \, f_c' \, b = \phi_s \, A_s \, f_y$

where c is the depth from extreme compression fibre to the neutral axis, f_c' is the concrete compressive strength, A_s is the steel reinforcement area, f_y is the steel yield stress, b is the width of the beam, and ϕ_c and ϕ_s are the concrete and steel resistance factors taken as 0.65 and 0.85, respectively. The distance from extreme compression fibre to the neutral axis, c, can be isolated as

[3.2] $$c = \frac{\phi_s A_s f_y}{\phi_c \alpha_1 \beta_1 f_c' b}$$

The stress block parameters, α_1 and β_1, are calculated from Equation [2.8a], and [2.8b], respectively. Equation [3.2] can be written in terms of mechanical reinforcement ratio, ω, where

[3.3] $$\omega = \frac{A_s f_y}{b d f_c'}$$

as

[3.4a] $$c = \frac{\phi_s \omega d}{\phi_c \alpha_1 b_1}$$

or

[3.4b] $$\frac{c}{d} = \frac{\phi_s \omega}{\phi_c \alpha_1 \beta_1}$$

Thus the requirement in Clause 9.2.4 of A23.3:19 can be expressed in terms of ω as "the lessor of 20% or [30- 50($\frac{1.3\,\omega}{\alpha_1 \beta_1}$)]%".

Lou et al (2014) tested a two-span continuous reinforced concrete beam loaded with equal point loads applied at the middle of the two mid spans. Two beam groups were investigated: Group 1 beams had less steel reinforcement at the interior support than at the midspan. The interior support section cracked and yielded first which reduced the flexural stiffness locally and caused additional moment to be redistributed to the span section. Group 2 beams had less reinforcement at the span section than at the interior support, so the yielding occurred first at the span section. It was concluded that a full collapse mechanism is easier to develop in a high strength concrete beam compared to a normal strength concrete beam.

The conclusion from Lou et all (2014) aligns with Equation [2.11], which shows the approximately inverse relationship between the ultimate curvature and ω, and Equation

[3.3], which shows that an increase in f_c' decreases ω. Hence the flexural curvature ductility is increased for an increasing f_c', which also increases the rotation capacity at the first plastic hinge and makes it more likely that a collapse mechanism will develop.

3.3 COMPUTATIONAL METHODS TO QUANTIFY MOMENT REDISTRIBUTION

The impact of higher reinforcing steel strength on the degree of moment redistribution that occurs at ULS was assessed numerically using the following three-step procedure:

1. The span sections of a two-span continuous beam with a given f_c' and reinforcing steel grade is designed to correspond to the given reinforcement ratio, ρ, at the interior support section.

2. The procedure described in Chapter 2 to determine bilinear moment-curvature relationships is used for these two critical cross sections.

3. The yielding and ultimate points for the two critical cross sections are used as input to the SAP2000 Finite Element Analysis program (Computers & Structures Inc., 2020) to determine the collapse load using nonlinear analysis.

An equal area method, described in Section 3.3.1, was applied to approximately calculate the rotational capacity, and location of the plastic hinge in the span section. This was used to verify the results obtained using SAP2000.

3.3.1 Applying Equal Area Method to Calculate Collapse Load

For the idealized continuous beam shown in Figure 3.2a, with the live load applied on both spans, the plastic collapse mechanism requires three plastic hinges to be present. The first plastic hinge forms at the interior support and the subsequent two plastic hinges form simultaneously at the critical span sections, Figure 3.2b. When the live load is applied on one span only, collapse occurs when two plastic hinges form: one in the loaded span and one at the interior support.

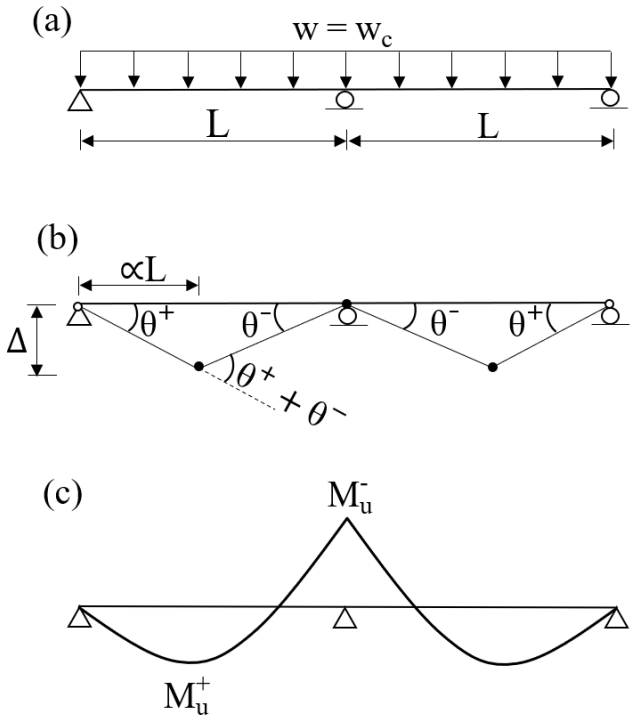

Figure 3.2: Collapse mechanism in a two-span beam: (a) Loading (b) Mechanism (c) Bending moment at collapse

An approximate procedure for determination of the collapse load, used to verify the results of SAP2000 analysis, is presented here. The procedure is based on the following assumptions:

1. The behavior outside the plastic hinge regions is linear-elastic-cracked; tension stiffening is ignored.
2. The moment-curvature relationship is bilinear, defined by the points: (0,0), (ϕ_y, M_y), (ϕ_u, M_u) where the yielding and ultimate moments and curvatures are as defined in Section 2.2.1.

The procedure is as follows:

1. Compute the total collapse load of the beam using the Virtual Work Theorem.
    a) The External Virtual Work (EVW) done by the applied load is

[3.5] $EVW = 2\ L\ \left(\frac{\Delta}{2}\right) w_c L = w_c L^2 \Delta$

where w_c is the collapse load and L is the span length. The internal virtual work, IVW, is the sum of the product of the plastic moment capacities, $M_u^{+/-}$, and the associated inelastic rotations, $\theta^{+/-}$ at the plastic hinge locations.

b) Internal Virtual Work (IVW) is

[3.6] $IVW = 2\ M_u^+(\theta^+ + \theta^-) + M_u^-(2\theta^-)$

From Figure 3.2b, the inelastic rotations can be related to the maximum deflection. The rotation at the exterior support is

[3.7] $\theta^+ = \frac{\Delta}{\propto L}$

where $\propto L$ is the distance from the plastic hinge at the critical span section to the external support. The rotation at each side of the interior support is

[3.8] $\theta^- = \frac{\Delta}{(1 - \propto)L}$

c) Set the EVW, Equation [3.5], equal to the IVW, Equation [3.6]

[3.9] $L^2\ w_c\ \Delta = 2\ M_u^+(\theta^+ + \theta^-) + \gamma_M M_u^+(\theta^-)$

Substituting Equations [3.7] and [3.8] into [3.9] to eliminate $\theta^{+/-}$ and simplifying yields

[3.10] $w_c = \frac{2M_u^+}{L^2\left\{\left(\frac{1 + \gamma_M \propto}{\propto(1 - \propto)}\right)\right\}}$

where γ_M is the ratio of magnitudes of the ultimate negative and positive moments, M_u^-/M_u^+.

d) Determine the location of span plastic hinge. The derivative of Equation [3.10] with respect to $\propto$ is

$$\textbf{[3.11]}\ \frac{dw}{d\propto} = \frac{d\left[\frac{2M_u^+}{L^2\left(\frac{1+\gamma_M\propto}{\propto(1-\propto)}\right)}\right]}{d\propto}$$

and setting $dw/d\propto = 0$ yields

$$\textbf{[3.12a]}\ \gamma_M\propto^2 + 2\propto - 1=0$$

and hence

$$\textbf{[3.12b]}\ \propto = \frac{\sqrt{1+\gamma_M} - 1}{\gamma_M}$$

2. Determine the inelastic rotation necessary to allow formation of second plastic hinge.

a) Determine the load, w_1, needed to initiate formation of the first plastic hinge. This behaviour at this point is linear-elastic so

$$\textbf{[3.13]}\ w_1 = \frac{8M_y^-}{L^2}$$

b) Determine the load increment, w_2, needed to initiate formation of the second plastic hinge

i. The shear force at the exterior support, V_1, due to w_1 computed assuming linear-elastic behavior, is

$$\textbf{[3.14]}\ V_1 = \frac{3}{8}w_1L$$

ii. The maximum moment in the span due to w_1, M_1, occurs when the shear force is 0

$$\textbf{[3.15]}\ M_1 = -V_1(\propto L) + w_1\frac{(\propto L)^2}{2}$$

iii. The incremental moment required to initiate yield at the span plastic hinge, M_2, is

[3.16] $M_2 = M_y^+ - M_1$

iv. The associated load increment, w_2 is

[3.17] $$w_2 = \frac{2M_2}{\propto L^2 (1 - \propto)}$$

c) Determine the deflections at midspan due to the combination of w_1 and w_2. The approximate linear-elastic deflection at midspan due to w_1, Δ_1, assuming pinned-fixed beam end connections due to symmetry is

[3.18] $$\Delta_1 = \frac{w_1 \propto L^4}{48E_c(0.85I_{cr}^+ + 0.15I_{cr}^-)} \{1 - 3\propto^2 + 2\propto^3\}$$

where E_c is the Young's modulus for concrete, and I_{cr}^+ and I_{cr}^- are the cracked moment of inertia for the span and support cross sections, respectively. The approximate additional simply supported beam deflection at midspan due to w_2, Δ_2, is

[3.19] $$\Delta_2 = \frac{w_2 \propto L^4}{24E_c I_{cr}^+} \{1 - 3\propto^2 + 2\propto^3\}$$

The total deflection, Δ, is

[3.20] $\Delta = \Delta_1 + \Delta_2$

d) The inelastic rotational demand, θ_{id}, is

[3.21] $$\theta_{id} = \frac{d\Delta_2}{dL} = \frac{w_2 \propto L^3}{6E_c I_{cr}^+} \{1 - 3\propto^2 + 2\propto^3\}$$

3. Determine the inelastic rotation capacity

a) Compute the failure load, w_f, approximately as

[3.22] $w_f = w_1 + w_2$

b) Compute the total shear force, V_{if}, at the internal support due to the total load

[3.23] $$V_{if} = \left(\frac{5}{8}w_1 + \frac{1}{2}w_2\right)L$$

c) Determine the approximate half length of the plastic hinge at the support, x. As shown in Figure 3.3, this half length is the distance from the centre of the hinge, where the applied moment is M_u^-, to the point where the applied moment is M_y^-, as shown schematically by the shaded region of the figure. Moment equilibrium requires

[3.24] $$\left(M_u^- - M_y^-\right) = -\frac{w_f}{2}x^2 + V_{if}x$$

from which x can be determined.

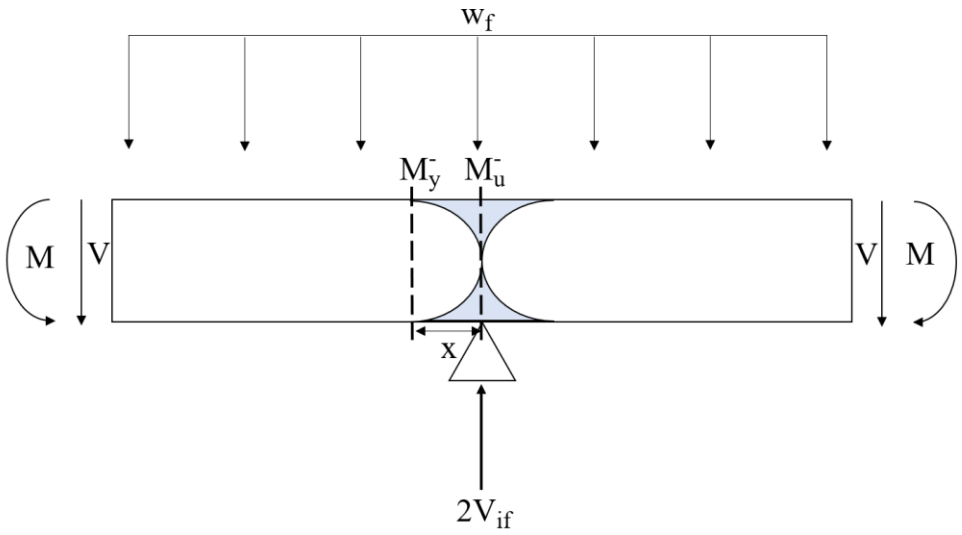

Figure 3.3: Free Body Diagram of the interior support hinge region

d) Determine the inelastic rotation, θ_{ir}, at the hinge

[3.25] $$\theta_{ir} = \frac{1}{2}(\varphi_u - \varphi_y)x$$

If $\theta_{ir} < \theta_{id}$, the inelastic rotation capacity at the plastic hinge is insufficient to allow a collapse mechanism to develop. Instead, the interior support cross section fails before the span plastic hinge forms.

3.3.2 Reinforcing Steel Design at Critical Cross sections

Figure 3.4 shows schematically the procedure for determining the span reinforcement ratio, ρ^+, corresponding to a given support reinforcement ratio, ρ^-. The procedure is as follows

1. Initialize:
    a. Define concrete compressive strength, steel grades.
    b. Define geometric parameters: b, d, L.
    c. Compute stress block parameter, α_1, using Equation [2.8a].
2. Assign a support reinforcement ratio which will increase with each iteration until the c/d limit in Clause 10.5.2 of A23.3:19 is reached.
3. Determine the steel area at the interior support, A_s^-, and the corresponding nominal support moment, M_u^-. For $A_s^- = \rho^- bd$, the depth of rectangular stress block, a, is

    [3.26] $$a = \frac{f_y A_s^-}{\alpha_1 f_c' b}$$

    The nominal support moment is

    [3.27] $$M_u^- = f_y A_s^- \left(d - \frac{a}{2}\right)$$

    Determine the distributed load, w, corresponding to this nominal ultimate support moment

    [3.28] $$w = M_u^- \frac{8}{L^2}$$

4. Determine the span moment, M_u^+, and the associated reinforcement ratio, ρ^+ from the applied load. The critical moment demands are computed assuming linear-elastic analysis. The negative moment at the interior is $\frac{wL^2}{8}$, corresponding to live load on

both spans. The positive moment, M_u^+, is derived for the critical load case of live load on one span only

[3.29] $M_u^+ = 0.07 w_d L^2 + 0.096\, w_l L^2$

Assuming dead load, w_d and live load, w_l are equal, Equation [3.29] simplifies to

[3.30] $$M_u^+ = \frac{wL^2}{12}$$

From Equation [2-12] in the CAC Concrete Design Handbook (CAC 2016)

[3.31] $$\rho^+ = \left[1 - \sqrt{1 - \frac{2M_u^+}{\alpha_1 f_c' b d^2}}\right] \frac{\alpha_1 f_c'}{f_y}$$

Hence, the span flexural reinforcement area, A_s^+, equals $\rho^+ bd$.

5. Increment ρ^- and repeat Steps 3 to 5.

These steel areas, material grades, and geometric properties are used as input for the moment-curvature analysis.

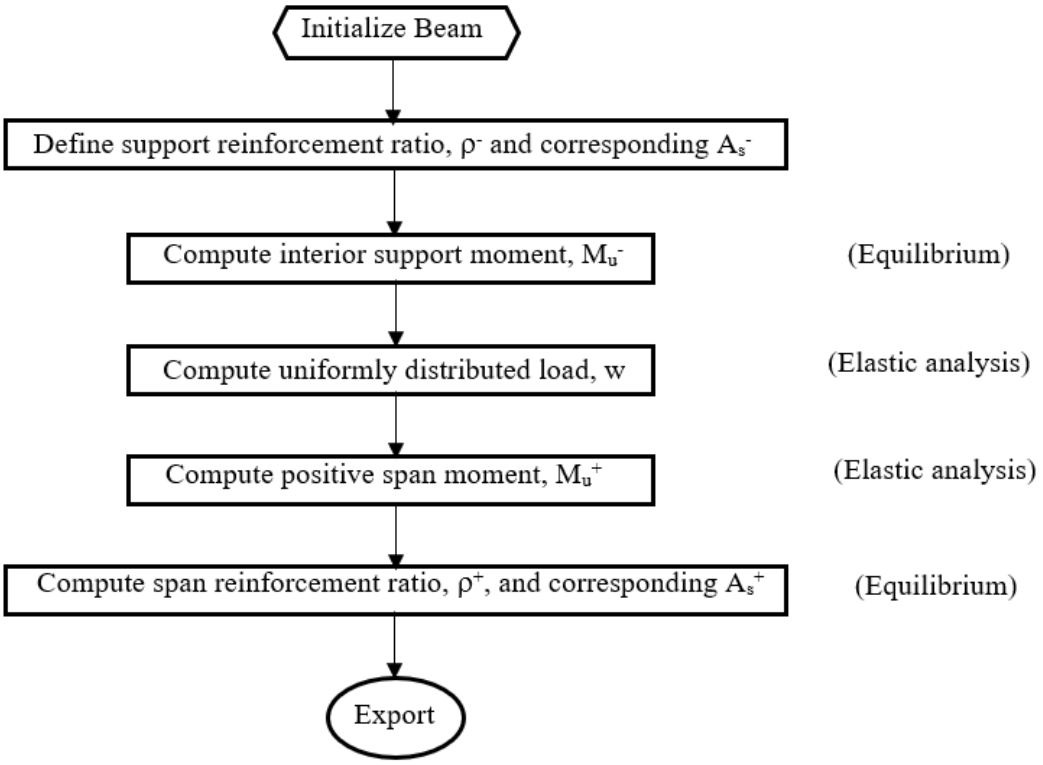

Figure 3.4: Procedure to determine positive moment reinforcement area, A_s^+, at span, given negative moment steel area, A_s^-, at support

3.3.3 Moment-Curvature Analysis

The material properties, section dimensions and steel areas are next used to generate moment-curvature relationships for the critical span and interior support cross sections using the procedure in Chapter 2. If there is no clearly defined yield moment and curvature then the equal area method, as described in Section 2.3.4, is used to determine an equivalent bilinear relationship. This is necessary for the beams reinforced with ASTM A1035/1035M Grade 100 steel. Beams reinforced with A615/615M A706/706M steels typically show a well-defined yield moment and curvature.

The moments and curvatures at yield and at ultimate are critical input for the subsequent non-linear SAP2000 analysis. The yield moment, where steel tensile stress reaches yield, defines the initiation of plastic hinge formation. The ultimate moment and corresponding ultimate curvature define whether the inelastic plastic hinge rotation capacity is sufficient,

given the inelastic rotation demand, to achieve a full plastic collapse mechanism. The Ultimate moment was defined as either: (1) the maximum moment value or (2) the moment corresponding to an extreme fibre concrete compressive strain of 0.0035.

The stress-strain relationship for concrete is as proposed by Carreira and Chu (1985) and the stress-strain relationship and associated parameters for the high-strength steel reinforcement are as proposed by Mander and Matamoros (2019). Further details of the moment-curvature analysis are provided in Chapter 2.

3.3.4 SAP2000 Analysis

Figure 3.5 shows the procedure for using the non-linear analysis capabilities of SAP2000 (Computers and Structures Inc., 2021) to quantify the moment redistribution.

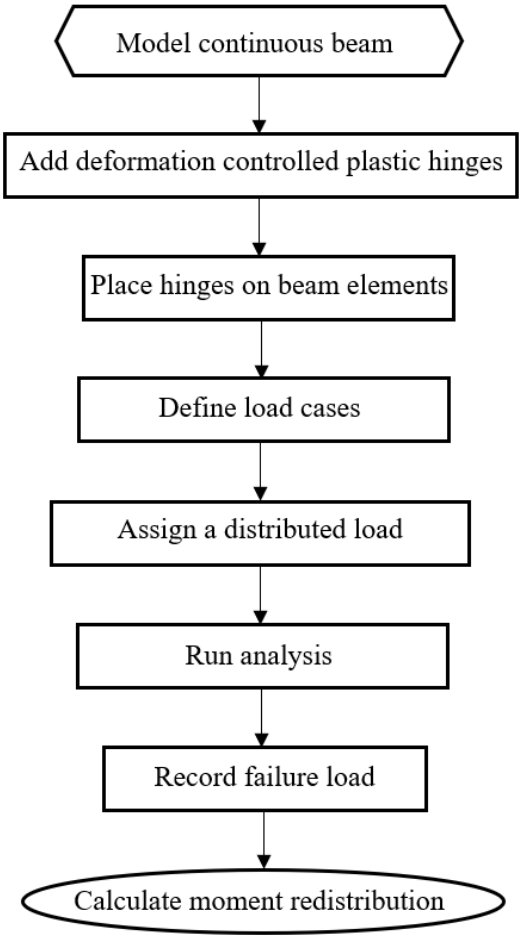

Figure 3.5: Procedure to determine failure load using SAP2000 nonlinear analysis

Figure 3.6a shows the beam model in SAP2000. Each of two spans has 50 plastic hinges distributed along the span length. The hinges also act as separators and discretize each span into smaller elements. The plastic hinges in SAP2000, as shown in Figure 3.6b, are 'deformation controlled (ductile)' which require a moment-curvature relationship to be defined.

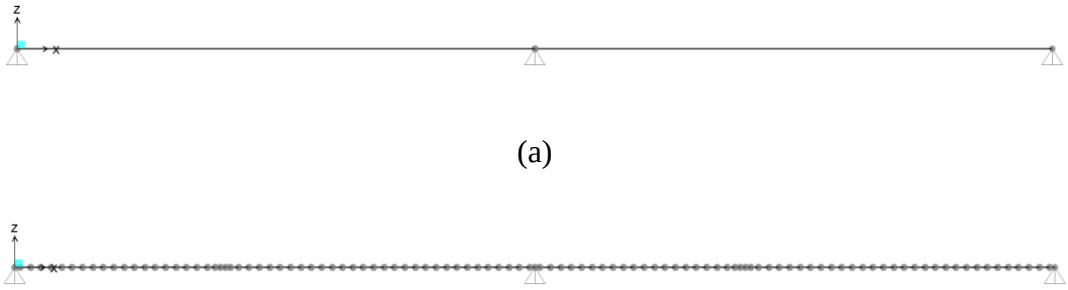

(a)

(b)

Figure 3.6: SAP2000 beam idealization: (a) Beam model in SAP2000 (b) Plastic hinge locations

The procedure is as follows:

1. Create a two-span concrete beam that is continuous over the interior support in SAP2000, as shown in Figure 3.6a.

2. Define the yielding and ultimate moment and curvature values for the interior support and span cross sections as the values taken from moment-curvature analysis described in Section 3.3.3.

3. Use the 'Assign' command to apply a uniformly distributed load on the two spans incrementally to allow the modelling of nonlinear behaviour in the beam. For each load increment

    a. SAP tabulates moments along length of beam.

    b. SAP compares the moment in each element with the specified yield and ultimate values. If the yield moment is exceeded, the stiffness at the hinge

is reduced to allow inelastic rotation to occur. If the ultimate moment at either critical section is reached, the beam is deemed to have failed.

4. Compute the maximum moments, M_{el}, due to the failure load, w_f, assuming a linear-elastic response. If the first plastic hinge forms at the interior support, the corresponding moment is $M_{el}^{-}= \frac{w_f L^2}{8}$. If the first plastic hinge forms at the span section, the corresponding moment is $M_{el}^{+}= \frac{w_f L^2}{12}$.

5. Compute the moment redistribution, r. If both spans are loaded with live loads simultaneously, the first plastic hinge forms at the interior support and the moment redistribution is calculated as

[3.32] $$r = \frac{M_{el}^{-} - M_{y}^{-}}{M_{el}^{-}}$$

where M_y^- is the yield moment at interior support as obtained from the moment-curvature analysis. If only one span is loaded with live load, the first plastic hinge forms at the critical span cross section and the moment redistribution is computed as

[3.33] $$r = \frac{M_{el}^{+} - M_{y}^{+}}{M_{el}^{+}}$$

where M_y^+ is the yield moment at critical span as obtained from the moment-curvature analysis.

6. Repeat Steps 2 through 6 for the range of reinforcement ratios investigated.

3.4 EXAMPLE CALCULATIONS

To illustrate the methodology described in Section 3.3, two example calculations are presented. A case where a full collapse mechanism is considered first, followed by a case where the inelastic rotation capacity at the first plastic hinge is exhausted before a full collapse mechanism forms.

3.4.1 Case Of Full Plastic Mechanism Forming

A two-span one-way slab, continuous over the interior support, has a rectangular cross section with a width, b, of 1000 mm, a height, h, of 200 mm and an effective depth, d, of 170 mm. The concrete compressive strength, f_c', is 70 MPa, and the reinforcement is ASTM A615/615M Grade 100 steel with a mean yield strength of 830 MPa. The reinforcement at the interior support, A_s^-, is 2380 mm^2, corresponding to ω of 0.165. The reinforcement at the span, A_s^+, is 1520 mm^2, which corresponds to ω of 0.106. Live load is applied simultaneously on both spans, which are each 5 m long.

Figure 3.7 shows the idealized bilinear moment-curvature relationships for the critical span and interior support cross sections. The member exhibits linear-elastic behaviour until the first plastic hinge forms at the interior support, indicated by Point A on the figure. As the load is increased, the moment at the interior support increases slightly until the plastic hinge at the span forms, Point B. The application of additional load eventually causes the interior support cross section to reach its maximum moment, M_u^- of 310 kN-m and curvature, φ_u of 8.6E-5 1/mm, Point C: this corresponds to the failure load of 106 kN/m. The moment at the interior support assuming linear-elastic behaviour, M_{el}^-, is 331.3 kN-m from Equation [3.28]. From Equation [3.32], the percentage of moment redistribution at the interior support cross section is 9.8%.

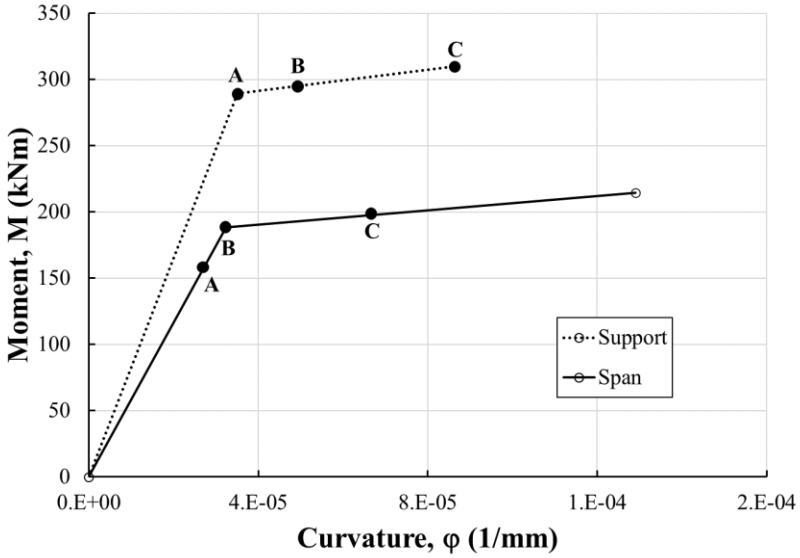

Figure 3.7: Bilinear moment-curvature relationships – Case of complete mechanism

Figure 3.8 shows the associated load-deflection response, with Points A, B and C again corresponding to the formation of the plastic hinge at the support, the formation of the plastic hinge in the spans, and the support reaching its maximum capacity, respectively. The formation of the plastic hinges causes the stiffness of the member to decrease.

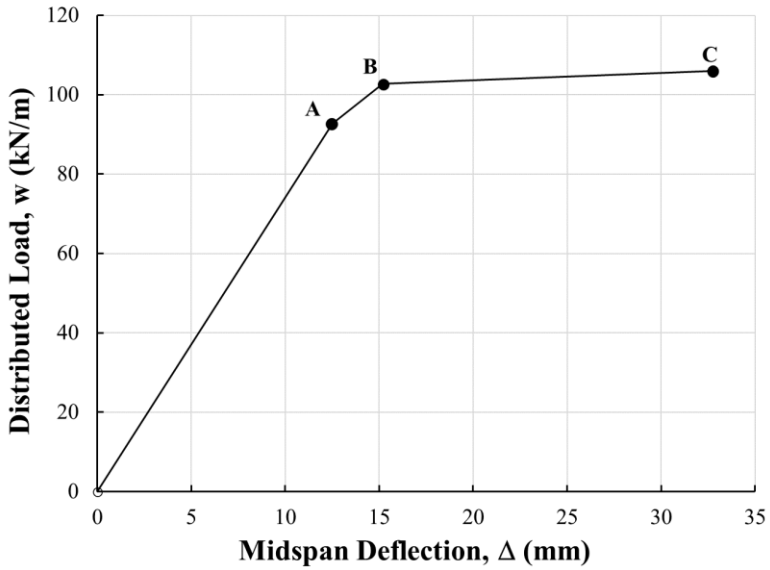

Figure 3.8: Load-deflection response

3.4.2 Case Of Incomplete Plastic Mechanism

The geometry of the cross section, span lengths, and steel and concrete strengths of the previous case are again adopted. The reinforcement areas at the interior support and span sections are 3740 mm^2 and 2300 mm^2 which correspond to ω of 0.26 and 0.16, respectively. Live load is again applied simultaneously on both spans.

Figure 3.9 shows the bilinear moment-curvature responses the span and support cross sections. The first plastic hinge again forms at the interior support, Point A on the figure. When additional load is applied, the maximum moment and curvature is reached at the interior support, Point B, before hinges form at the critical span cross section. The curvature ductility factors, φ_u/φ_y, for the support and span cross sections are 1.2 and 2.5, respectively. The low curvature ductility at the support limits its inelastic rotation capacity, θ_i, at each side of the support which can be quantified as

[3.34] $$\theta_i = \int_0^x \varphi_i dl$$

where x is the half the length of the support plastic hinge and φ_i is the inelastic curvature within the hinge. Equation [3.34] is a simplified approximation as it ignores any tension stiffening that may be taking place within the plastic hinge.

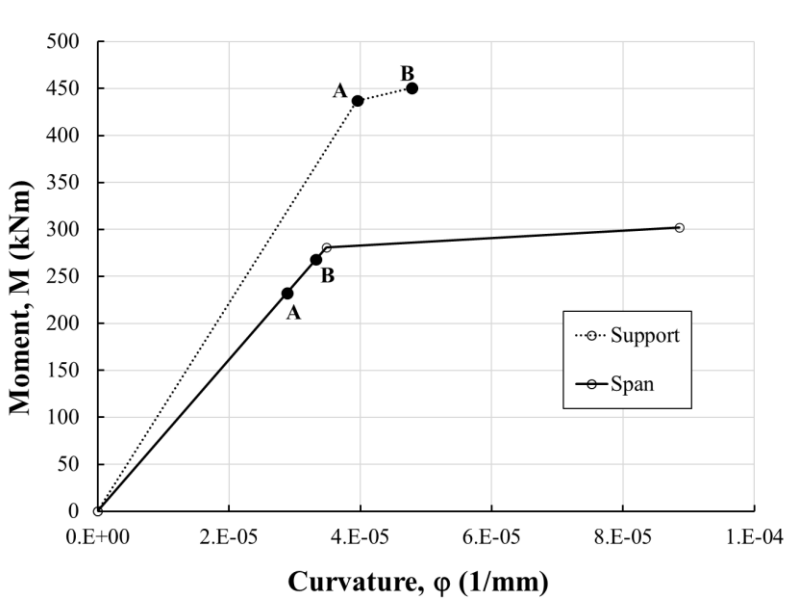

Figure 3.9: Idealized bilinear moment-curvature relationships – Case of incomplete mechanism

Figure 3.10 shows the associated load-deflection response. The response is linear-elastic initially until the plastic hinge forms at the interior support, Point A. The member stiffness is again reduced at greater loads, but the additional deflection that occurs before the interior support section fails, Point B, is marginal.

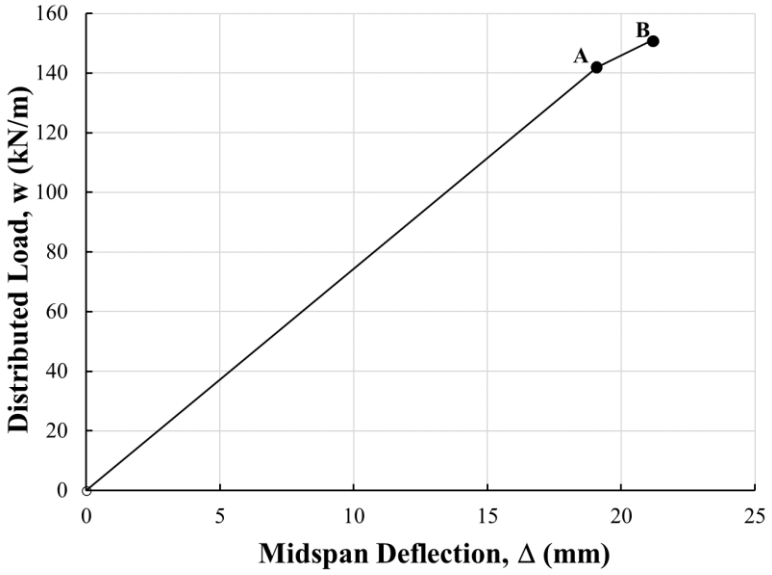

Figure 3.10: Load-deflection response – Case of incomplete mechanism

3.5 PARAMETRIC STUDY

This section presents the results of a detailed parametric analysis. Two steel grades are considered: ASTM A615/615M Grade 100 (690 MPa) (ASTM 2020) and A706/706M Grade 60 (420 MPa) (ASTM 2016). These grades are selected because they have relatively low and high curvature ductilities, respectively, for a given ω (discussed in Chapter 2). Two concrete compressive strengths are considered: f_c' of 30 and 70 MPa.

Figures 3.11 and 3.12 show the variation of the percentage of moment redistribution with the mechanical reinforcement ratio, ω, for the two steel grades and f_c' of 30 and 70 MPa, respectively. When the live load is on one span only, any difference due to the two steel grades is negligible because a full plastic collapse mechanism develops in all cases irrespective of f_c'. The first plastic hinge forms in the span section, which has less reinforcement and so is more ductile than the support section. The support section yields and reaches its ultimate capacity first. When the live load is on both spans, a full plastic mechanism forms if the mechanical reinforcement ratio of the support section, ω, is less than approximately 0.25 or 0.2 for $f_c^{'}$ of 30 or 70 MPa, respectively, as seen in Figures 3.11 and 3.12. The influence of the steel grade on the moment redistribution percentage is negligible if a full plastic collapse mechanism develops. For greater ω values, the inelastic rotation capacity of the plastic hinge at the support is reached, a full plastic collapse mechanism does not form, and the moment redistribution percentage is reduced. The reduced moment redistribution percentage is particularly evident for the ASTM A615/615M Grade 100 steel whether f_c' is 30 MPa, Figure 3.11, or 70 MPa, Figure 3.12.

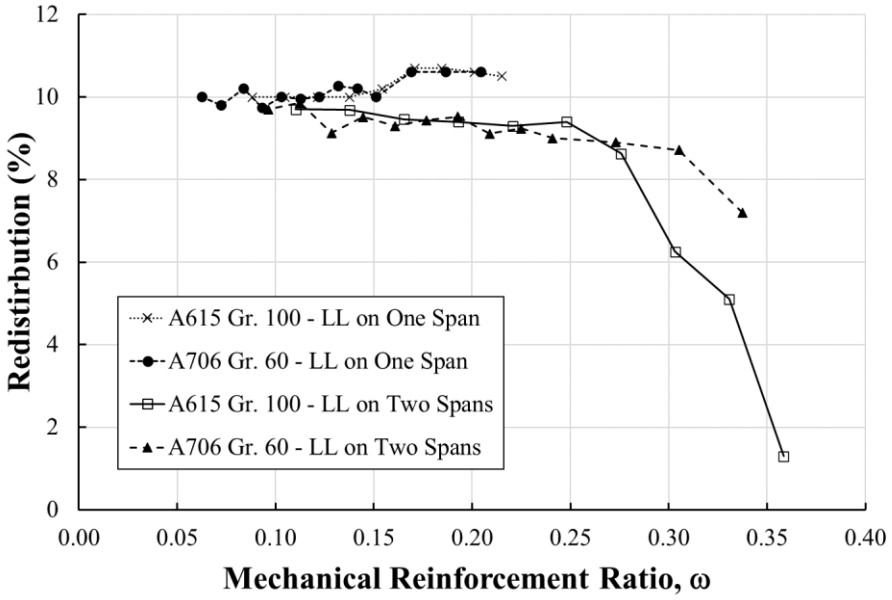

Figure 3.11: Moment redistribution for ASTM A615/615M Grade 100 and ASTM A706/706M Grade 60 (f_c'=30 MPa)

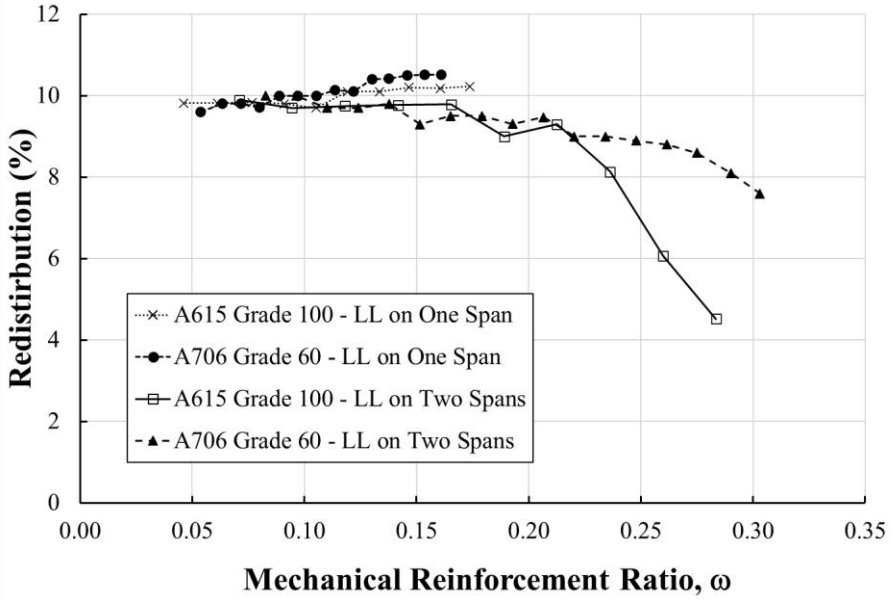

Figure 3.12: Moment redistribution for ASTM A615/615M Grade 100 and ASTM A706/706M Grade 60 (f_c'=70 MPa)

Figure 3.13 shows the idealized bilinear moment-curvature relationships for both steel grades at the interior support and span cross sections for f_c' of 70 MPa. For both steel grades, ω at the interior support is 0.25 so an incomplete mechanism is formed. The yielding and ultimate moments and ultimate curvatures for both grades are similar. The yielding curvature, ϕ_y, for the section with A615/615M Grade 100 reinforcement is, however, markedly greater that that for the section with A706/706M Grade 60 reinforcement. This reduces the curvature ductility, the inelastic rotation capacity, and the percentage of moment redistribution. The section reinforced with the higher steel grade has smaller steel area for a given ω value, so the cracked moment of inertia and associated stiffness will be lower.

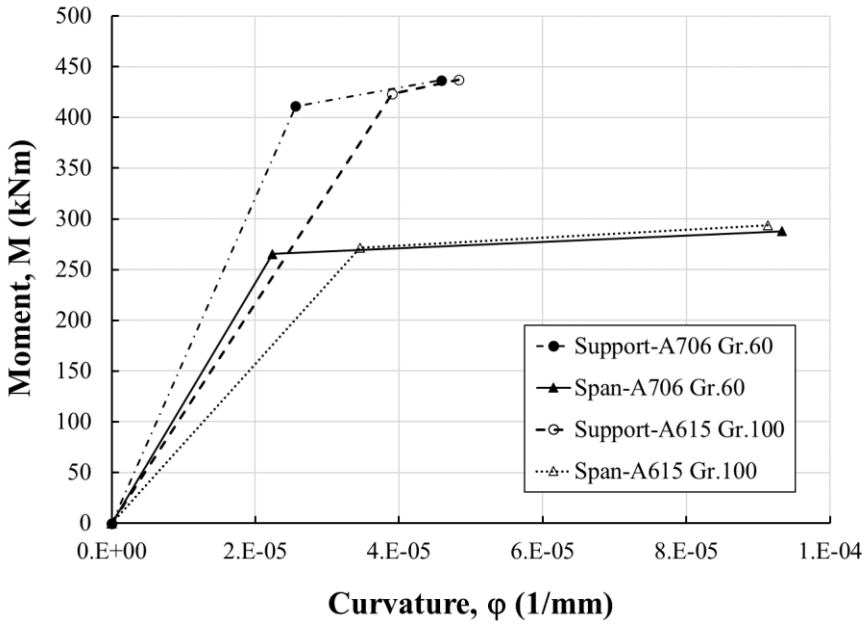

Figure 3.13: Idealized moment-curvature relationships for ω = 0.25, f_c' = 70 MPa

Figure 3.14 shows the variation of moment redistribution percentage for beams reinforced with A615/615M Grade 100 steel when f_c' is 30 and 70 MPa. Figure 3.15 is the companion figure for the A706/706M Grade 60 steel grade. When one span is loaded, a complete mechanism forms for the entire range of ω investigated. The corresponding redistribution percentages are consistent irrespective of the concrete strength or the steel grade. When live load is applied on both spans, a complete collapse mechanism forms for ω less than

approximately 0.20 when the reinforcement is A706/706M Grade 60 and 0.25 when the reinforcement is ASTM A615/615M Grade 100. At greater values of ω, a complete mechanism does not form at failure because the plastic hinge at the interior support fails before the critical span section can yield. When live load is applied on both spans, increasing f_c' stops the complete mechanism formation at a smaller ω value. When live load is applied on one span, a complete collapse mechanism is developed irrespective of f_c' value.

The ultimate extreme fibre concrete strain was limited to 0.0035. The ultimate moment associated with concrete strains exceeding 0.0035 were not investigated. As discussed in Chapter 2, however, the flexural curvature ductility, φ_u/φ_y increases when this limit is ignored. A higher φ_u/φ_y will increase the inelastic rotation capacity at a plastic hinge and the beam will be more likely to develop a complete collapse mechanism.

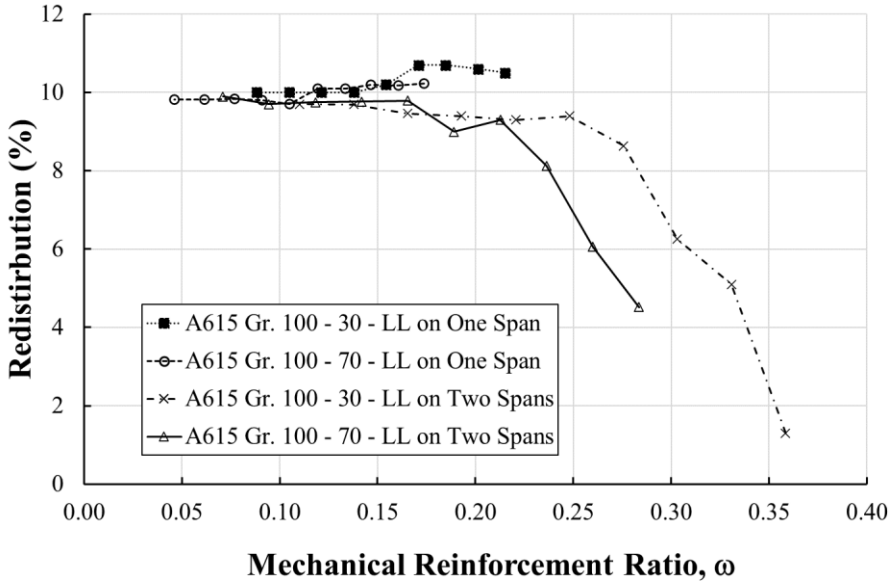

Figure 3.14: Moment redistribution for f_c' of 30 MPa and 70 MPa (ASTM A615/615M Grade 100)

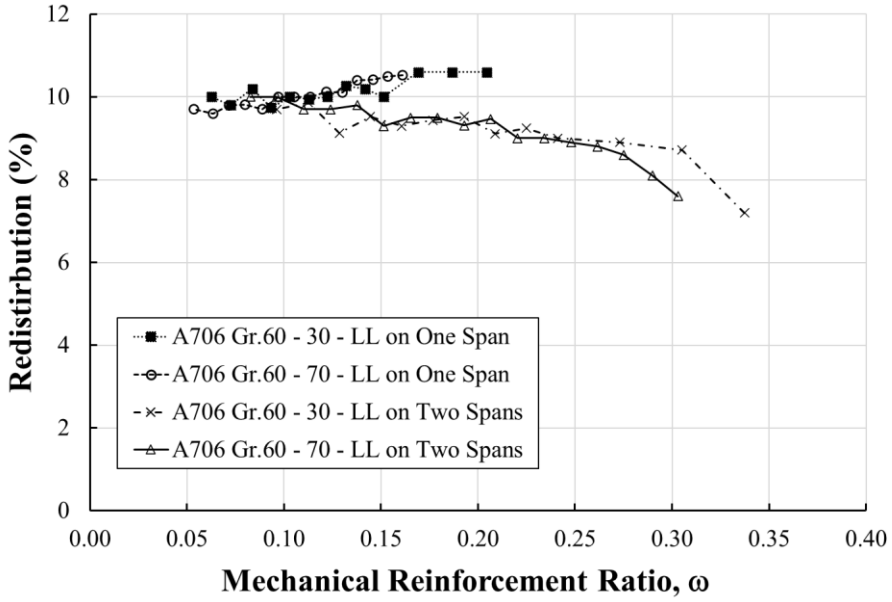

Figure 3.15: Moment redistribution for f_c' of 30 MPa and 70 MPa (ASTM A706/706M Grade 60)

Figure 3.16 shows the bilinear moment-curvature relationships for a beam cross section reinforced with ASTM A615/615M Grade 100 steel and f_c' of 30 and 70 MPa. The ω values are 0.25 and 0.16 for the interior support and span cross sections, respectively. The curvature ductility of the support for an f_c' of 70 MPa is a bit smaller than that for f_c' of 30 MPa. This is due to a reduced flexural stiffness: a reduced A_s lowers I_{cr}, Equation [2.4], and so reduces the cracked flexural stiffness EI_{cr}. Equation [2.5] shows that the yield curvature is a function of the depth of the compression region, k, which reduces as A_s or ρ are reduced. For a given ω, increasing f_c' increases A_s which leads to a greater yielding curvature and a smaller curvature ductility. The smaller curvature ductility for a cross section reinforced with A615/615M Grade 100 steel corresponds to a smaller inelastic rotation capacity at the plastic hinge, so the maximum ω corresponding to a full plastic collapse mechanism is reduced.

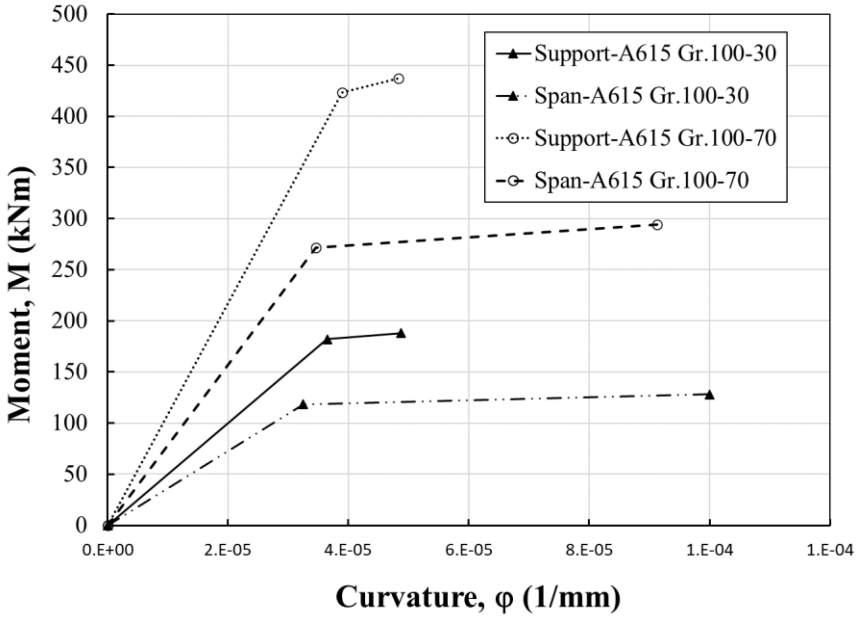

Figure 3.16: Moment-curvature relationships for ASTM A615/615M Grade 100 steel - f_c' of 30 and 70 MPa

3.6 COMPARISON WITH A23.3:19 REQUIREMENTS

In Figures 3.17 a. and b., the maximum permissible redistribution specified in A23.3:19, given by Equation [3.4b], is superimposed on the results from the parametric study for concrete strengths of 30 and 70 MPa, respectively. The A23.3:19 provisions provide a conservative lower bound on the actual moment redistribution percentages for these cases.

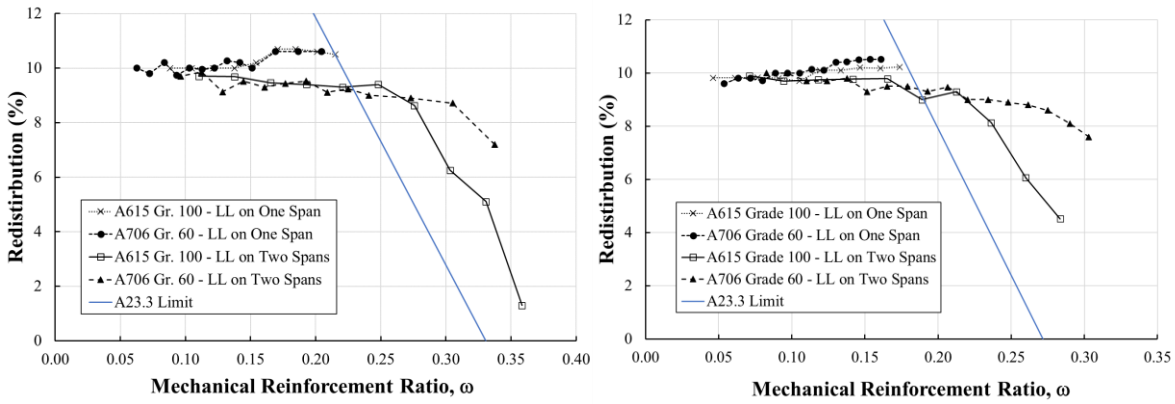

Figure 3.17: Comparison of A23.3:19 maximum redistribution percentage with observed redistribution: (a) f_c'= 30 MPa (b) f_c'= 70 MPa

3.7 IMPACT OF MOMENT REDISTRIBUTION ON SERVICEABILITY LIMIT STATES

At Serviceability Limit States (SLS), the behaviour of the critical moment section is elastic-cracked. The steel stress at SLS is approximately 0.6 f_y (Clause 10.6.2 in A23.3). If a cross section is designed at ULS accounting for moment redistribution, however, the steel area is reduced and the SLS steel stresses will be greater. The crack widths at SLS, which are proportional to the SLS steel stresses will increase. In particular, the steel stress at SLS may markedly exceed the value of 0.6 f_y. In this section, a procedure is presented to determine the maximum permissible redistribution, r_{max}, to satisfy crack width criterion specified in ACI 318:19 (ACI 2019), which are more current than that in A23.3:19 (CSA 2019). The procedure is as follows:

1. Develop an expression that relates the resisting moment to the factored applied dead and live moments, accounting for redistribution. The required resistance, M_r, is

   [3.35] $M_r = M_f^e(1 - r)$

   where r is the reduction of factored moment due to moment redistribution, and M_f^e

is computed using linear-elastic analysis

[3.36] $M_f^e = 1.25M_d + 1.5M_l$

here, M_d and M_l are the moments due to specified dead and live loads, respectively and load factors 1.25 and 1.5 are from the National Building Code of Canada (NBCC 2015). For $K = M_l/M_d$, this can be written as

[3.37] $M_f^e = M_d(1.25 + 1.5K)$

Substituting Equations [3.37] into [3.35] to eliminate M_f^e

[3.38] $M_r = M_d(1.25 + 1.5K)(1 - r)$

2. Compute the steel stress at SLS, f_s. Assuming linear-elastic cracked behaviour

[3.39] $$f_s = \frac{\{nM_s(d - kd)\}}{I_{cr}}$$

where: n, the modular ratio, equals E_s/E_c; M_s is the applied service moment; (kd) is the depth of compression zone; and, I_{cr} is the cracked moment of inertia. The depth of the compression zone is computed using Equation [2.3]. Noting that $M_s = M_d + M_l = M_d\,(1+K)$

[3.40] $$M_d = \frac{M_s}{1 + K}$$

Substituting Eq. [3.40] into Eq. [3.38] to eliminate M_d

[3.41] $$M_r = \frac{\{M_s(1.25 + 1.5K)(1 - r)\}}{(1 + K)}$$

Rearranging Equation [3.41] to isolate M_s and substituting this into Equation [3.39] to eliminate M_s yields

[3.42] $$f_s = \frac{n(1 + K)M_r(d - kd)}{(1.25 + 1.5K)(1 - r)I_{cr}}$$

The resisting moment is computed as

[3.43a] $$M_r = \phi_s A_s f_y \left(d - \frac{\phi_s A_s f_y}{2\phi_c \alpha_1 f_c' b} \right)$$

where ϕ_s and ϕ_c are the resistance factors for steel and concrete, respectively. This can be written as

[3.43b] $$M_r = \phi_s \rho f_y \left(1 - \frac{\phi_s \rho f_y}{2\phi_c \alpha_1 f_c'} \right) bd^2$$

From Equation [2.4], the cracked moment of inertia can be expressed as

[3.44] $$I_{cr} = \left[\frac{k^3}{3} + n\rho(1-k)^2 \right] bd^3$$

Substituting Equations [3.43b] and [3.44] into Equation [3.42] to eliminate M_r and I_{cr}

[3.45] $$f_s = \frac{(1 + K)}{(1.25 + 1.5K)} \frac{f_y}{(1 - r)} \frac{\phi_s \rho \left(1 - \frac{\phi_s \rho f_y}{2\phi_c \alpha_1 f_c' bd} \right) (1 - k) n}{\frac{(k^3)}{3} + n\rho(1 - k)^2}$$

3. Determine the maximum permissible steel stress, $f_{s,max}$ which satisfies the crack width criteria in ACI 318:19 (ACI 2019). Article 24.3.2 limits the maximum spacing, s, to the lesser of

[3.46a] $$s < 380 \left(\frac{280}{f_s} \right) - 2.5 c_{cl}$$

or

[3.46b] $$s < 300 \left(\frac{280}{f_s} \right)$$

where f_s is in MPa and the clear cover, c_{cl}, is in mm. These equations can be written

in terms of maximum steel stress, $f_{s,max}$, for a given spacing as

[3.47a] $$f_{s,max}=\frac{380\times280}{s+2.5c_{cl}}$$

or

[3.47b] $$f_{s,max}=\frac{380\times280}{s}$$

The variation of $f_{s,max}$ with spacing, s, is shown in Figure 3.18.

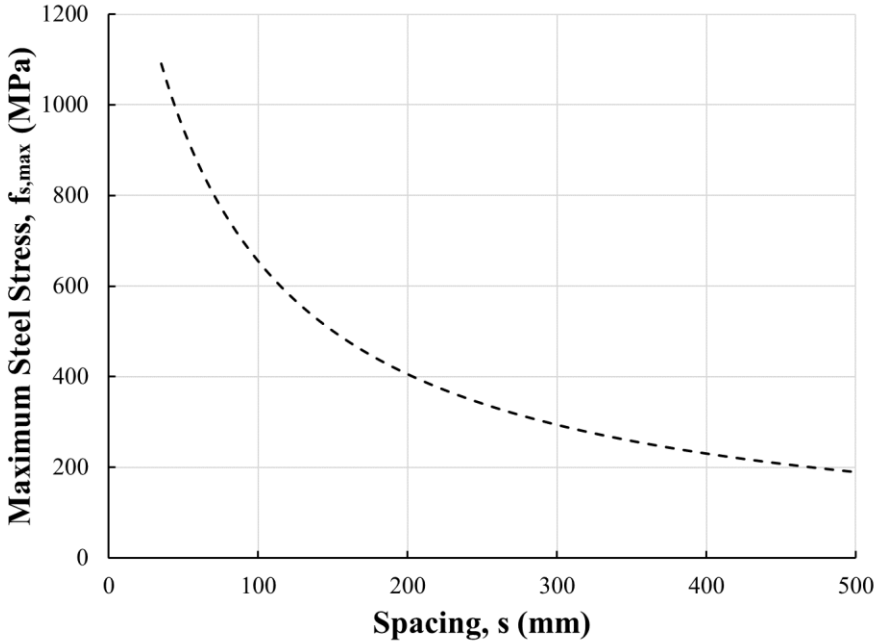

Figure 3.18: Maximum steel stress for given reinforcement spacing (ACI 2019)

4. Determine the maximum permissible redistribution, r_{max} for a given spacing, s, and clear cover, c_{cl}.

    a. Substitute the givens, s and c_{cl}, into Equations [3.47a] and [3.47b] and take $f_{c,max}$ to be the smaller of the two values.

    b. Substituting $f_{c,max}$ into Equation [3.44] and solve for r_{max}. This is computed as

$$\textbf{[3.48]}\ r_{max} = \frac{(1 + K)}{(1.25 + 1.5K)} \frac{f_y}{f_{s,max}} \frac{\phi_s \rho f_y \left(1 - \frac{\phi_s \rho f_y}{2\phi_c \alpha_1 f_c'}\right)(1 - k)n}{\frac{(k^3)}{3} + n\rho(1 - k)^2}$$

Figure 3.19 shows the variation of r_{max} with ρ for ASTM A706/706M Grade 60 and ASTM A615/615M Grade 100 reinforcement, bar spacings of 100 mm and 250 mm, f_c' of 30 MPa, and a clear cover of 25 mm. The maximum redistribution for each steel grade is also shown. It is clear that the maximum redistribution is markedly less for the higher strength, A615/615M Grade 100 steel. It is also clear that the designs that satisfy the A23.3:19 limit will be satisfactory for some combinations of steel grade, concrete strength, reinforcement ratio, and spacing, such as the two relationships for bar spacings of 100 mm. Other design, however, will exhibit unsatisfactory crack widths at other combinations of these variables, such as the two relationships for bar spacings of 250 mm. Thus, it is required that Clause 9.2.4 of A23.3:19 be revised to require that crack widths should be checked using the computed reinforcing steel stress at SLS, f_s, at any cross section where the reinforcing steel area has been reduced using moment redistribution.

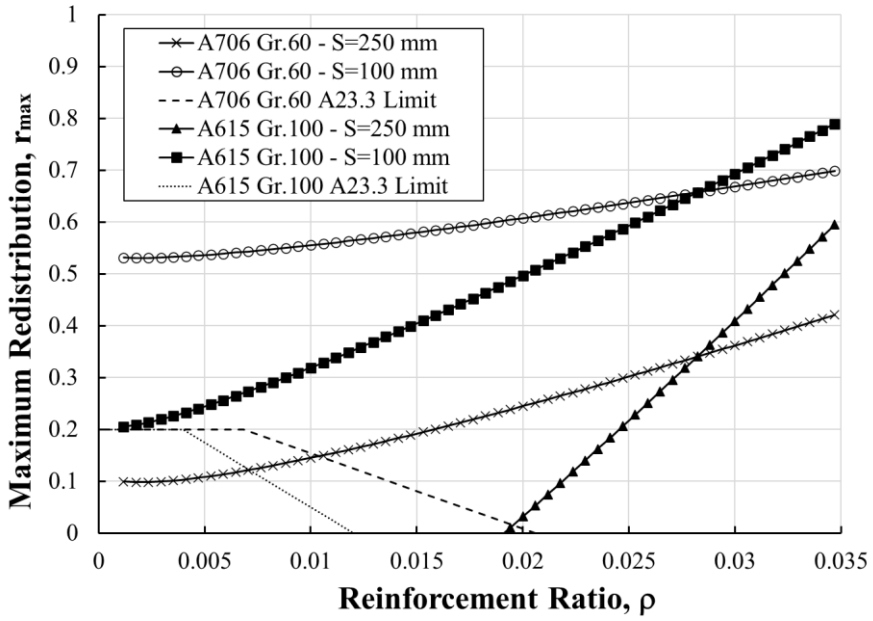

Figure 3.19: Variation of maximum permissible redistribution with reinforcing ratio, ρ

3.8 SUMMARY AND CONCLUSION

The objective of the research presented in this chapter was to verify whether beams reinforced with High Strength Reinforcement, with a specified yield stress greater than 500 MPa, complies with the current redistribution limits given in Clause 9.2.4 of CSA Standard A23.3:19 “Design of Concrete Structures”. A parametric study investigated the effect of using ASTM A615/615M Grade 100 or ASTM A706/706M Grade 60 reinforcement on the moment redistribution exhibited by a two-span beam that is continuous over the internal support. Concrete compressive strengths of 30 and 70 MPa were considered and loading cases with the live load on one span only or on both spans were investigated. The impact of Serviceability Limit State on the maximum permissible redistribution was also investigated.

The parametric study for at Ultimate Limit State essentially required three steps. First, the flexural reinforcement area at critical span cross section was determined given the corresponding interior support reinforcement area. Second, an idealized bilinear moment-

curvature relationship was determined for these cross sections using the programming code described in Section 2.3.3. Finally, nonlinear analysis was conducted in SAP2000 (Computers & Structures Inc., 2020) using the computed curvatures and moments at yield and ultimate input and the moment redistribution was quantified. This procedure was repeated for different internal support reinforcement ratios.

The impact of moment redistribution at Serviceability Limit State (SLS) was investigated by determining the maximum permissible redistribution, r_{max}, using the maximum steel stress, $f_{s,max}$ as given in ACI 318:19 to satisfy crack widths, given a reinforcement spacing, s, and a clear cover, c_{cl}.

The following conclusions are drawn:

1. If a full plastic collapse mechanism forms at member failure, the moment redistribution percentage is independent of the grade and quantity of the steel reinforcement.

2. If the first hinge to form has insufficient inelastic rotation capacity, it will fail locally before a full plastic collapse mechanism forms.

3. The curvature ductility factor, ϕ_u/ϕ_y, and inelastic rotation capacity reduce as the mechanical reinforcement ratio, ω increases. Thus, the maximum permitted redistribution must reduce for beams with increasing ω values.

4. A beam reinforced with High Strength Reinforcement will have a lower curvature ductility factor than a beam with the same ω reinforced with conventional reinforcement. The maximum permissible moment redistribution is therefore less. The magnitudes of the ultimate curvature, ϕ_u, are similar at a given ω but the yield curvature, ϕ_y, of the beam reinforced with HSR can be markedly greater because the steel area and cracked section modulus are less.

5. For the cases investigated, the current provisions of Clause 9.2.4 in CSA A23.3:19 are conservative with respect to the maximum redistribution permitted.

6. The maximum moment redistribution permissible can be limited to ensure that the crack widths at critical cross sections at SLS are acceptable. If the steel area is reduced by accounting for moment redistribution at Ultimate Limit State, it is recommended that crack widths be checked at these cross sections using the computed steel stress at SLS, instead of assuming a value of $0.6f_y$, as is currently permitted in A23.3:19.

Chapter 4

4 Deflections In Concrete Beams Reinforced with High Strength Steel

4.1 INTRODUCTION

Figure 4.1 shows the instantaneous and long-term midspan deflection history of a simply supported beam over its 25-year lifetime. The beam has a width of 200 mm, a height of 360 mm, and spans 5000 mm. It has a concrete compressive strength, f_c', of 50 MPa, steel reinforcement yield stress, f_y, of 500 MPa, a midspan reinforcement ratio, ρ, of 0.6% and live-to-dead load ratio of 1. The moments due to the beam's own weight, superimposed dead load, sustained live load and transient live load are 16.5, 1.8, 4.6 and 13.8 kNm, respectively. The ultimate shrinkage strain, ε_{shu}, is taken as 780 microstrain (CAC 2016), the ultimate creep coefficient, C_u, is taken as 2.35 and the associated correction factor, Q_{cr}, is taken as 1. The deflections include deflection due to shrinkage, Δ_{sh}; instantaneous and long term (creep) deflections due to the beam's own weight, $\Delta_{OW,i}$, and $\Delta_{OW,c}$, respectively; instantaneous and long term (creep) deflections due to superimposed dead load, $\Delta_{SDL,i}$ and $\Delta_{SDL,c}$, respectively; instantaneous and long term (creep) deflections due to sustained live load, $\Delta_{SLL,i}$ and $\Delta_{SLL,c}$, respectively; and, instantaneous deflection due to transient live loads, $\Delta_{LL,i}$. The total deflection, Δ_t, is 29 mm, or $L_n/172$, after 25 years where L_n is the clear span length. Table 9.3 of A23.3:19 (CSA 2019) limits "that part of the total deflections occurring after the installation of non-structural elements" to $L_n/480$ or $L_n/240$ for non structural elements that are likely or not likely to be damaged by large deflections, respectively. If the non-structural elements are assumed to contribute to the superimposed dead load, this incremental deflection, Δ_{inc}, that occurs after the superimposed dead load is added, in this case 14 mm, is checked against the $L_n/480$ or $L_n/240$ limit.

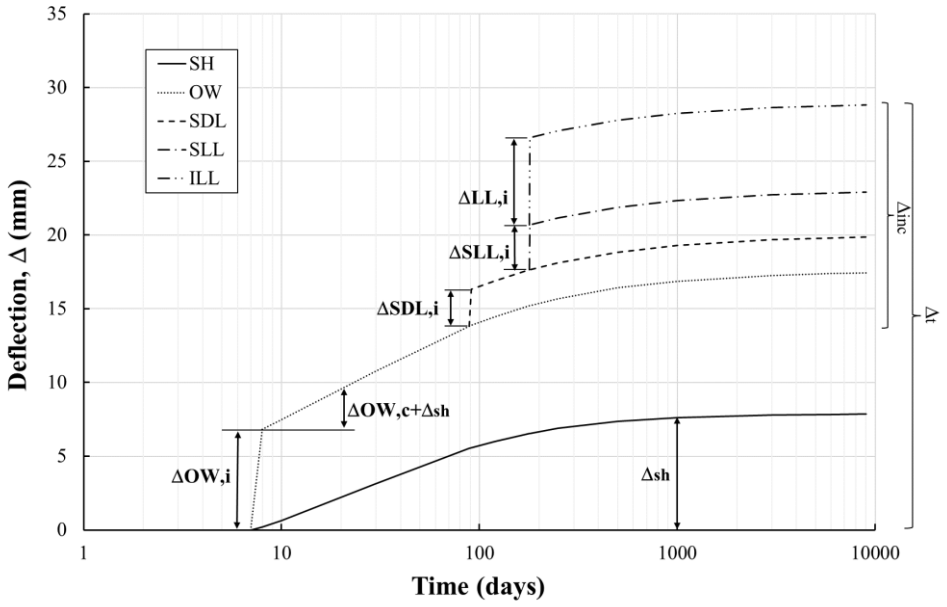

Figure 4.1:Beam midspan deflections

The incremental deflection that occurs after the SDL is applied can be computed as

[4.1] $\Delta_{inc} = (1 - \tau_s)\,\Delta_{sh} + (1 - \tau_c)\,\Delta_{OW,c} + \Delta_{SDL,c} + \Delta_{SLL,c} + \Delta_{SLL,i} + \Delta_{LL,i}$

where τ_c is the fraction of the total creep deflection that occurs in the time interval, t_{dse}, between the application of the own weight and superimposed dead loads. Similarly, τ_s is the fraction of the total shrinkage deflection that occurs in the time interval 't' between the end of moist curing and the time of application of the superimposed dead load. These fractions can be computed using the following equations (CAC 2016)

[4.2] $$\tau_c = \frac{t_{dse}^{0.6}}{10 + t_{dse}^{0.6}}$$

and

[4.3] $$\tau_s = \frac{t}{C_s + t}$$

According to the *CAC Concrete Design Handbook* (CAC 2016), C_s is taken as 35 for concrete subjected to 7 days of moist curing or 55 for concrete subjected to 1 to 3 days of steam curing.

As shown in Figure 4.1, instantaneous deflections in reinforced concrete beams are due to the beam's own weight, the superimposed dead load, and the live load. The long-term deflections are due to shrinkage, particularly for beams with different reinforcement areas in the tension and compression regions, and creep due to own weight, superimposed dead loads, and sustained live loads.

CSA A23.3:19 Table 9.2 specifies a minimum height, h_{min}, for beams that are simply supported, or have one or both ends continuous. If the beam height is less than this limit, deflections must be computed and compared with the limits specified in Table 9.3. The values listed in Table 9.2 pertain to beams reinforced with steel that has a minimum specified yield strength f_y of 400 MPa. For higher yield strengths, h_{min} is increased by the factor $(0.4 + f_y/670)$, where f_y has units of MPa.

4.1.1 Objectives

The objectives of the research reported in this chapter are as follows:

1. Determine whether beams with high strength reinforcement (HSR) that just satisfy the h_{min} limit in Table 9.2 have long-term incremental deflections less than $L_n/240$. This objective is necessary because:

    a. HSR reduces the steel area needed to achieve a given factored moment resistance M_r.

    b. A reduced steel area reduces the cracked moment of the inertia of beam cross section, I_{cr}, and so reduces the cracked flexural rigidity E_cI_{cr} and effective cracked flexural rigidity E_cI_e.

    c. A smaller flexural rigidity causes increased deflections under specified loads.

2. Investigate whether the height correction factor, s_f, can be relaxed while still satisfying the $L_n/240$ deflection limit in A23.3. This is important because reducing the beam height can reduce construction costs.

4.1.2 Chapter Outline

The objective of this chapter is to check if current deflection criteria are adequate for HSR, which requires computing deflections for beams with high yield stress reinforcements. Chapter 4.2 therefore calculates the instantaneous, creep, and shrinkage deflections using Gilbert's method (Gilbert 2011).

Section 4.3 shows the method for calculating the associated dead loads, consisting of a beam's own weight and superimposed dead load, and the live loads, consisting of the applied sustained live load and other transient live loads.

Section 4.4 carries out a preliminary investigation, showing the effects of changing several variables on the service load moments and flexural rigidity of the beam. A sensitivity analysis is then conducted to determine how the incremental deflections vary with concrete compressive strengths, reinforcing steel yield stresses, end support conditions, and ratios of applied live to dead loads. A minimum height correction factor is specified in A23.3:19 to increase beam height as the reinforcing steel yield stresses are increased. The sensitivity analysis results are therefore presented for two cases: this factor is applied in the first set of results and subsequently ignored in the second set of results. The deflections are computed for simply supported beams, and two- and three-span beams that are continuous over the interior support(s).

Section 4.5 refines the minimum height correction factor for beam configurations with a specified steel yield stress, ratio of service live-to-dead loads, and for varying concrete compressive strengths and reinforcement ratios.

Section 4.6 summarizes the chapter and lists the conclusions.

4.2 METHOD FOR CALCULATING DEFLECTIONS

Gilbert's (2011) method was used to compute instantaneous, creep, and shrinkage deflections. Table 4.1 shows the loading and concrete strength development history assumed for the analyses. The concrete compressive strength is assumed not to increase after it reaches its specified 28-day strength, f_c'.

Table 4.1: Loading and concrete strength development history

Concrete age (Days)	**Load type at given age**	**Strength as fraction of f_c'**
7	Own Weight	75
90	Superimposed Dead Load	100
180	Sustained Live Load	100
180+	Instantaneous Live Load	100

To compute the effective moment of inertia, I_e, A23.3:19 uses an equation involving a moment, M_a, defined as the "maximum moment in member at load stage at which deflection is computed or at any previous load stage". It is assumed that the maximum moment occurs during construction and equals the moment due to the specified own weight, superimposed dead, and live loads.

Figures 4.2a and 4.2b show the application of live load to single spans of the two- and three-span beams, respectively. This "patterned" loading arrangement maximizes the deflections in the spans that carry the live loads.

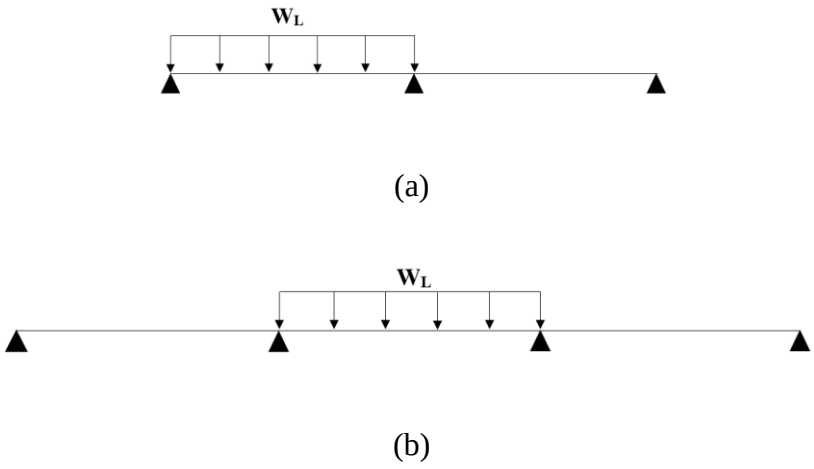

Figure 4.2: Live load application in continuous beams: (a) Two-span beam (b) Three-span beam

The steps in the deflection calculation are as follows:

1. Determine the gross cross section area, A_c, centroid, $\bar{y}_c$, and moment of inertia, I_g, assuming a rectangular cross section. Let 'b' be the beam cross section width, and 'h' be the minimum cross section height as determined from Table 9.2 in A23.3:19. Then

   [4.4] $A_c = bh$

   [4.5] $\bar{y}_c = \frac{h}{2}$

   [4.6] $I_g = \frac{bh^3}{12}$

2. Determine the modular ratio and rupture stress of the concrete when it is 7 or 28 days old

   a. Modulus of elasticity at 7 days, $E_{c,7}$

      [4.7] $E_{c,7} = 4500\sqrt{f_{c,7}}$

where $f_{c,7}$ is the concrete compressive strength at age 7 days and ranges between 20 and 40 MPa.

Modulus of elasticity at 28 days (and older ages), $E_{c,28}$

[4.8] $E_{c,28} = 4500\sqrt{f'_c}$

where f'_c is the concrete compressive strength at age 28 days and ranges between 20 and 40 MPa.

b. Modular ratio at 7 days, n_7

[4.9] $n_7 = \frac{E_s}{E_{c,7}}$

where E_s is the young's modulus for steel.

Modular ratio at 28 days (and older ages), n_{28}

[4.10] $n_{28} = \frac{E_s}{E_{c,28}}$

c. Rupture stress at 7 days, $f_{r,7}$

[4.11] $f_{r,7} = 0.6\sqrt{f_{c,7}}$

Rupture stress at 28 days (and older ages), $f_{r,28}$

[4.12] $f_{r,28} = 0.6\sqrt{f'_c}$

In accordance with the assumed loading history shown in Table 4.1, deflections due to shrinkage and own weight (instantaneous and creep) are based on the 7-day modular ratio and rupture stress (Equations [4.9] and [4.11], respectively). All other deflections are computed using the 28-day values, Equations [4.10] and [4.12], respectively.

4.2.1 Instantaneous Deflection

The method to compute instantaneous deflections involves four steps, as follows:

1. Determine the transformed cross section area, centroid, and moment of inertia of the uncracked section.

    a. Find the transformed area, A_t. Let 'A_s' be the steel tensile reinforcement area

    [4.13] $A_t = A_c + (n - 1)A_s$

    b. Find the transformed centroid, $\bar{y}_t$. Let 'd' be the effective depth of the reinforcing steel

    [4.14] $$\bar{y}_t = \frac{A_c\bar{y}_c + (n - 1)A_s d}{A_t}$$

    c. Find the transformed moment of inertia, I_t

    [4.15] $$I_t = I_c + A_c(\bar{y}_t - \bar{y}_c)^2 + (n - 1)A_s(d - \bar{y}_t)^2$$

2. Determine the cracked moment of inertia, I_{cr}

    [4.16] $$I_{cr} = \frac{b(kd)^3}{3} + nA_s(d - kd)^2$$

    where (CAC 2016)

    [4.17] $$kd = \frac{\sqrt{2db + 1} - 1}{B}$$

    and

    [4.18] $$B = \frac{b}{nA_s}$$

3. Determine the effective moment of inertia and instantaneous curvatures:

    a. Find the cracking moment, M_{cr}

[4.19] $M_{cr} = \frac{f_r I_t}{h - \bar{y}_t}$

b. Find the effective moment of inertia, I_e, using the Bischoff Equation (Bischoff 2007)

[4.20] $I_e = \frac{I_{cr}}{1 - 0.5\left(1 - \frac{I_{cr}}{I_t}\right)\left(\frac{M_{cr}}{M_a}\right)^2} < 0.6I_t$

The requirement that I_e be less than $0.6I_t$ is recommended by Gilbert (2011).

c. Compute instantaneous midspan curvature, φ_m

[4.21] $\varphi_m = \frac{M}{E_c I_e}$

where M is the applied moment due to the specified load, M_{ow}, M_{SDL} or M_{LL} for own weight, superimposed dead load, or live load, respectively.

4. Find the instantaneous deflection, Δ_i

[4.22] $\Delta_i = \frac{L_n^2}{96}\left(\varphi_l + 10\varphi_m + \varphi_r\right)$

where φ_l is the curvature at the left support, φ_m is the curvature at midspan, and φ_r is the curvature at the right support. As the moments (and curvatures) at the ends of a simply supported beam are zero, Equation [4.22] simplifies to

[4.23] $\Delta_i = \frac{L_n}{96}\left(10\varphi_m\right)$

4.2.2 Creep Deflection

The method to compute creep deflections due to sustained loads is presented in the three steps below. Creep is quantified using an ultimate creep coefficient, C_u, that ranges between 1.3 and 4.15 (CAC 2016). This value is modified by correction factors Q_{cr} that account for the age at loading, t_0, relative humidity, volume/surface area ratio and other factors (CAC 2016).

5. Find curvature weights, ζ, based on the long-term cracking moment, $M_{cr}(t)$

   [4.24] $M_{cr}(t) = 0.7M_{cr}$

   [4.25] $\zeta = 1 - \left(\frac{M_{cr}(t)}{M_a}\right)^2$

6. Find the uncracked and cracked creep curvatures, $\varphi_{c,un}$ and $\varphi_{c,cr}$, respectively, and compute average creep curvature at midspan, $\varphi_{avm,c}$

   [4.26] $\varphi_{c,un} = 1 + (45\rho - 900\rho^2)(1 + \frac{\rho'}{\rho})$

   where ρ and ρ', are the tension and compression reinforcement ratios, respectively.

   [4.27] $\varphi_{c,cr} = \frac{0.48}{\sqrt{\rho}}\frac{I_{cr}}{I_e}^{0.33}\left(1 + (125\rho + 0.1)\left(\frac{\rho'}{\rho}\right)^{1.2}\right)$

   [4.28] $\varphi_{avm,c} = \left(\frac{\zeta}{\varphi_{c,cr}} + \frac{1 - \zeta}{\varphi_{c,un}}\right)\varphi_m Q_{cr} C_u$

   where φ_m is the instantaneous midspan curvature calculated using Equation [4.21].

7. Compute the creep deflection, Δ_c, using Equation [4.22]. For a simply supported beam, the curvatures at the ends due to creep, $\varphi_{avl,c}$ and $\varphi_{avr,c}$ are zero so

[4.29] $\Delta_c = \frac{L_n^2}{96}\left(10\varphi_{avm,c}\right)$

For live load applied on a two-span beam, Figure 4.2a, the instantaneous and creep curvature at the left support, φ_l, is 0, midspan curvature, φ_m, is calculated using Equation [4.21], and right support curvature, φ_r, is calculated by substituting the applied moment at the interior support into 'M' in Equation [4.21]. For live load applied on a three-span beam, Figure 4.2b, the instantaneous and creep curvatures at the left and right support are the same due to symmetry and midspan curvature is calculated separately using the same procedure as that for the two-span beam.

4.2.3 Shrinkage Deflection

The method to compute the shrinkage deflection, Δ_{sh}, is presented in the following two steps. The ultimate shrinkage strain, ε_{shu}, is taken as 780 microstrain (CAC 2016).

8. Determine the uncracked and cracked shrinkage curvatures, $\varphi_{sh,un}$ and $\varphi_{sh,cr}$, respectively, and compute average curvature due to shrinkage, $\varphi_{avm,sh}$

[4.30] $\varphi_{sh,un} = (100\rho - 2500\rho^2)\left(\frac{2d}{h} - 1\right)\left(1 - \frac{\rho'}{\rho}\right)^{1.3}\frac{\varepsilon_{shu}}{h}$

[4.31] $\varphi_{sh,cr} = 1.2\left(\frac{I_{cr}}{I_e}\right)^{0.67}(1 - 0.5\frac{\rho'}{\rho})\frac{\varepsilon_{shu}}{d}$

[4.32] $\varphi_{avm,sh} = \zeta\varphi_{sh,cr} + (1 - \zeta)\varphi_{sh,un}$

9. Find shrinkage deflection, Δ_{sh}. The curvature due to shrinkage is constant along the span of a simply supported beam assuming that the steel tensile reinforcement is continuous from left end support to the right end support. Thus

[4.33] $\Delta_{sh} = \frac{L_n^2}{96}\left(\varphi_{avl,sh} + 10\varphi_{avm,sh} + \varphi_{avr,sh}\right)$

where $\varphi_{avl,sh}$, $\varphi_{avm,sh}$, and $\varphi_{avr,sh}$ are the shrinkage curvatures at the left support, midspan, and right support, respectively. Since these shrinkage curvatures are equal for a simply supported beam, Equation [4.33] simplifies to

[4.34] $$\Delta_i = \frac{L_n^2}{96}\left(12\varphi_{avm,sh}\right)$$

The shrinkage curvatures at the left support and midspan of a two-span beam under the loading illustrated in Figure 4.2a are the same while the shrinkage curvature at the right support is computed separately. In a three-span beam, Figure 4.2b, the shrinkage curvatures at the left and right supports are the same due to symmetry while the midspan shrinkage curvature is computed separately.

4.3 METHOD TO DETERMINE LIVE AND DEAD LOADS

4.3.1 Simply Supported Beams

The midspan reinforcement ratio is chosen and corresponding moment capacity, M_r, is determined according to A23.3:19 (CSA 2019) using the concrete stress block approximation. Live and dead loads are determined after computing the corresponding specified moments at the critical sections according to CSA A23.3:19. The load combination used is

[4.35] $M_r = 1.25M_d + 1.5M_l$

Expressing the ratio of live to dead load moments as K, Equation [4.35] can be expressed as

[4.36] $M_r = M_d(1.25 + 1.5K)$

The dead load moment is therefore

[4.37] $$M_d = \frac{M_r}{(1.25 + 1.5K)}$$

The live load moment is

$$\textbf{[4.38]}\ M_l = \frac{M_r - 1.25M_d}{1.5}$$

4.3.2 Continuous Beams

The reinforcement ratio at an interior support and corresponding moment capacity, M_r^-, are determined. The associated applied factored uniformly distributed load, w_f, is calculated using the approximate moment coefficients in Table 9.1 of A23.3:19. For a two-span beam that is continuous over the interior support

$$\textbf{[4.39]}\ w_f = \frac{M_r^- L^2}{9}$$

For a three-span beam, the w_f corresponding to the moment at the first interior support is (CAC 2019)

$$\textbf{[4.40]}\ w_f = \frac{M_r^- L^2}{10}$$

The dead load is therefore

$$\textbf{[4.41]}\ w_d = \frac{w_f}{(1.25 + 1.5k)}$$

The live load, w_l, is Kw_d. The loads from the approximate moment coefficients are the used to calculate the corresponding in-service linear-elastic live and dead load moments given in Table 4.2 for the critical interior support(s) and span sections.

Table 4.2: Linear-elastic moment summary for 2-span and 3-span beams continuous over interior support(s)

Span	M_d interior sup.	M_d span	M_l interior sup.	M_l span
2	$\frac{w_d L^2}{8}$	$\frac{9w_d L^2}{128}$	$\frac{w_l L^2}{16}$	$\frac{49w_l L^2}{512}$
3	$\frac{w_d L^2}{10}$	$\frac{w_d L^2}{40}$	$\frac{w_l L^2}{20}$	$\frac{47w_l L^2}{625}$

The superimposed dead load and own weight moments were assumed to be 10% and 90% of the total dead load computed using Equation [4.41], respectively. The sustained and instantaneous live load moments were assumed to be 25% and 75% of the total live load moment, respectively.

4.4 PARAMETRIC STUDY

4.4.1 Scope

The total and incremental deflections of reinforced beams with heights that satisfy the limits specified in Table 9.2 of A23.3:19 are computed to determine whether these limits are appropriate for beams reinforced with HSR. A total of 288 beams were investigated for the following range of parameters:

- Ratios of specified live to dead loads, K, of 0.5, 1, and 1.5;
- Steel yield strengths, f_y, of 400, 500, 600, and 700 MPa;
- Concrete compressive strengths, f_c', of 30 and 50 MPa (23 and 38 MPa at 7 days);
- Simply supported, two-span continuous, and three-span continuous beams;

- Reinforcement ratios, ρ, of 0.006, 0.009, 0.012, 0.015.

Equations [4.7] and [4.8] are used to determine the modulus of elasticity, E_c, at 7 days, and 28 days, respectively, when f_c' ranges between 20 MPa and 40 MPa as specified in A23.3:19 (CSA 2019). However, these equations are used to find E_c for a f_c' of 50 MPa in this investigation because of their simplicity, and because the error between the actual E_c and the E_c from these equations, when f_c' is 50 MPa, is 1.3%. A Note to Clause 8.6.2 of A23.3:19 cautions that E_c may fluctuate between 80% and 120% of the value computed using Equations [4.7] and [4.8].

The impact of the yield stress correction factor, s_f, on deflections is investigated. The yield stress correction factor is defined in A23.3:19 as

[4.42] $$s_f = 0.4 + \frac{f_y}{670}$$

where f_y is the yield stress in MPa. A higher reinforcement yield stress increases s_f which is then used as a multiplicative factor to determine the minimum beam height for which deflections need not be checked.

Two distinct parametric studies were carried out. The first, described in Section 4.4.2 "Results with Height Correction Factor", determined incremental deflections, Δ_{inc}, and span-to-incremental deflection ratios, L_n/Δ_{inc}, for beams with minimum heights from A23.3:19 Table 9.2 as modified using the height correction factor, Eq. [4.42]. In the second, described in Section 4.4.3 "Results without Height Correction Factor" the minimum heights from A23.3:19 Table 9.2 were not modified, which is equivalent to assuming that s_f equals 1.0 irrespective of the steel yield strength.

Table 4.3 shows the results of a preliminary parametric study conducted to investigate the effects of the listed parameters on h_{min}, nominal moment resistance, M_n, dead load moment, M_d, live load moment, M_l, and I_{cr} as given in Equation [4.16]. The control beam (B1) is simply supported with a midspan ρ of 0.006 which is increased to 0.009 in B_2, f_y of 500 MPa which is increased to 700 MPa in B_3, K of 1 which is increased to 1.5 in B_4, and f_c' of

50 MPa which is reduced to 30 MPa in B_5. The yield stress correction factor given by Equation [4.41] was accounted for in this preliminary study.

Table 4.3: Effects of various parameters on applied moments and cracked moment of inertia

Change	**h_{min} (mm)**	**M_a (kNm)**	**M_d (kNm)**	**M_l (kNm)**	**I_{cr} (mm^4)**
B_1: Control	358	37.9	18.9	18.9	2.1×10^8
B_2: Increase ρ	358	55.4	27.7	27.7	2.9×10^8
B_3: Increase f_y	451	85.7	42.9	42.9	4.5×10^8
B_4: Increase K	358	37.3	14.9	22.4	2.1×10^8
B_5: Reduce f_c'	358	36.7	18.4	18.4	2.6×10^8

Increasing ρ by 50% in B_2 increases the live and dead loads on the beam by 47% but also increases I_{cr} by 38%. These factors counteract each other, so the net effect of increasing ρ by 50% is to increase deflections by roughly 6.5%. Increasing f_y in B_3 by 40% also increases h_{min} by 26%. The combination of these factors increases the live and dead loads by 127% but I_{cr} also increases by 114%. These factors gain counteract, so the effect of increasing f_y by 40% is to increase deflections by approximately 11%. Increasing K by 50% in B_4 increases live loads by 19% and decreases dead loads by 21% while I_{cr} does not change. An increase in K would therefore increase the incremental deflections that occur after the superimposed dead load is applied when the concrete is three months old, due to an increase in live load. The total deflection would be reduced, however, because the smaller dead load reduces the instantaneous and creep deflections due to the own weight and superimposed dead loads. The higher K factor also reduces M_a slightly, by 1.6%, which slightly increases the weight factor Equation [4.25], giving more weight to the cracked curvatures. This reduces the creep deflections but increases the shrinkage deflections slightly. Finally, reducing f_c' by 40% in B_5 reduces the applied dead and live load moments

by 2.6%, reduces the concrete modulus of elasticity by 22.5% and reduces I_{cr} by 23%. The effect of these counteracting factors on the deflections is essentially negligible.

4.4.2 Results With Height Correction Factor

Tables 4.4 and 4.5 show the effects of increasing f_y, ρ, and K on the total and incremental deflections, respectively. The incremental deflections are those that occur after the superimposed dead load is applied when the concrete is assumed to be three months old. The effect of an increase of f_y, ρ, or K on the deflection is represented by +, - or 0, if the deflection is increased, reduced, or unchanged, respectively, when the factor is increased.

Table 4.4: Effect of f_y, ρ or K on total deflection (Height correction factor considered)

Deflection due to	**Increase f_y**	**Increase ρ**	**Increase K**
Shrinkage	-	+	~0
Own weight	+	+	-
Superimposed DL	+	+	-
Sustained LL (creep)	-	+	+
Instantaneous LL (total)	+	+	+

Table 4.5: Effect of f_y, ρ or K on incremental deflection (Height correction factor considered)

Deflection due to	**Increase f_y**	**Increase ρ**	**Increase K**
Shrinkage	-	+	~0
Own weight (creep)	-	+	-
Superimposed DL (creep)	-	+	-
Sustained LL (creep)	-	+	+
Instantaneous LL (total)	+	+	+

4.4.2.1 Shrinkage

Shrinkage deflection is reduced with increasing f_y. This is because the steel area needed to achieve the necessary moment demand is reduced and so reduces the axial stiffness, k_N, of the reinforcing steel, given by

[4.43] $$k_N = \frac{EA}{L}$$

where E_s and A_s are the elastic modulus of the reinforcement, respectively, and L is an arbitrary length. This stiffness reduction causes a reduced restraint of shrinkage deformations and so smaller curvatures due to restrained shrinkage. Conversely, a higher ρ increases shrinkage deflection.

The K value, the ratio of live to dead loads, affects the weight factor, Equation [4.25], because a higher K slightly reduces the total nominal capacity and increases the weight factor. The difference in results is negligible, however, because giving more weight to the cracked curvatures reduces the creep deflections but increases the shrinkage deflections.

4.4.2.2 Own Weight (OW) And Superimposed Dead Load (SDL)

The total deflections due to OW and SDL include both creep and instantaneous deflections. In contrast, the incremental deflections due to OW and SDL include only creep deflections because Δ_{inc} is the deflection that occurs after the concrete is three months old, and so after the OW and SDL loads are applied.

Increasing f_y while maintaining ρ and K constant increases the beam height, the beam depth, and therefore also increases the steel reinforcement area. The applied dead load moments also significantly increase and therefore the instantaneous curvature due to dead load slightly increases, Equation [4.21]. The ratio of long-term cracking moment, Equation [4.24], to total applied moment is reduced which causes the weight factor, Equation [4.25], to marginally increase. The cracked creep curvature, Equation [4.27], increases while the uncracked creep curvature remains constant. This decreases the creep curvature and therefore the creep deflection due to dead load. Hence an increase in f_y increases the

instantaneous dead load deflections and reduce the creep deflections due to dead load if ρ and K are unchanged.

Increasing ρ for a given f_y and K increases dead load moments and therefore the instantaneous deflections due to dead loads. The cracked creep curvature, Equation [4.27], decreases and the creep curvature, Equation [4.28], increases. Hence increasing ρ increases both the instantaneous and creep dead load deflection if f_y and K are unchanged.

Increasing K, while maintaining f_y and ρ constant, increases the live load moments and consequently reduces the dead load moments which reduces dead load deflections.

4.4.2.3 Sustained Live Load (SLL) And Instantaneous Live Load (ILL)

The entries for Sustained Live Load in Tables [4.4] and [4.5] only consider creep deflections. These increases for higher ρ while f_y and K are unchanged, and decrease for higher f_y values when ρ and K are unchanged, as previously stated. Increasing K increases the live load moments and therefore increases the live load deflections.

Figure 4.3 shows the variation of the ratio of effective length to incremental deflection, L_n/Δ_{inc}, with the span reinforcement ratio, ρ, for two-span beams with one end continuous with reinforcing steel f_y of 400 MPa and 700 MPa, K values of 0.5, 1, and 1.5, and f_c' of 30 MPa. For all K values, L_n/Δ_{inc} decreases with increasing ρ. A higher ρ increases the cracked moment of inertia, I_{cr}, and associated flexural rigidity which reduces deflections. In all investigated cases, the deflections meet the requirements of A23.3:19 because L_n/Δ_{inc} is greater than 240 – that is, Δ_{inc} is less than $L_n/240$.

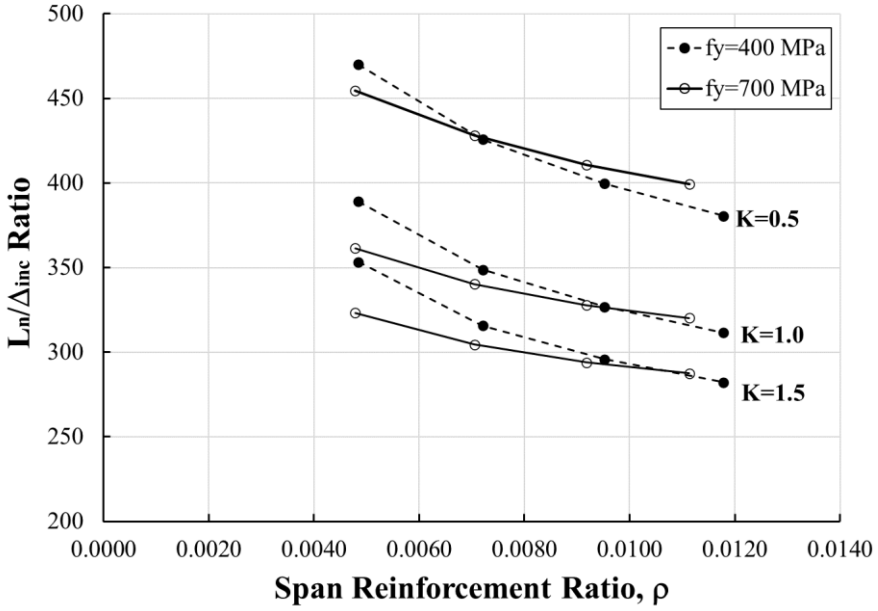

Figure 4.3: Variation of L_n/Δ_{inc} with ρ, two-span beams continuous over interior support

Figure 4A.1 in Appendix 4 is similar to Figure 4.3 but is computed for f_c' of 50 MPa. The higher f_c' increases E_c and the subsequent flexural stiffness but the applied service loads are also slightly increased. The different in deflections due to this change of f_c' is marginal.

Figure 4.4 shows the variation of incremental deflection with span reinforcement ratio for two-span beams that are continuous over the interior support. The analysis considers beams with f_y of 400 MPa and 700 MPa, K of 0.5, 1, and 1.5, and f_c' of 30 MPa. The span lengths are 5 m and the deflections shown are for the span that carries the live load. Increasing ρ increases the factored moment resistance, approximately proportionally, and so increases the service live and dead loads. The greater ρ also increases I_{cr} and I_e, so the overall effect of ρ on Δ_{inc} is relatively slight. A larger K value increases the incremental deflections, as discussed in Section 4.4.1, as the live load increases and so the incremental deflections increase significantly. Differences between f_y are minor: there is roughly a 2 mm difference between the two f_y for the critical case when K = 1.5 and ρ = 0.015. At higher ρ values, a higher f_y is more favourable because the deeper beam actually deflects less.

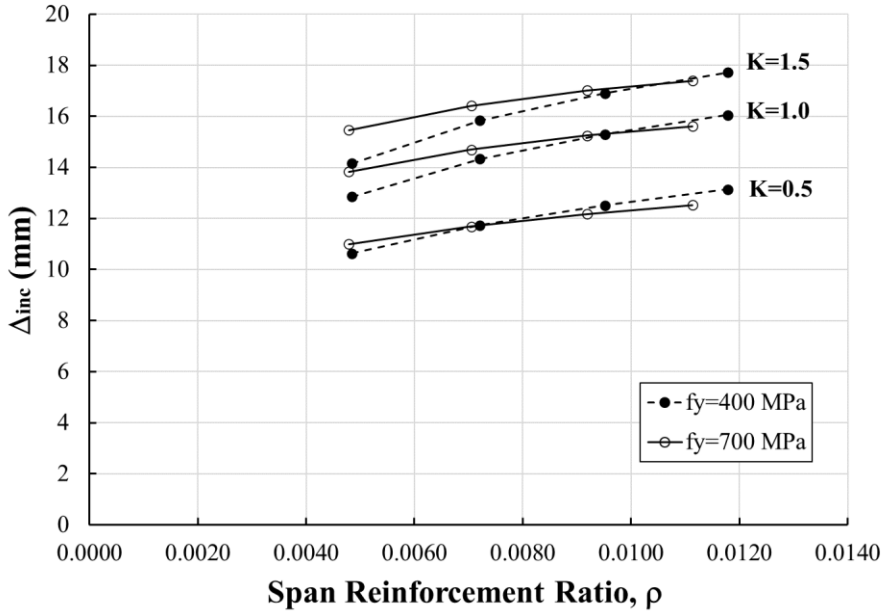

Figure 4.4: Variation of Δ_{inc} with ρ, two-span beams continuous over interior support

Figure 4.5 shows the variation of the ratio of effective length to incremental deflection, L_n/Δ_{inc}, with the span reinforcement ratio, ρ, for a simply supported beam with reinforcing steel f_y of 400 MPa and 700 MPa, K of 0.5, 1, and 1.5, and f_c' of 30 MPa. The deflections shown are slightly larger at smaller ρ values compared those shown in Figure 4.3 and are similar at higher ρ values.

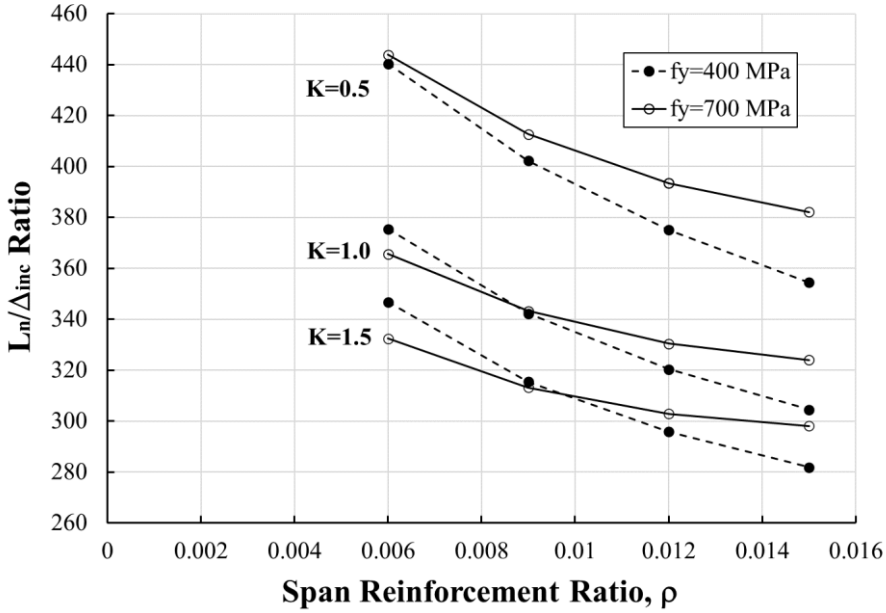

Figure 4.5: Variation of L_n/Δ_{inc} with ρ, simply supported beams

Figure 4.6 shows the variation of the ratio of effective length to incremental deflection, L_n/Δ_{inc}, with the span reinforcement ratio, ρ, for three-span beams continuous at both interior supports. The computations are based on beams with reinforcing steel f_y of 500 MPa and 700 MPa, K values of 0.5, 1, and 1.5, and f_c' of 30 MPa. Equation [4.20], which calculates the effective moment of inertia and states the condition that $0.6I_t$ cannot be exceeded, was not satisfied at low ρ with an f_y of 400 MPa. Hence the lower f_y was set to 500 MPa. The smallest L_n/Δ_{inc} ratio in the figure is 340 which satisfies the limit of 240 specified in A23.3:19.

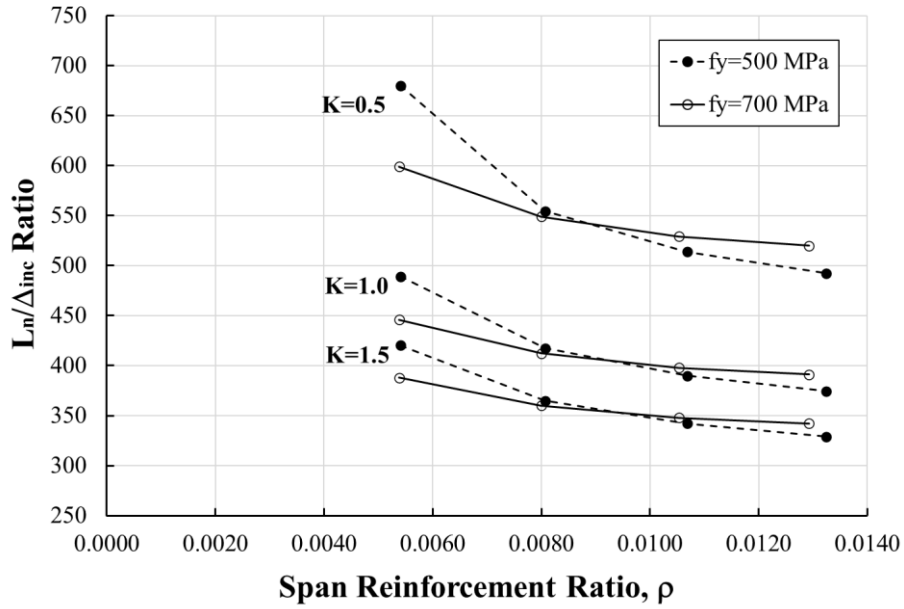

Figure 4.6:Variation of L_n/Δ_{inc} with ρ, three-span beams continuous over the interior supports

Figure 4.7 shows the variation in the incremental deflection, Δ_{inc}, with the span reinforcement ratio, ρ, for three-span beams continuous at both interior supports. The computations again are based on f_y of 500 MPa and 700 MPa, K values of 0.5, 1, and 1.5, and f_c' of 30 MPa. The deflections presented are the smallest of the three end support configurations investigated. A higher f_y yields smaller deflections at high ρ, as was previously observed for simply supported, and two-span beams.

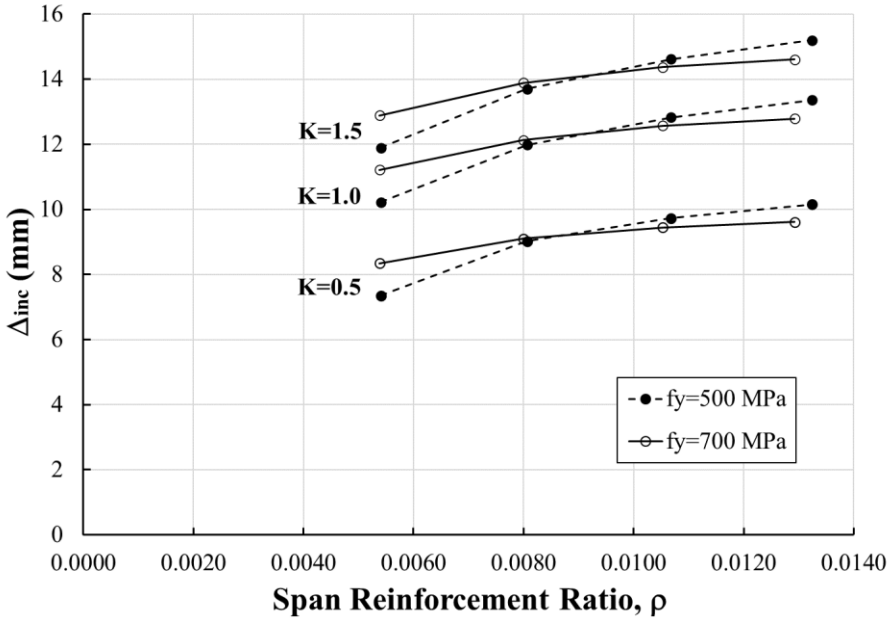

Figure 4.7: Variation of Δ_{inc} with ρ, three-span beams continuous over the interior supports

4.4.3 Results Without Height Correction Factor

Figure 4.8 shows the variation of the span to incremental deflection ratio, L_n/Δ_{inc}, with ρ for simply supported beams with f_c' of 50 MPa. In this case, however, when the yield stress correction factor on h_{min}, Equation [4.42], is assumed equal to 1.0. As the steel yield stress is increased for a given ρ, the deflection is increased which reduces the L_n/Δ_{inc} ratio. As ρ is increased for a given f_y, the deflection is increased. For given ρ and K values, a higher f_y markedly increases the applied dead and live load moments, M_l and M_d, which increase the deflections at service loads. For beams reinforced with Grade 700 steel (MPa) and a ρ greater than 0.013, L_n/Δ_{inc} is less than 240 regardless of the K value, so the beam deflections exceed the limit specified in A23.3:19. A higher K value increases incremental deflections because live loads increase.

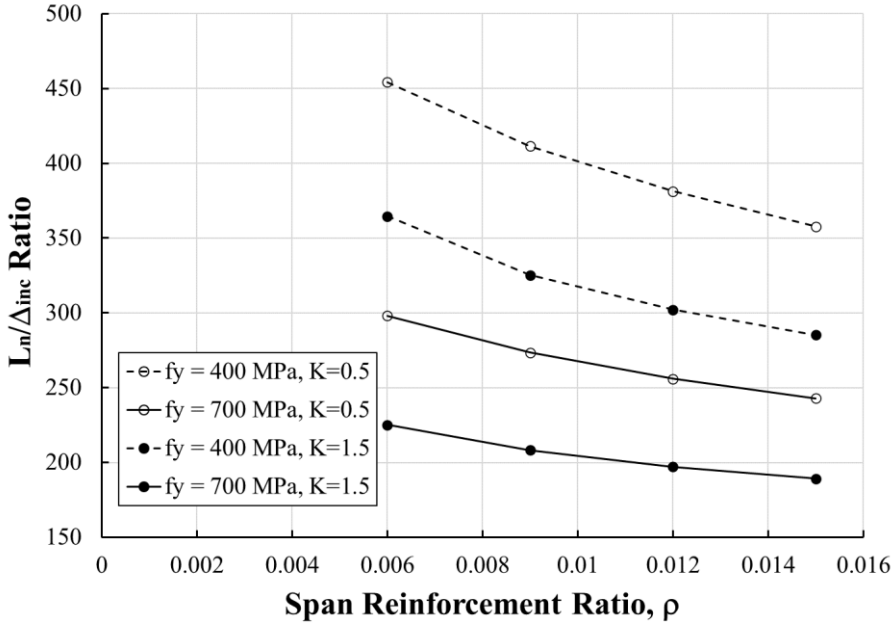

Figure 4.8: Variation of L_n/Δ_{inc} with ρ, without height modification, simply supported beams with a higher f_c'

Figure 4.9 shows the variation of the span to incremental deflection ratio with ρ for simply supported beams with f_c' of 30 MPa when the yield correction factor for h_{min}, Equation [4.42], is taken equal to 1.0. The values for K of 1.5 and f_y of 700 MPa are again all less than 240, and so do not satisfy the A23.3:19 limit.

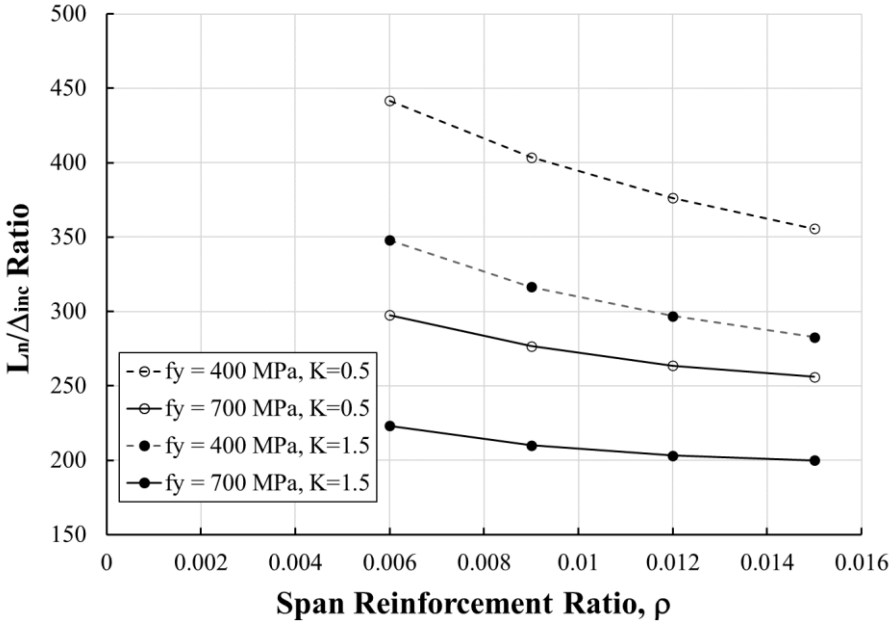

Figure 4.9: Variation of L_n/Δ_{inc} with ρ, without height modification, simply supported beams with a lower f_c'

Figure 4.10 shows the variation of the span to incremental deflection ratio with ρ for two-span beams that are continuous over the interior support, with f_c' of 30 MPa, when the yield stress height correction factor for h_{min}, Equation [4.42], is taken equal to 1.0. The values for K of 1.5 and f_y of 700 MPa are again all less than 240, and so do not satisfy the A23.3:19 limit.

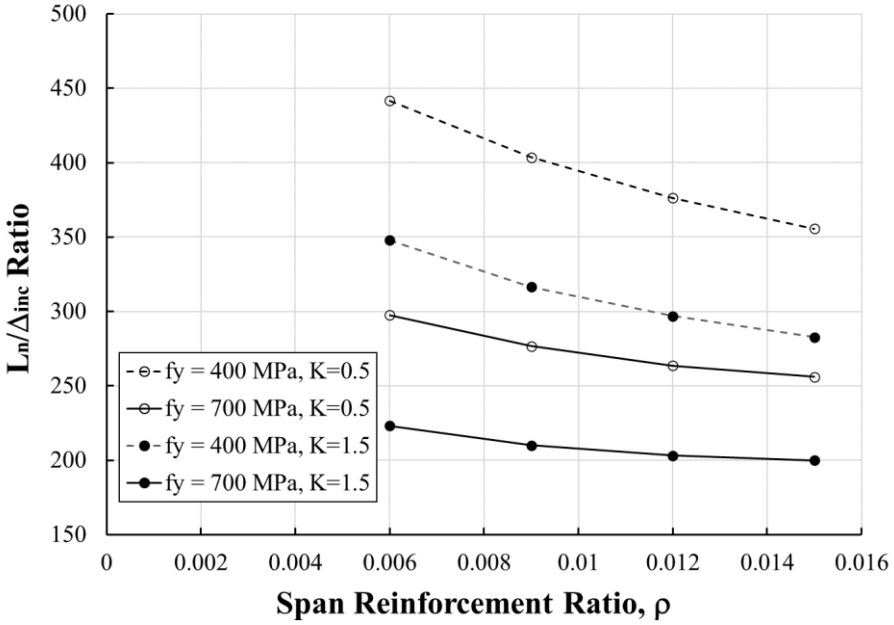

Figure 4.10: Variation of L_n/Δ_{inc} with ρ, without height modification, two span beam continuous over interior support

4.5 REFINING THE YIELD STRESS CORRECTION FACTOR FOR h_{min}

As f_y increases above 400 MPa, the height correction factor, s_f, as given in Equation [4.42], also increases. However, as shown in Section 4.4.2, adopting the limiting beam height always gives conservative deflection results and so may not be cost effective. As the deflections consistently increase with ρ, the critical case will be for the maximum reinforcement ratio, ρ_{max}, defined as

[4.43] $$\rho_{max} = \alpha_1 \beta_1 \frac{\phi_c}{\phi_s} \frac{f'_c}{f_y} \frac{\varepsilon_u}{\varepsilon_u + \varepsilon_y}$$

where ε_u is the ultimate concrete compression strain, taken as 0.0035, ε_y is the steel yield strain, taken as f_y/E_s, f_y is 700 MPa, E_s is 200000 MPa. In accordance with A23.3:19 (CSA 2019) α_1 and β_1 are the concrete stress block parameters, computed from Equations [2.8a] and [2.8b], respectively.

The current provisions of Clause 10.5.2 of A23.3:19 actually limit ρ_{max} to 80% of the value given by Equation [4.43]: for simplicity, this refinement is ignored in the present work so the reduced s_f values in this section will still be conservative.

Figure 4.11 shows the ratio of clear span, L_n, to incremental deflection, Δ_{inc}, for simply supported beams. The computations are based on reinforcing steel f_y of 700 MPa, ρ from 0.6 % to ρ_{max} , K of 1.5, and f_c' of 30, 50, 70, and 90 MPa. For a f_c' greater than 40 MPa, the elastic modulus for concrete at 7 days, $E_{c,7}$, in this investigation is computed as

[4.44] $$E_{c,7} = (3300\sqrt{f_{c,7}} + 6900)\left(\frac{\gamma_c}{2300}\right)^{1.5}$$

for the 7-day concrete compressive strength, $f_{c,7}$, and the elastic modulus for concrete at 28 days, $E_{c,28}$, is computed as

[4.45] $$E_{c,28} = (3300\sqrt{f_c'} + 6900)\left(\frac{\gamma_c}{2300}\right)^{1.5}$$

for the 28-day concrete compressive strength, f_c'. The unit weight of concrete, γ_c, is taken as 2400 kg/m^3.

In each case the s_f value has been reduced by a constant factor to yield a maximum incremental deflection of $L_n/240$ at ρ_{max}. For example, the h_{min} for a beam with f_c' of 30 MPa can be reduced by 19% and satisfy the A23.3:19 $L_n/240$ incremental deflection limit at ρ_{max}. Similarly, the h_{min} for a beam with f_c' of 90 MPa be reduced by 2%. As noted in Section 4.4.2, increasing f_c' causes increased deflections for a given ρ value and f_y of 700 MPa.

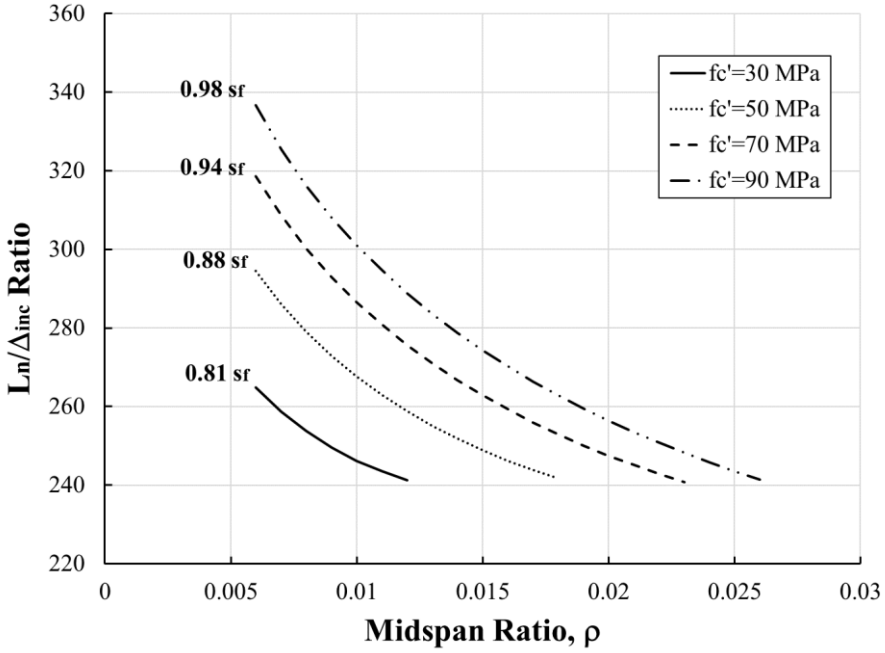

Figure 4.11: Variation of L_n/Δ_{inc} with midspan ratio, ρ: factored minimum height correction factor in simply supported beams

4.6 SUMMARY AND CONCLUSIONS

The research reported in this chapter has focussed on code provisions for deflections of beams reinforced with High Strength Steel Reinforcement (HSR). CSA A23.3:19 Table 9.2 specifies a minimum height, h_{min}, for beams that are simply supported, or have one or both ends continuous. If the beam height is less than this limit, deflections must be computed and compared with the limits in Table 9.3 of A23.3:19. The values listed in Table 9.2 pertain to beams reinforced with steel that has a minimum specified yield strength f_y of 400 MPa. For higher yield strengths, h_{min} is increased by the factor $(0.4 + f_y/670)$, where f_y has units of MPa.

The total and incremental deflections were investigated for concrete beams with concrete compressive strengths, f_c', of 30 and 50 MPa, reinforcing steel yield strengths, f_y of 400, 500, 600, and 700 MPa, and K values, the ratio of specified live to dead loads, of 0.5, 1, and 1.5. The incremental deflection is that which occurs after deflection-sensitive elements

are installed, which is assumed in the present study to correspond to the application of the superimposed dead load when the concrete is three months old. Shrinkage deflection, creep and instantaneous deflections due to own weight, superimposed dead load, sustained live loads, and deflection due to instantaneous live loads were investigated in simply supported beams, two-span beams continuous over the interior support, and three-span beams continuous over both interior supports. The impact of the beam height correction factor, s_f, which increases for a greater f_y value, was also investigated and refined for specific beam configurations. For each beam considered, h_{min} was determined from Table 9.2 of A23.3:19 and, for a given ρ, f_y, and K, the factored moment capacity and associated service dead and live load moments were calculated. Gilbert's Method (Gilbert 2011) was then used to calculate the instantaneous, creep, and shrinkage deflections in beams.

The following conclusions are drawn

1. The yield stress correction factor for h_{min} specified in Table 9.2 of A23.3:19 for beams reinforced with higher yield strength steels cannot be ignored. Beams that satisfy the h_{min} requirement when reinforced with Grade 400 reinforcement consistently do not satisfy the incremental deflection limit of clear span/240 as specified in A23.3:19 when higher-grade reinforcement is used.

2. If the yield stress correction factor specified in Table 9.2 of A23.3 is used to modify h_{min} for beams reinforced with higher-grade reinforcement, beams that exactly meet this h_{min} requirement have acceptable incremental deflections. For 288 cases investigated, the limit of clear span/240 was satisfied.

3. For a given yield strength and service live-to-dead load ratio, the incremental deflections increase for higher reinforcement ratios, ρ.

4. For a given reinforcement ratio and yield strength, the incremental deflection increases with higher service live-to-dead load ratios, K.

5. The ratios of incremental deflection to clear span ratios are relatively insensitive to the yield strength, f_y, for all cases considered when the yield stress correction factor for h_{min} is accounted for.

6. The yield stress correction factor for h_{min} can be reduced depending on the f_c', f_y, K, and the end support conditions. For a K of 1.5, f_c' ranging from 30 to 90 MPa, steel f_y of 700 MPa in a simply supported beam, a 19% reduction in s_f is possible with f_c' of 30 MPa and a 2% height reduction is possible with f_c of 90 MPa at maximum ρ.

Chapter 5

5 Summary, Conclusions, And Recommendations

5.1 SUMMARY

The objective of the research reported in this thesis was to investigate the flexural behaviour of concrete beams reinforced with High Strength Reinforcement (HSR) and to determine whether current provisions in CSA Standard A23.3:19 “Design of Concrete Structures” (CSA 2019) are appropriate for beams reinforced with HSR. To assess whether beams reinforced with HSR provide less warning of failure than those reinforced with conventional reinforcement, a parametric study was conducted. A moment-curvature code, created specifically for this project, allowed the curvature ductility ratios of beams reinforced with different steel quantities, types, and grades to be quantified and compared. The curvature ductility also influences the inelastic rotation capacities of plastic hinges and so the impact of different steel quantities, types, and grades on the maximum permissible moment redistribution could be assessed. As a beam reinforced with HSR requires a reduced steel area to satisfy Ultimate Limit State requirements compared to a beam with conventional reinforcement, the cracked moment of inertia is reduced at Serviceability Limit States. Another research objective was to investigate the serviceability of beams reinforced with HSR, particularly crack widths and deflections. Reinforcing steels that met the specifications of ASTM A615/615M Grades 60 & 100 (ASTM 2020a), ASTM A706/706M Grade 60 & 80 (ASTM 2016), and A1035/1035M Grade 100 (ASTM 2020b) were investigated.

Chapter 2 presented a sensitivity analysis to determine the effect of reinforcing steel quantity, type and grade, concrete compressive strength and other variables on the curvature ductility ratios, ultimate steel stresses, ultimate maximum concrete compressive strains, and the transition from tension-initiated to compression-initiated flexural failures. Various concrete and steel stress-strain idealizations reported in the literature were presented used to derive moment-curvature relationships based on the underlying first principles. The variation of the flexural curvature ductility ratios with the mechanical

reinforcement ratio was quantified using regression analysis. The variation of the ultimate steel stress with the mechanical reinforcement ratio was also quantified using regression analysis. The extreme fibre concrete compressive strain at ultimate moment was investigated for different reinforcement quantities, types and grades, and was compared to the value of 0.0035 specified in Clause of 8.5.3 in A23.3:19 to verify its appropriateness for beams reinforced with HSR. The balanced conditions that mark the transition between tension-initiated and compression-initiated flexural failures were also investigated.

Chapter 3 presented a parametric study to determine the effect of the reinforcement quantity, type and grade and concrete compressive strength on the moment redistribution in two-span beams that are continuous over the interior support. The moment redistribution was quantified using a 3-step process: (1) the reinforcement at critical positive (midspan) and negative (interior support) sections was designed; (2) moment-curvature relationships for these critical sections were derived; and, (3) these relationships were input to the SAP2000 finite element analysis software to determine the failure load, from which the moment redistribution was determined. Two cases of moment redistribution, involving the formation of complete and incomplete collapse mechanisms, were encountered. The in-service crack widths at cross sections designed at Ultimate Limit States accounting for moment redistribution were investigated, and the maximum permissible moment redistribution was quantified to ensure that crack width criteria in ACI 318:19 (ACI 2019) were satisfied.

Chapter 4 presented a parametric study to determine the effect of the reinforcement quantity, type and grade and concrete compressive strength on the short- and long- term deflections of simply supported beams, two-span beams continuous over the interior support, and three-span beams continuous over the interior supports. Gilbert's method (Gilbert 2011) was applied to compute shrinkage deflections, and instantaneous and creep deflections due to dead and live loads. Beam deflections can be deemed adequate without detailed calculations if minimum height criteria specified in Table 9.2 of CSA A23.3:19 (CSA 2019) are met. The investigation focused on the adequacy of the equation specified for use with this table to increase the minimum permissible beam height when the reinforcement yield stress exceeds 400 MPa. This yield stress correction factor equation

was refined to make it less conservative, while still ensuring that the actual deflection of a member that satisfies the minimum height requirements using the refined equation is less than the acceptable limit.

5.2 CONCLUSIONS

1. The curvature ductility ratio, defined as the ratio of ultimate to yield curvatures φ_u/φ_y, is approximately inversely proportional to the mechanical reinforcement ratio, ω, defined as $A_s f_y/bdf_c'$. It can be shown that the ultimate curvature, φ_u, is inversely proportional to ω. For different steel grades, magnitudes of the ultimate curvature are similar at a given ω but the yield curvatures, φ_y, of beams reinforced with HSR are markedly greater because the steel area and cracked section modulus are reduced. Thus, the curvature ductility ratio is less for beams reinforced with HSR.

2. For a given value of ω, beams reinforced with A706/706M Grade 60 steel have the highest curvature ductility ratios, and beams reinforced with ASTM A615/615M Grade 100 and A1035/1035M Grade 100 steels have the lowest curvature ductility ratios. If extreme fibre concrete compressive strain, $\varepsilon_{c,max}$, at ultimate is limited to 0.0035, then the differences between the variation of φ_u/φ_y with ω are statistically significant for each steel grade investigated. If $\varepsilon_{c,max}$ is not limited, then the difference between the variation of φ_u/φ_y with ω is not statistically significant for cross sections reinforced with A615/615M Grade 60 and A706/706M Grade 80 reinforcement.

3. Equations are derived for computing the ultimate steel stress as a function of ω for the steel grades investigated. These are suitable for design-office use.

4. The extreme fibre concrete compressive strain at ultimate is reduced significantly as f_c' increases while the steel type has a relatively smaller impact. The A23.3:19-specified value of 0.0035 can be unconservative when ω is greater than 0.20.

5. To ensure a tension-initiated flexural failure, A23.3:19 specifies a c/d limitation, where c is the depth of the compression region at ultimate and d is the effective reinforcement depth. This equation is appropriate for cross sections reinforced with the various types of high strength reinforcement investigated.

6. If a full plastic collapse mechanism forms when a continuous beam member fails, the moment redistribution percentage is independent of the grade and quantity of the steel reinforcement.

7. If a full plastic collapse mechanism does not form, because the inelastic rotational capacity of the first plastic hinge that forms is insufficient, the percentage of moment redistribution reduces as the steel yield stress increases. The maximum redistribution percentages permitted by Clause 9.2.4 of A23.3:19 are appropriate, however, for all grades of reinforcement investigated.

8. The maximum permissible moment redistribution can be limited to ensure that crack widths at critical cross sections at Serviceability Limit States are acceptable. If the steel area at a cross section is reduced by accounting for moment redistribution at Ultimate Limit State, it is recommended that crack widths at this cross section be checked using the computed in-service steel stress, instead of assuming a value of $0.6f_y$, as is currently permitted in A23.3:19.

9. The use of reinforcement with higher yield strengths leads to lesser steel areas, smaller cracked and effective moments of inertia, and so greater deflections than those obtained with conventional yield strengths. If the minimum height criteria specified in Table 9.2 of CSA A23.3:19 (CSA 2019) are met, beam deflections can be deemed adequate without further calculation. Beams reinforced with HSR do not satisfy the incremental clear span deflection limit of span/240 specified in A23.3:19 when the height correction factor specified in the notes to Table 9.2 is ignored. For all 288 beam cases investigated, however, the limit of clear span/240 was satisfied when the yield stress correction factor for h_{min} was used.

10. The yield stress correction factor for h_{min} can be reduced depending on the concrete compressive strength, steel yield strength, and other factors. For a simply supported beam with fy of 700 MPa, a 19% reduction in s_f is possible with f_c' of 30 MPa and 2% reduction is possible with f_c' of 90 MPa.

5.3 RECOMMENDATIONS FOR FUTURE WORK

5.3.1 Calibration Of Steel Resistance Factor For HSR

The reduced curvature ductility ratios of beams reinforced with high strength reinforcement that have a given mechanical reinforcement ratio, ω, and so a given factored moment resistance, imply that these beams will exhibit less warning of failure at collapse. In accordance with CSA S408-11 "Guidelines for the Development of Limit State Design Standards" (CSA 2011), the target reliability indices for these failure modes should be more stringent, which may require reduced reinforcing steel resistance factors, ϕ_s, currently specified to be 0.85, for beams reinforced with HSR. The resistance factor should be recalibrated to incorporate the loss of ductility.

The equation for the reliability index, β, is (Ravindra et al, 1978)

[5.1] $$\beta = \frac{\ln\left(\frac{\overline{R}}{\overline{Q}}\right)}{\sqrt{V_R^2 + V_Q^2}}$$

where $\overline{Q}$ is the mean load effect and is a function of applied loads on the beam, and V_R^2 and V_Q^2 are the coefficients of variation of the resistance and load effect, respectively. The mean resistance of the reinforced concrete beam, $\overline{R}$, can be written as

[5.2] $\overline{R} = R_n (\overline{P}\ \overline{M}\ \overline{F})$

where R_n is the nominal resistance, computed using the design provisions of A23.3:19 and $\overline{P}$, $\overline{M}$, and $\overline{F}$ the bias coefficients for the professional, material and fabrication factors.

The calibration would follow procedures described in CSA S408-11 (CSA 2011) that have been employed recently by Bartlett and Zhang (2018) for welded-wire reinforcement in bridges and Zhang and Bartlett (2019) for partial material resistance factors for ACI 318.

5.3.2 Moment Redistribution Provisions in A23.3:19

Clause 9.2.4 in A23.3:19 defines the maximum permissible moment redistribution in terms of increasing or reducing negative moments. It should be revised to indicate clearly that the maximum permissible redistribution is limited to the smaller of 20% or 30%-50(c/d) %, where c and d are the neutral axis depth and depth of the member at the cross section where the moments are being reduced using moment redistribution, respectively. It should also require that, if the steel area at a cross section is reduced by accounting for moment redistribution at Ultimate Limit State, crack widths at this cross section must be checked using the computed in-service steel stress, instead of assuming a value of 0.6 f_y as is currently permitted. This recommendation involves a simple code change without requiring further research.

References

American Concrete Institute (ACI) 2019. *Building Code Requirements for Structural Concrete and Commentary* (ACI 318:19). American Concrete Institute, Michigan, USA.

ASTM. 2016. *Standard Specification for Deformed and Plain Low-alloy Steel Bars for Concrete Reinforcement (ASTM A706/A706M)*. American Society for Testing and Materials (ASTM) International, West Conshohocken, PA.

ASTM. 2020a. *Standard Specification for Deformed and Plain Carbon-steel Bars for Concrete Reinforcement (ASTM A615/A615M)*. American Society for Testing and Materials (ASTM) International, West Conshohocken, PA.

ASTM. 2020b. *Standard Specification for Deformed and Plain, Low-carbon, Chromium Steel Bars for Concrete Reinforcement (ASTM A1035/A1035M).* American Society for Testing and Materials (ASTM) International, West Conshohocken, PA.

Bartlett, F.M. and Zhang, L.H. 2018: "Resistance Factor for Welded Wire Fabric Steel Reinforcement". *Electronic Proceedings, 10th International Conference on Short and Medium Span Bridges*, Quebec City, 10 pp.

Bischoff, P.H. 2007. "Rational Model for Calculating Deflections of Reinforced Concrete Beams and Slabs." *Canadian Journal of Civil Engineering*, **34**: 992-1002.

Canadian Standards Association (CSA) 2021. *Carbon Steel Bars for Concrete Reinforcement (CSA G30.18:21)*. Canadian Standards Association, Toronto, ON.

Canadian Standards Association (CSA). 2019. *Design of Concrete Structures* (CSA A23.3:19). Canadian Standards Association, Toronto, ON.

Canadian Standards Association (CSA). 2011. *Guidelines for the Development of Limit States Design Standards* (CSA S408:11). Canadian Standards Association, Toronto, ON.

Carreira, D. J. & Chu, K. H. 1985. “Stress-Strain Relationship for Plain Concrete in Compression.*” Journal of the American Concrete Institute*. **82** (6): 797-804.

Computers and Structures Inc. 2020. *CSI SAP-2000 Analysis Reference Manual*. Berkeley, California.

Gilbert, R. I. 2011. “The Serviceability Limit States in Reinforced Concrete Design”, Procedia Engineering, **14**: 385-395.

MacGregor, J. G. and Bartlett, F. M. 2000. “Reinforced Concrete: Mechanics and Design-First Canadian Edition”, Pearson Canada; Toronto, ON.

Mander, T. J., and Matamoros, A. B. 2019. “Constitutive Modeling and Overstrength Factors for Reinforcing Steel. *ACI Structural Journal*.” **116** (3): 219-232

Mast, R. F., Dawood, M., Rizkalla, S. H., & Zia, P. “Flexural strength design of concrete beams reinforced with high-strength steel bars.” *ACI Structural Journal*, **105** (5): 570-577.

National Research Council of Canada. 2015. *National Building Code of Canada* (NBCC 2015). National Research Council of Canada, Ottawa, Canada.

Ravindra, M. K. and T. V. Galambos. 1978. “Load and Resistance Factor Design for Steel.” *Journal of the Structural Division*, ASCE, **104** (ST9) Sept. 1978: 74-82

R. Park and T. Pauley. 1975. *Reinforced Concrete Structures.* John Wiley & Sons Inc. New York, NY.

Shahrooz, B. M., Reis, J. M., Wells, E. L., Miller, R., Harries, K. A., & Russell, H. G. 2010. “Flexural behavior and design with high-strength bars and bars without a well-defined yield point.” *Journal of the Transportation Research Board* (2172), 103-111. DOI: http://dx.doi.org/10.3141/2172-12.

Thorenfeldt, E., Tomaszewicz, & Jensen, J. J. 1987. “Mechanical Properties of High-Strength Concrete and Application in Design.” Proceedings of the Symposium

"Utilization of High-Strength Concrete", Stavanger, Norway. Tapir, Trondheim, 149-159.

Tiejiong Lou, Sergio M. R. Lopes & Adelino V. Lopes. 2014. "Evaluation of Moment Redistribution in Normal-Strength and High-Strength Reinforced Concrete Beams". *Journal of Structural Engineering* **140**(10): 04014072

Wee, T.H., Chin, M.S. and Mansur, M.A. 1996. "Stress Strain Relationship of High Strength Concrete in Compression." *Journal of Materials in Civil Engineering*. **8** (2): 70-76

Whitney, C.S. (1937). "Design of Reinforced Concrete Members Under Flexure and Combined Flexure and Direct Compression." *ACI Journal,* **33** (2): 483-498.

Yosefani, A. 2018. "Flexural Strength, Ductility, and Serviceability of Beams that Contain High-Strength Steel Reinforcement and High-Grade Concrete." *Thesis, submitted to partially fulfil the requirements of the Doctor of Philosophy degree*, Portland State University, Portland, OR.

Zhang, T., and Bartlett, F. M. 2019: "Partial Material Strength Reduction Factors: for ACI 318?" *American Concrete Institute Structural Journal*, **116** (3): 159-169.

Appendix 2A: Concrete Stress-Strain Idealizations

Concrete idealization Thorenfeldt et al (1987)

[2A.1] $$\frac{f_c}{f_c'} = \frac{n\frac{\varepsilon_c}{\varepsilon_0}}{n - 1 + \left(\frac{\varepsilon_c}{\varepsilon_0}\right)^{nk}}$$

[2A.2] $$n = 0.8 + \frac{f_c'}{2500}$$

[2A.3] $$\varepsilon_0 = \frac{f_c'}{E_c}\frac{n}{n - 1}$$

[2A.4] $$k = 0.67 + \frac{f_c'}{9000}$$

where: ε_0 is the strain corresponding to the peak compressive stress, f_c'; f_c and ε_0 are the concrete compressive stress and strain, respectively; and E_c is the elastic modulus of concrete.

Concrete idealization Wee et al (1996)

[2A.5] $$f_c = f_c'\left[\frac{k_1 B\left(\frac{\varepsilon_c}{\varepsilon_0}\right)}{k_1 B - 1 + \left(\frac{\varepsilon_c}{\varepsilon_0}\right)^{k_2 B}}\right]$$

[2A.6] $$k_1 = \left(\frac{50}{f_c'}\right)^3$$

[2A.7] $$k_2 = \left(\frac{50}{f_c'}\right)^{1.3}$$

where: $k_{1,2}$ are parameters with values of 1 if $f_c' < 50$ MPa and calculated using Equations [2A.6] and [2A.7] for $f_c' > 50$ MPa; and B is calculated using Equation [2.15].

Appendix 2B: Steel Stress-Strain Idealizations

Steel Idealization Mast et al (2008) For ASTM A1035/1035M Grade 100 Steel

If $\varepsilon_s < 0.0027$ then

[2B.1] $f_s = \varepsilon_s E_s$

If $\varepsilon_s > 0.0027$ then (in MPa)

[2B.2] $f_s = \left(1172 - \frac{2.379}{\varepsilon_s + 0.00104}\right)$

where: f_s and ε_s are the reinforcing steel stress and strain, respectively; and E_s is the elastic modulus of steel.

Steel Idealization Yosefani (2018) (in ksi) For A615/615M Grade 100 Steel

***Eq. derived from experimental plot**

$f_s = 29000\varepsilon_s, \left(0 < \varepsilon_s < \varepsilon_y\right)$

$f_s = f_y, \left(\varepsilon_y < \varepsilon_s < \varepsilon_{sh}\right)$

$f_s = f_y \left[1.2 - 0.2\left(\frac{\varepsilon_u - \varepsilon_s}{\varepsilon_u - \varepsilon_{sh}}\right)^2\right], \left(\varepsilon_{sh} < \varepsilon_s < \varepsilon_u\right)$

where: ε_y is the strain corresponding to steel yield stress, f_y, ε_{sh} is the strain at the onset of strain hardening, and ε_u is the steel strain at ultimate.

Appendix 4A: Incremental Deflections

Figures 4A.1, 4A.3, and 4A.5 show the variation of the ratio of effective length to incremental deflection, L_n/Δ_{inc}, with the span reinforcement ratio, ρ, for two-span beams continuous over the interior support, simply supported beams, and three-span beams continuous at both interior supports, respectively. The f_c' is 50 MPa, K has values of 0.5, 1, and 1.5, and the steel yield stress f_y is 400 MPa or 500 MPa (for the three-span beam only), and 700 MPa. Figures 4A.2, 4A.4, and 4A.6 shows the variation in the incremental deflection, Δ_{inc}, with the span reinforcement ratio, ρ, for the three different support configurations.

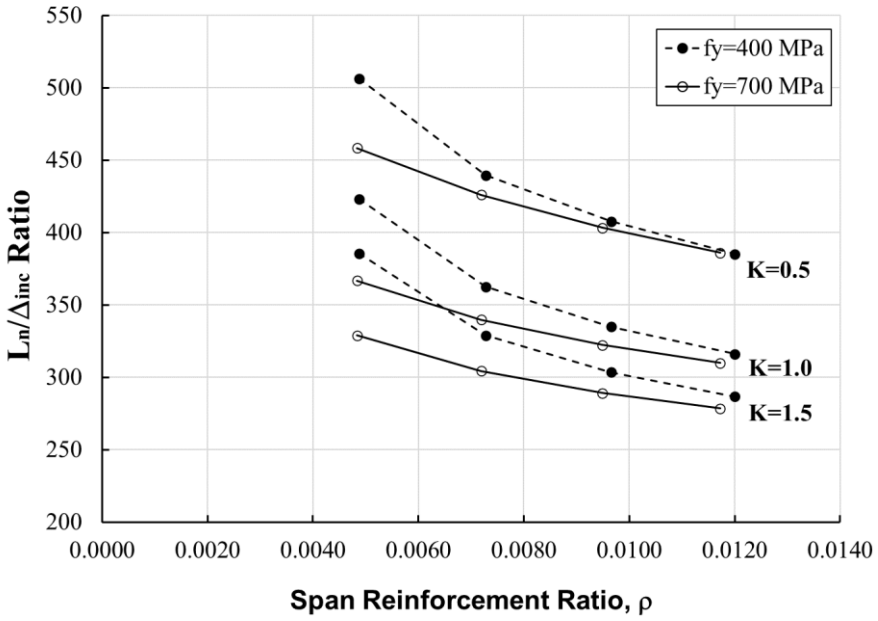

Figure 4A.1: Variation of L_n/Δ_{inc} with ρ, two-span beams continuous over the interior support

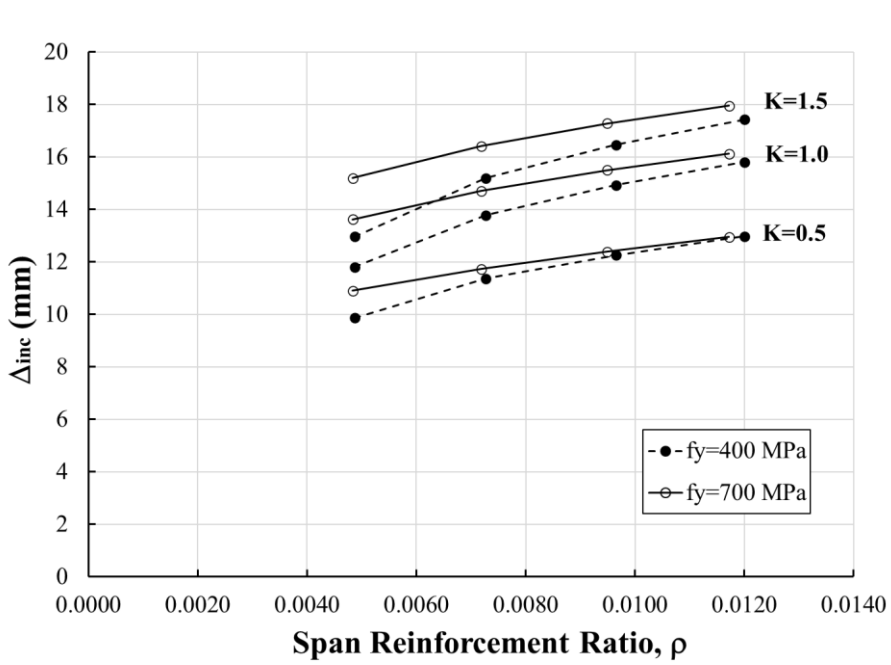

Figure 4A.2: Variation of Δ_{inc} with ρ, two-span beams continuous over the interior support

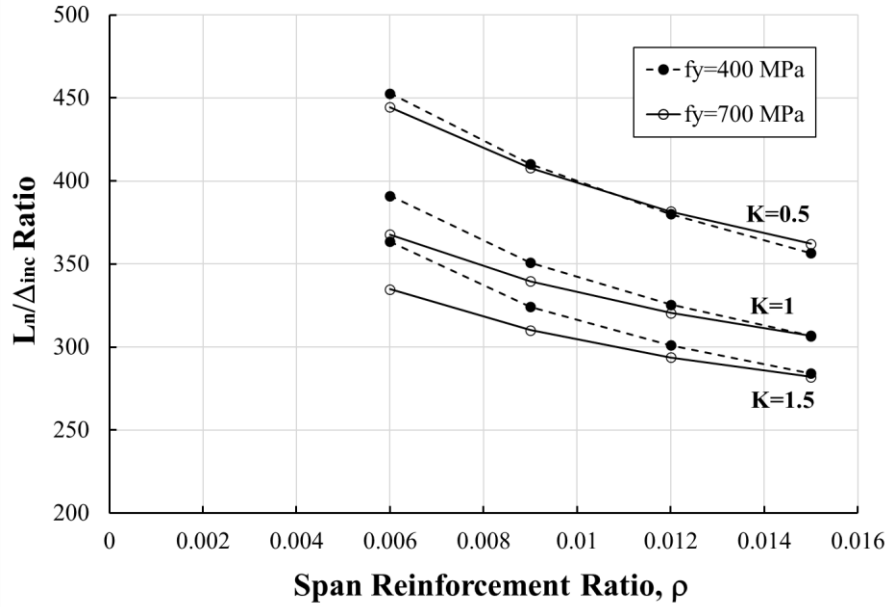

Figure 4A.3: Variation of L_n/Δ_{inc} with ρ, simply supported beams

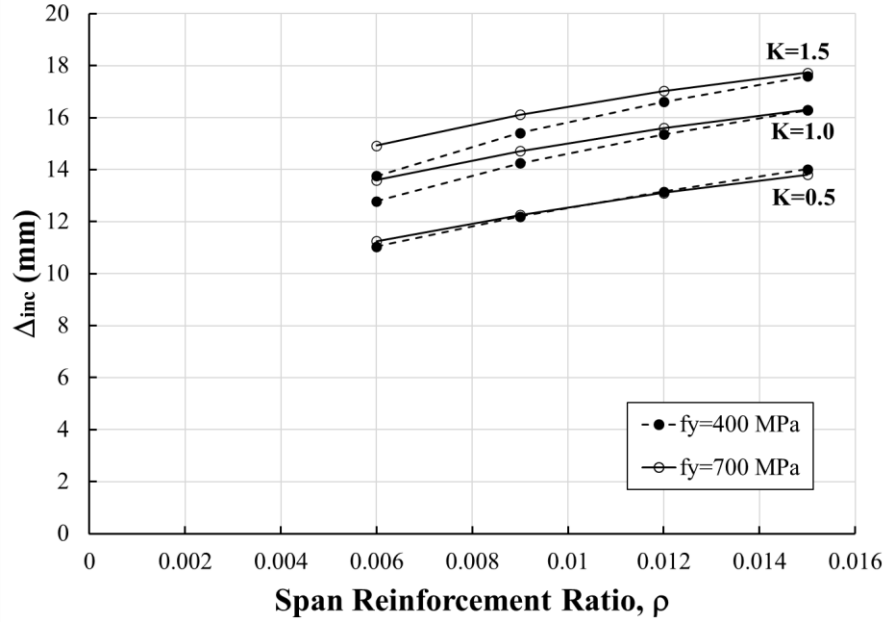

Figure 4A.4: Variation of Δ_{inc} with ρ, simply supported beams

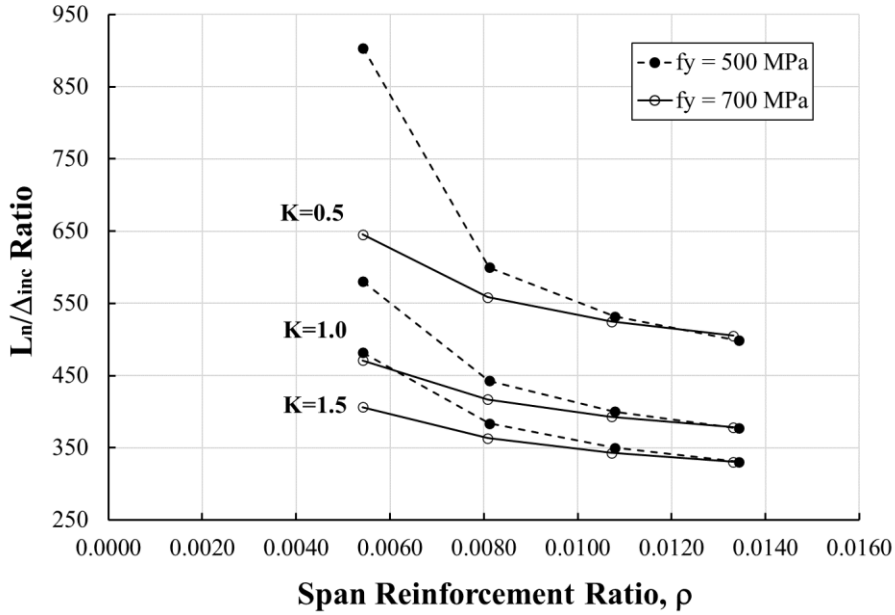

Figure 4A.5:Variation of L_n/Δ_{inc} with ρ, three-span beams continuous over the interior supports

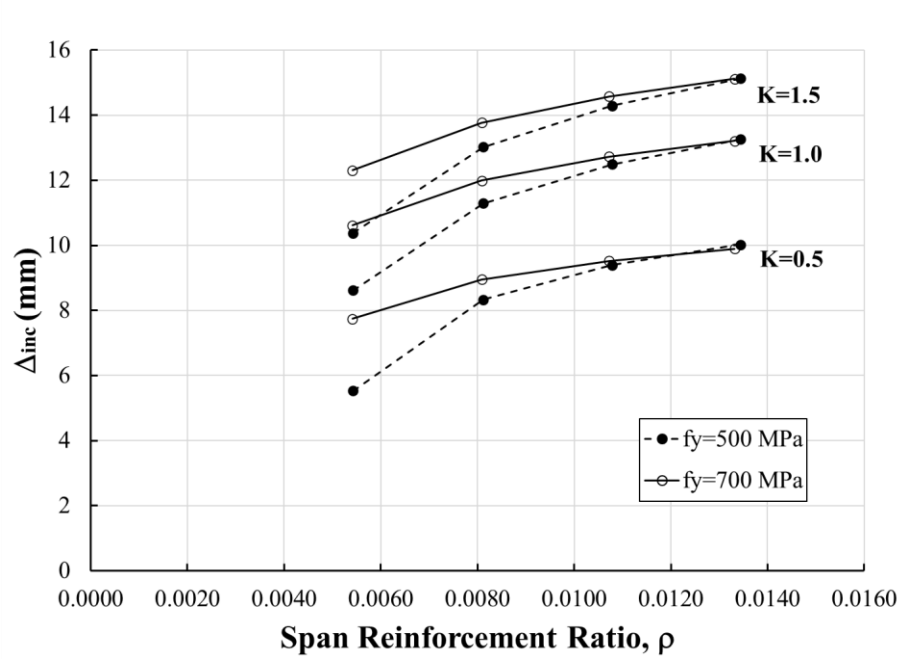

Figure 4A.6: Variation of Δ_{inc} with ρ, three-span beams continuous over the interior supports

Curriculum Vitae

Name	Sohaib Akbar
Degrees and Post-secondary Education	Bachelor of Engineering Science (BESc) 2020 The University of Western Ontario London, Ontario, Canada
	(Anticipated) Masters of Engineering Science (MESc) 2022 The University of Western Ontario London, Ontario, Canada
Related Work Experience	Teaching Assistant The University of Western Ontario 2021-2022

Publications

Akbar, S., Bartlett, F.M., Youssef, A.M. (2023). "Flexural Ductility of Concrete Beams Reinforced with High Strength Steel." *Proceedings of the Canadian Society of Civil Engineering Annual Conference 2021*. CSCE 2021 (held virtually). Lecture Notes in Civil Engineering, vol 248. Springer, Singapore. http://doi.org/10.1007/978-981-19-1004-3_51

Akbar, S., Bartlett, F. M. and Youssef, M. A. (In Press) "Moment Redistribution Limits for Beams with High Strength Steel Reinforcement." *Proceedings*, CSCE 2022 Annual Conference, Whistler, BC, 10 pp.